UNCLASSIFIED

AD 292131

Reproduced
by the

ARMED SERVICES TECHNICAL INFORMATION AGENCY
ARLINGTON HALL STATION
ARLINGTON 12, VIRGINIA

UNCLASSIFIED

NOTICE: When government or other drawings, specifications or other data are used for any purpose other than in connection with a definitely related government procurement operation, the U. S. Government thereby incurs no responsibility, nor any obligation whatsoever; and the fact that the Government may have formulated, furnished, or in any way supplied the said drawings, specifications, or other data is not to be regarded by implication or otherwise as in any manner licensing the holder or any other person or corporation, or conveying any rights or permission to manufacture, use or sell any patented invention that may in any way be related thereto.

292131

63-2-1

AD No. 292131 ASTIA FILE COPY

THE MICROWAVE CHARACTERISTICS AND APPLICATIONS OF FERROELECTRIC CERAMICS

By
M. DiDomenico, Jr.

Technical Report
Prepared under Office of Naval Research Contract
Nonr 225(48) (NR 373-361)

M.L. Report No. 960
October 1962

575100

Reproduction in whole or part is permitted for any purpose of the United States Government

ASTIA
JAN 3 1963
TISIA A

$12.00

Microwave Laboratory
W. W. Hansen Laboratories of Physics
Stanford University
Stanford, California

ERRATA

for M. L. Report No. 960

1. Page 34, line 17 after Part A; change "the gain wavelength" to read "the guide wavelength."
2. Page 35, line 9 from bottom; change "lies safely in the" to read "lies entirely in the."
3. Page 40, line 6 after Eq. (22); change "for $E \leqq 5$ kv/cm" to read "for $\Delta E \leqq 5$ kv/ cm."
4. Page 47, line 7 from bottom; change "from 0.1 to 9.5 kMc" to read "from 9.1 to 9.5 kMc."
5. Page 54, line 8; change "mismatched" to read "mismatches "
6. Page 67, line 16; change "elements L, G_1, C_1" to read "elements L_1, G_1, C_1 "
7. Page 71, Eq. (43); change "v" to "V".
8. Page 94, Eq. (63b) and the following line; change "ξ" to read "ζ" in two places.
9. Page 97, lines 2 and 4 after Eq. (73); change "$\beta_k = k\omega\sqrt{\mu c_0}$" and "$Z_0 = \sqrt{\mu}/c_0$" to read "$\beta_k = k\omega\sqrt{\mu c_0}$" and "$Z_0 = \sqrt{\mu/c_0}$ "
10. (a) Page 113, line 16; change "attneuators" to read "attenuators."
    (b) Page 113, lines 5 and 6 from bottom; change "what important design considerations are made for" to read "what the important design considerations are in"
11. (a) Page 119, Eq. (B.1); delete the prime in "$j'\omega\epsilon E$" to read "$j\omega\epsilon E$ "
    (b) Page 119, in equations following Eq. (B.1) at end of page; delete one E_2' from "$E_2' = E_2' = E_1' e^{-\eta' - j\phi'}$" to read "$E_2' = E_1' e^{-\eta' - j\phi'}$ "
12. Page 121, Eq. (B.5); change "v" following the integral to "V"
13. Page 125, line 4; change "os" to "as"
14. Page 131, Eq. (D.7); delete "$-V_f$" after the first integral sign.
15. Page 134, Eq. (E.7); change the last term to read "$|I_g|^2/(g_{01} + n^2 Y_0)^2$"
16. Page 141, line 5; change "parameter $\zeta = 3 c_2$ by" to read "parameter $\xi = 3 c_2$ by"
17. Page 142, Eq. (G.3); change "$A_e(z)$" to read "$A_3(z)$"

Microwave Laboratory
W. W. Hansen Laboratories of Physics
Stanford University
Stanford, California

THE MICROWAVE CHARACTERISTICS AND APPLICATIONS OF FERROELECTRIC CERAMICS

by

M. DiDomenico, Jr.

Technical Report
October 1962

Prepared under Office of Naval Research
Contract Nonr 225(48)(NR373-361)
Jointly supported by the U. S. Army Signal Corps,
the U. S. Air Force, and the U. S. Navy
(Office of Naval Research)

M. L. Report No. 960

ABSTRACT

The purpose of this investigation was to study both theoretically and experimentally the uses of ferroelectric ceramics in microwave device applications. At microwave frequencies, ferroelectric ceramics behave as nonlinear dielectrics and exhibit small signal as well as large signal scaler nonlinear characteristics in both the dielectric constant and the rf dielectric conductivity. The meaning of the small signal nonlinear behavior is that the rf dielectric properties are functions of an applied dc bias field. Since a knowledge of the microwave characteristics of the materials is of the utmost importance for device feasibility studies, the preliminary part of this study gives a comprehensive review of the experimentally measured characteristics of the ferroelectric titanates, and in particular of the ceramic 73 per cent $BaTiO_3$ - 27 per cent $SrTiO_3$.

From the known small signal characteristics of this ceramic material, an X-band electrically tunable ferroelectric phase shifter was constructed. The phase shifter is reciprocal and consists of a thin slab of the ceramic completely filling the transverse plane of a rectangular waveguide with suitable dielectric matching sections placed symmetrically about the slab so as to form a bandpass filter. Phase shift was controlled by applying a dc electric field to the ferroelectric. The measured characteristics of this device showed that phase shifts of 40° - 50° degrees are attainable over a 400 Mc band centered about 9.3 kMc with insertion losses ranging from 2 - 6 db. In addition to the experimental study of the phase shifter, the general incremental behavior of such small signal devices as phase shifters, attenuators, and tunable cavities is also discussed.

The nonlinear behavior of the 73 per cent $BaTiO_3$ - 27 per cent $SrTiO_3$ ceramic was further used to construct a harmonic generator operating from 3 kMc to 9 kMc. A third harmonic conversion efficiency of 8.5 per cent was attained for a peak input power of 2200 watts. The theoretical analysis of the harmonic generator was carried out for the case where the nonlinear coupling element comprises both nonlinear reactance and nonlinear resistance.

By fitting the expression obtained for the conversion efficiency to the experimental data, the large signal dielectric constant and rf conductivity of the above mentioned ceramic were found to be given by $\epsilon'(E) = \epsilon_0 \left[2200 - 7.5 \times 10^{-11} E^2\right]$ farad/m , and $\sigma(E) = \epsilon_0 \left[160\ \bar{\Omega} + 29 \times 10^{-12}\ \bar{\Omega}\ E^2\right]$ mhos/m , where E is in volts per meter. These results were measured at 3 kMc and for temperatures in the range of 49 - 52°C.

Since the ferroelectric ceramic under consideration is made up of both nonlinear reactive and nonlinear resistive terms, it can be treated as a generalized nonlinear dielectric medium. To study the properties of traveling-wave harmonic generation in such a dielectric medium a perturbation solution was developed for the steady-state response of nonlinear TEM transmission lines and nonlinear cylindrical waveguides of arbitrary cross section. In order to assess the characteristics of ferroelectric traveling-wave harmonic generators, an example is worked out for an S-band rectangular waveguide completely filled with the ceramic and excited in the TE_{10} mode at the fundamental frequency of 3 kMc. The predicted behavior of this device is then compared with the experimental characteristics of the cavity-type ferroelectric harmonic generator so as to determine the advantages and disadvantages of each type of device. The comparison brings out the superiority of the resonant system and indicates ways of improving the distributed system. Finally, based upon the treatment of the waveguide problem, the processes of frequency and mode conversion in nonlinear waveguides are discussed, both in general and with regard to the above example of the rectangular guide.

* suit-10

ACKNOWLEDGEMENTS

I wish to express my gratitude to my research supervisor, Professor R. H. Pantell, for his interest and guidance throughout the course of this project, and for his many contributions to the work. It is indeed a pleasure to express my appreciation to Dr. B. A. Auld for his very helpful assistance throughout much of this work. I would also like to thank Dr. D. A. Johnson for many helpful discussions concerning the experimental work.

Finally, I wish to express my thanks to Mr. A. S. Braun for his supervision in the preparation of this manuscript, and to Mrs. M. Formentini and Miss Elaine Gilderoy for the typing.

TABLE OF CONTENTS

LIST OF FIGURES

CHAPTER I

INTRODUCTION

Ferroelectric materials have been the subject of widespread and intensive investigation in recent years, both with regard to understanding the underlying physical behavior of the materials and from the point of view of utilizing their basic nonlinear dielectric properties in microwave devices. Ferroelectrics are unique among dielectrics in that they are capable of sustaining a spontaneous polarization over a certain temperature range which usually extends from absolute zero to a critical temperature known as the ferroelectric Curie point. Over the temperature range of spontaneous polarization the material displays a hysteresis loop between the polarization and applied field analogous to the hysteresis loop observed in the magnetization curve of a ferromagnetic material. At temperatures above the Curie point, the spontaneous polarization disappears. In this temperature range the materials possess a very large field-dependent induced polarization resulting in a characteristic nonlinear dielectric behavior with high dielectric constant. It is this nonlinear relationship between induced polarization and applied field, which extends well into the microwave portion of the spectrum (both for large rf signals and for small signals in conjunction with a strong dc bias), that makes ferroelectrics attractive from the standpoint of microwave device applications.

Although the literature on the subject of ferroelectricity contains a great deal of information on the experimental characteristics of ferroelectrics in single crystal and polycrystalline form, very little progress has been made toward understanding the physical mechanisms responsible for their behavior. Since most of the experimental data given for ferroelectrics has been concerned with their low frequency properties, most applications have been limited to such things as the use of the square loop hysteresis characteristic in computer technology or the construction

of miniaturized nonlinear capacitors for use in low frequency circuit applications. The amount of information which is currently available on the microwave characteristics of ferroelectrics is very limited, and as a consequence there has been practically no work reported on the use of ferroelectrics at microwave frequencies.

The purpose of this report is to describe an investigation which was undertaken to study, both theoretically and experimentally, how the small signal and nonlinear large signal characteristics of ferroelectric titanate ceramics can be used in microwave device and microwave circuit applications. Since no consistent description of the dielectric properties of the materials exists from a physical point of view, it is necessary to rely on a phenomenological description of the material properties as deduced from experimental data in the form of curves. Using such an approach, it was possible to analyze the behavior of microwave circuits containing ferroelectrics, and to successfully design devices which utilize the nonlinear properties of these materials.

The ferroelectric chosen for this study was a polycrystalline ceramic with composition 73 per cent $BaTiO_3$ - 27 per cent $SrTiO_3$. The microwave properties of this ceramic as well as those of a number of other mixed barium-strontium titanate ceramics have been measured by Johnson[1] and others.[2-5] This particular ceramic was chosen for two reasons. The first is that its general properties are representative of those of the ferroelectric-titanate class of ceramics; and the second is that in comparison with the other ceramic materials of this class considered in reference 1, the 73 per cent $BaTiO_3$ - 27 per cent $SrTiO_3$ ceramic has a large degree of nonlinearity for temperatures ranging about $40^{\circ}C$ above its Curie point which is approximately $20^{\circ}C$. Accordingly, this ceramic composition can be operated near room temperature with very simple temperature stabilizing equipment. Moreover, this material has a high breakdown field strength (in excess of 30 kv/cm). Generally speaking, ceramics were used, as opposed to single crystals, since they are easily manufactured, easily fabricated to almost any desired shape with excellent mechanical properties, available in large samples at moderate costs, and also isotropic, while at the same time strongly nonlinear.

Owing to the fact that virtually no experimental work has been done on the utilization of ferroelectrics in microwave devices, it was felt that attention should be given not only to the design and construction of ferroelectric devices but also to their analytical description. For this reason, an attempt has been made to appraise theoretically the use of ferroelectrics in a number of small signal and large signal devices, and to investigate experimentally their behavior. The distinction between small signal and large signal devices is based upon the characteristics of the nonlinearity of the ferroelectric material that is used. In the small signal case the rf dielectric constant is a function of an applied dc bias field giving rise to what is henceforth referred to as a dc nonlinearity; in the large signal case the rf dielectric constant is a function of the instantaneous rf field intensity within the material and is thus representative of a nonlinear dielectric behavior. The two specific devices which were considered experimentally were an X-band electrically tunable phase shifter, and a harmonic generator capable of tripling from a fundamental frequency of 3 kMc to an output frequency of 9 kMc. The phase shifter is an example of a small signal device and the harmonic generator typifies a large signal device. Both of these devices represent a successful application of ferroelectrics at microwave frequencies, and were chosen because they are of considerable practical importance, and because they show the feasibility for using these materials in representative microwave devices.

It should be noted that other materials, such as ferrites and semiconductor diodes, have been successfully used in microwave devices of this nature. Ferroelectrics represent a potentially competitive element and as such have received considerable attention as possible candidates for use in devices; it is therefore of significance to be able to evaluate critically the utility of these materials in relation to ferrites and diodes. From the materials standpoint, ferroelectrics have a number of obvious advantages. For example, depending upon their size they can be treated as lumped or distributed elements. At small signals their loss characteristics are independent of power level. Diodes, on the other hand, are available only as lumped elements and their losses tend to increase with power level even for small signals. Unlike ferrite materials,

ferroelectric ceramics are isotropic and can be biased electrostatically with negligible amounts of dc control power. Since the bias is provided by electric fields rather than magnetic fields, the biasing equipment can be very simple and inexpensive. Furthermore, the response time of the rf dielectric properties to changes in dc bias will be short compared to what may be obtained in the corresponding case of ferrites. In contradistinction to both ferrites and diodes, the large signal characteristics of ferroelectric ceramics display a nonlinearity which is an even function of field strength in the absence of bias; ferrites and diodes are usually operated in the biased state and exhibit an odd nonlinear characteristic. This type of large signal behavior is obviously an advantage or a disadvantage depending upon the application under consideration. Ferroelectrics have two decided disadvantages at microwave frequencies. They have relatively high loss, and have very high dielectric constant which makes matching into these materials a difficult problem. In addition, their dielectric properties are temperature dependent.

The remainder of the work presented here is organized into four chapters. Chapter II is primarily concerned with the microwave characteristics of ferroelectric ceramics and the manner in which their macroscopic electrical behavior can be described. Included as an introduction is a brief discussion of the physical properties of ferroelectrics in single crystal and polycrystalline form at and below microwave frequencies. An extensive discussion is given of the small signal dc nonlinear characteristics of the ferroelectric ceramic composed of 73 per cent $BaTiO_3$ - 27 per cent $SrTiO_3$ and of the large signal characteristics of this ceramic. The final portion of the chapter deals with the problem of microwave losses in nonlinear ceramics, and presents a discussion of the advantages and disadvantages in microwave applications of ferroelectric materials compared with ferrite and diode materials.

In Chapter III a general discussion of the small signal applications of ceramic nonlinear dielectrics is given with regard to phase shifting, cavity tuning, and attenuating. Implicit in these applications are also switching, tunable filtering, and impedance matching. The dc nonlinear characteristics of the ceramic composition of 73 per cent $BaTiO_3$ - 27 per cent $SrTiO_3$ are used in the design and construction of an

X-band phase shifter whose incremental phase shift can be controlled with a dc voltage in a predictable way. This phase shifter is reciprocal and consists of a thin slab of the nonlinear ceramic completely filling the transverse plane of a rectangular waveguide, with suitable dielectric matching sections placed symmetrically about the slab so as to form a band-pass filter.

Chapter IV is concerned with the large signal applications of the ferroelectric-titanate ceramics. The specific problems treated in this chapter are harmonic generation in lumped and distributed circuits. Both nonlinear reactance and nonlinear resistance are included in these problems since both effects are present simultaneously in ferroelectrics. In this sense, therefore, the ferroelectric medium is a generalized nonlinear dielectric. The work on harmonic generation in lumped circuits deals with the theoretical and experimental aspects of frequency multiplication in cavity-type microwave circuits. The experimental phase of the work is devoted to studying the behavior of a frequency tripler which operates from 3 kMc to 9 kMc. The operating characteristics of this device were found to be in excellent agreement with those predicted theoretically. The remaining portion of the chapter treats the problem of traveling-wave harmonic generation along nonlinear transmission lines and in nonlinear waveguides of arbitrary cross-section. This work is strictly of an analytical nature and makes use of perturbation theory to describe the processes of frequency and mode conversion in distributed nonlinear systems.

The final chapter, Chapter V, is devoted to a discussion of the conclusions reached and to giving some suggestions for future work.

CHAPTER II

THE MICROWAVE CHARACTERISTICS OF FERROELECTRIC-TITANATE CERAMICS

Althought the ultimate goal of this work is to make use of the microwave characteristics of ferroelectric-titanate ceramics in the design and construction of microwave devices, it is nonetheless important to understand from a fundamental viewpoint the behavior and limitations of these materials especially insofar as they determine and affect the performance of the devices in which the materials are incorporated. Accordingly, this chapter presents a brief survey of some of the outstanding physical properties of ferroelectrics, and gives a comprehensive discussion of their experimentally measured small signal and large signal microwave characteristics.

A. PHYSICAL PROPERTIES OF FERROELECTRICS[6-11]

Based upon their chemistry and crystal structure, ferroelectrics may be classified into three groups.[10,11] Rochelle salt, potassium dihydrogen phosphate (KDP), and barium titanate are examples of well-known ferroelectrics belonging to the different groups. The material of primary concern here is the $BaTiO_3$ - type ferroelectric which is a member of the oxygen octahedron group. This group consists of ionic crystals having the perovskite structure.[10,11] Barium titanate is the most important member of the perovskites and represents the simplest crystal structure exhibiting ferroelectricity. It is for this reason that it has received very intensive theoretical and experimental investigation throughout the literature.[7]

Most dielectric materials are nonpolar or have a vanishing electric dipole moment in the absence of an external field. For such dielectrics there is a linear relationship between the polarization and applied field. Due to the behavior of their crystalline structure with temperature, ferroelectric materials become polar below a critical temperature known as the ferroelectric Curie point and are consequently capable of supporting a spontaneous polarization. Materials of this type have very unusual dielectric properties which give rise to nonlinear behavior. In order that a crystal display a spontaneous moment, it is necessary that the lattice structure lack a center of symmetry or that it be noncentrosymmetric. This can be seen by picturing a crystal as a constellation of permanent dipoles which have a configuration compatible with the crystalline symmetry. For those crystals having a center of symmetry one finds that the dipole configuration is equivalent to arranging the dipoles in antiparallel pairs. Thus, it is evident that the centrosymmetric crystal structure (or, for that matter, any crystal structure which produces an equivalent effect) will not support a permanent dipole moment. A macroscopic permanent dipole moment or spontaneous polarization can only exist if the crystalline symmetry is of such a nature that it does not give rise to a dipole configuration in the form of antiparallel pairs. Crystals having this property exhibit the phenomenon of piezoelectricity. Since it is possible for a crystal to be piezoelectric without being ferroelectric (e.g., quartz) but not vice versa, ferroelectrics may be generally classified as a subgroup of piezoelectric-type crystals.

The outstanding property of ferroelectric materials is that in the polar state the direction of the spontaneous polarization can be reversed by the application of a low frequency external field which is below the breakdown field strength of the crystal. Because crystals are most commonly made up of a number of domains or regions of uniform polarization, one finds that the curve of the net macroscopic polarization vs applied field is in the form of a hysteresis loop. The occurrence of hysteresis between the polarization P and the applied field E causes the material to exhibit nonlinear dielectric properties which are brought about by the fact that as the field E increases the domains become aligned and eventually cause the crystal to become a single domain. When this

condition is reached the polarization saturates. It is apparent then that the domain structure of ferroelectric crystals is responsible for the presence of dielectric nonlinearities below T_c . However, the domain wall nonlinearities are present only at low frequencies where the motion of the domain boundaries can follow the changes in the exciting field. In the microwave region (above 1000 Mc) the relaxation of domain wall motion causes this nonlinear mechanism to be completely negligible.

The foregoing discussion clearly describes how the nonlinearities arise below T_c in the low frequency region. However, it in no way accounts for the presence of dielectric nonlinearities above T_c where the material is nonpolar and where the domain structure is absent. To understand the cause for the nonlinear dielectric behavior above T_c , it is necessary to consider the variations in the dielectric properties of the material produced by changes in temperature. When this is done one finds that the field-induced variations in the polarization, which are responsible for the dielectric nonlinearities and occur in both the polar and nonpolar state, are closely allied with the temperature dependence of the dielectric properties.

If one examines the behavior of the dielectric constant of ferroelectric crystals with respect to temperature, the most prominent characteristic observed is that, as the crystals are cooled through their Curie point, the dielectric constant ϵ defined by

$$\epsilon = \left.\frac{\partial D}{\partial E}\right|_{E=0} = \epsilon_0 + \left.\frac{\partial P}{\partial E}\right|_{E=0} , \qquad (1)$$

where $D = \epsilon_0 E + P$, increases rapidly, reaching a very large value typically of the order of $10^4 - 10^5$ and then drops sharply to an almost constant value. Figure 1 illustrates this behavior. The cusp in the dielectric constant appearing in the vicinity of T_c is due to the fact that as one passes through the transition temperature from the unpolarized to the polarized or ferroelectric phase the crystal structure undergoes an abrupt phase transition. It is noteworthy to mention that in the region above T_c the dielectric constant is observed to follow a Curie-Weiss law[12] (i.e. $\epsilon = C/(T - T_c)$ where C is a constant); this region

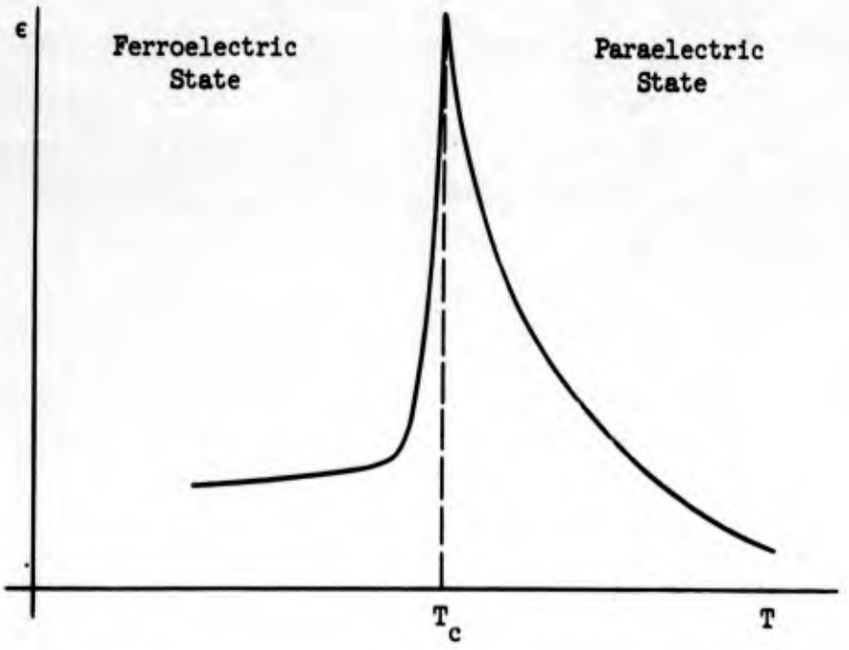

FIG. 1--Schematic representation of the dielectric constant of a ferroelectric crystal in the neighborhood of the Curie point.

is consequently known as the paraelectric phase. Precisely the same type of behavior as shown in Fig. 1 occurs for polycrystalline and ceramic materials, the only difference being that the Curie point is not as well defined for these materials and that the peak in the dielectric constant is not as high.

Merz[13] has made measurements on the dielectric constant and spontaneous polarization of single domain $BaTiO_3$ crystals as a function of temperature. The results of his measurements show the existence of three separate phase transitions in the $BaTiO_3$ crytal lattice. In the paraelectric state the $BaTiO_3$ lattice has the cubic perovskite structure and is centrosymmetric. The phase transition occurring at $T_c = 120^{\circ}C$ determines the Curie point and the onset of the ferroelectric state. Each of the three phase transitions appearing at and below T_c cause a loss of symmetry in the crystal lattice, and hence account for the presence of a noncentrosymmetric crystalline structure which is required of crystals in the ferroelectric state. As a function of temperature, it is found that for $3^{\circ}C < T < 120^{\circ}C$ the crystal is tetragonal with spontaneous polarization along the [001] crystal axis. Between $-80^{\circ}C$ and $3^{\circ}C$ the orthorhombic structure

exists with polarization along the [011] axis, and below -80°C the crystal becomes rhombohedral and is polarized along the [111] crystal axis.

In the prior discussion of the temperature dependence of the dielectric constant of ferroelectric crystals, it was pointed out that in the immediate neighborhood of the Curie point the crystal lattice undergoes a phase transition (see Fig. 1). The phase transition which occurs at T_c is caused by a change in the crystal structure (and therefore the energy and volume of the crystal) as it goes from one equilibrium position to another. The changes in the polarization of the crystal lattice can either be discontinuous, as in the case of first-order transitions, or continuous, as with second-order transitions. It is evident, therefore, that in the vicinity of the Curie point the lattice is in an unstable configuration and can consequently be greatly influenced by the application of an external field. It can then be seen, in a qualitative way, that the production of large variations in the polarization by changes in the external field may be accounted for by considering the coupling between the external field and the basic structural instabilities in the lattice. According to this description, which may be used to formulate a thermodynamic model for the crystal, one can induce changes in the polarization or dielectric constant by applying either a strong dc field to the material or an intense time-varying field. To be more precise, since the polarization, electric field, and temperature are all related by the free energy of the crystal, one finds that as one approaches the transition temperature the relationship between the polarization and applied field should become nonlinear due to the fact that the polarization becomes very large in this region. If one examines the behavior of the polarization above T_c, as done by Devonshire,[14] one finds that in the presence of an external field there is a large induced polarization in the paraelectric temperature region and that this polarization approaches the spontaneous polarization as the crystal is cooled below T_c. Thus there is no well defined Curie point in a biased crystal since the external field tends to induce a phase transition at temperatures above T_c. One may conclude from this discussion that the cause for the dielectric nonlinearity at temperatures very close to T_c is related to the stability of the lattice. Since it is observed experimentally that the degree of

nonlinearity decreases as one departs from the Curie point, it is to be expected that these same arguments apply at temperatures somewhat above and below T_c and can hence be used to describe the dielectric nonlinearity in the paraelectric phase.

B. THEORIES PERTAINING TO FERROELECTRICITY[9-11, 14, 15]

Although there is a large body of experimental data describing the physical properties of ferroelectrics, there is relatively little quantitative understanding of the underlying mechanisms responsible for the existence of the ferroelectric state. Because of the simplicity of its crystal structure the material which has the most promise of being understood theoretically is the $BaTiO_3$ - type ferroelectric. Jaynes[15] has given a comprehensive review of the theories proposed for $BaTiO_3$ and has discussed in some detail the objections to the various theories as well as their limitations.

The simplest theory which has been developed for interpreting the phenomenon of ferroelectricity is the dipole theory[11] in which the crystal is assumed to be made up of a large number of freely rotating electric dipoles analogous to the simple dipole model used to explain ferromagnetism. The fundamental problem encountered in the dipole theory is the calculation of the internal local fields acting on the dipoles. In the case of magnetic materials, where one essentially has noninteracting or freely-rotating dipoles, the local field problem can be treated directly by assuming that the internal field is proportional to the magnetization. A similar assumption can be made for ferroelectric materials; however, due to the complexities which exist in even simple lattices the computation of the local field from a molecular viewpoint is much more difficult in ferroelectric than in ferromagnetic substances. The assumption that a crystal can be represented as a classical dipole array accounts for the possibility of spontaneous polarization below the Curie point and the Curie - Weiss law behavior above the Curie point. However, the dipole theory only predicts the existence of one Curie point whereas materials such as Rochelle salt have two Curie points. This fact, together with the fact that the dipole theory does not take into account the coupling of the mechanical and electrical

forces in the crystal, forms the basis for the objections to the theory. Furthermore, the dipole theory predicts Curie temperatures which are high enough to cause most polar liquids to be ferroelectric -- a conclusion which is not supported experimentally.

Of the theories which have been proposed to explain the behavior of barium titanate, the molecular interaction theories are the most significant. In the first of these, known as the ionic displacement theory, it is assumed that the Ti^{4+} ion residing at the center of the oxygen octahedron in the perovskite lattice shifts from its centrosymmetric position at temperatures above T_c to a noncentrosymmetric position at temperatures below T_c . One can thus account for the production of a permanent dipole moment in each unit cell of the crystal, and can account for the presence of a spontaneous polarization by the cooperative effect of all of the dipoles in the crystal. Another theory which is very similar is the oxygen displacement theory where it is assumed that the effect of the phase change in the crystal structure at the Curie point is to cause the O^{2-} ions to move perpendicularly out of the plane of the Ba^{2+} ions and thereby to generate a spontaneous moment. Each of the theories qualitatively explains the observed phenomena by considering the coupling between the electrical and mechanical forces in the lattice via the temperature dependent behavior of the crystal. However, as discussed by Jaynes[15] and Dekker[11] there are a number of objections to the ionic displacement theories. The most outstanding of these is related to the question of the actual motion of the ions in the crystal lattice.

Perhaps the most successful theory of ferroelectricity is the phenomenological theory developed by Devonshire[14] which is independent of the specific molecular mechanisms in the crystal giving rise to the ferroelectric state. The theory is accordingly based upon purely thermodynamic arguments. The basis of Devonshire's formalism is that the free energy is a function of polarization and mechanical stress and thus includes the coupling between the electrical and elastic properties of the ferroelectric crystal. Although this description is capable of qualitatively accounting for the observed phase transitions in stressed and unstressed crystals, it gives no physical insight into what mechanisms are responsible for this behavior.

C. THE MICROWAVE PROPERTIES OF FERROELECTRIC CERAMICS

Ferroelectric materials have been investigated most extensively at frequencies below 1000 Mc. In the microwave region (above 1000 Mc) relatively little information is available on the dielectric properties of these materials. The most significant difference between the low frequency and microwave characteristics of ferroelectrics is that below T_c the hysteresis in the P vs E curve is absent in the microwave region. This is substantiated by measurements made on the time required to switch the polarization by 180° in a single domain, which for $BaTiO_3$ single crystals has been shown to have a corresponding frequency limit in the megacycle range.[16]

Recently, Stanford[17] has shown that in the vicinity of the Curie point and in the region of 1000 Mc there is a dispersion in the dielectric constant of the ferroelectric titanates which appears only in the ferroelectric phase. This is in general agreement with the measurements of Powles and Jackson[18] made on polycrystalline barium titanate. The appearance of this dispersion in the dielectric constant is apparently closely related to Kittel's theory of domain boundary motion,[19] indicating that domain wall relaxation processes are responsible for the observed dispersion. These measurements give further evidence that the hysteresis in the P vs E curve is absent at microwave frequencies.

Very little other data exists on the microwave properties of the ferroelectric titanates. The small signal dielectric constant and loss tangent of the single domain crystals of $BaTiO_3$ as well as the effect of the dc field on the microwave characteristics of this material has been measured by Benedict and Durand[3] at 24 kMc. Jaynes and Varenhorst[20] have measured the small signal complex dielectric constant of $BaTiO_3$ single crystals and ceramics as a function of frequency and temperature from 2 Mc to 4000 Mc and from 80°C to 150°C, respectively, for a number of bias voltages. Other measurements[2,4,5] have also been made on the microwave characteristics of ferroelectrics, using various techniques.

Johnson[1] has made a systematic study of the small signal and large signal microwave characteristics of the ceramic composed of 73 per cent $BaTiO_3$ - 27 per cent $SrTiO_3$ between 3 kMc and 10 kMc. In addition he has measured the small signal dielectric constant of this ceramic for frequencies extending into the millimeter wave region. His measurements were performed on ceramics rather than single crystals since one of the objectives was to obtain design data useful in device applications where ceramic materials are more practical. Compared to single crystals ceramics have the disadvantage of having higher loss tangents. However, the dielectric constants of these materials are not as large as those obtained with single crystals nor do their dielectric properties vary as drastically with temperature. Since it is desirable in device applications to operate the materials above their Curie point where the rf losses are relatively small, and since it is desirable at the same time to have this operating region be near room temperature, it is necessary to dope the $BaTiO_3$ crystal with other elements so as to lower its Curie point. Jackson and Reddish[21] have shown that by replacing the barium ions in the lattice by strontium ions, the Curie point of the (Ba - Sr) TiO_3 composition can be reduced considerably. Hence, the ceramic composition of 73 per cent $BaTiO_3$ - 27 per cent $SrTiO_3$ (which is of interest here) has a Curie point at room temperature ($T_c = 20^{\circ}C$) . This is $100^{\circ}C$ lower than the Curie point of pure barium titanate; the ceramic can therefore be operated conveniently as a nonlinear dielectric material near room temperature.

1. Small Signal Characteristics at Millimeter Wavelengths

The curve shown in Fig. 2 of the relative dielectric constant of the nonlinear ceramic referred to above as a function of frequency reveals at a glance the dispersive character of the dielectric constant at microwave frequencies. This curve extends over the greater portion of the microwave spectrum (from 3 to 300 kMc) and illustrates the magnitude and variation of the dielectric constant throughout this part of the spectrum. Furthermore, as discussed below, it indicates over what range of frequencies the dielectric nonlinearity can be used in microwave devices.

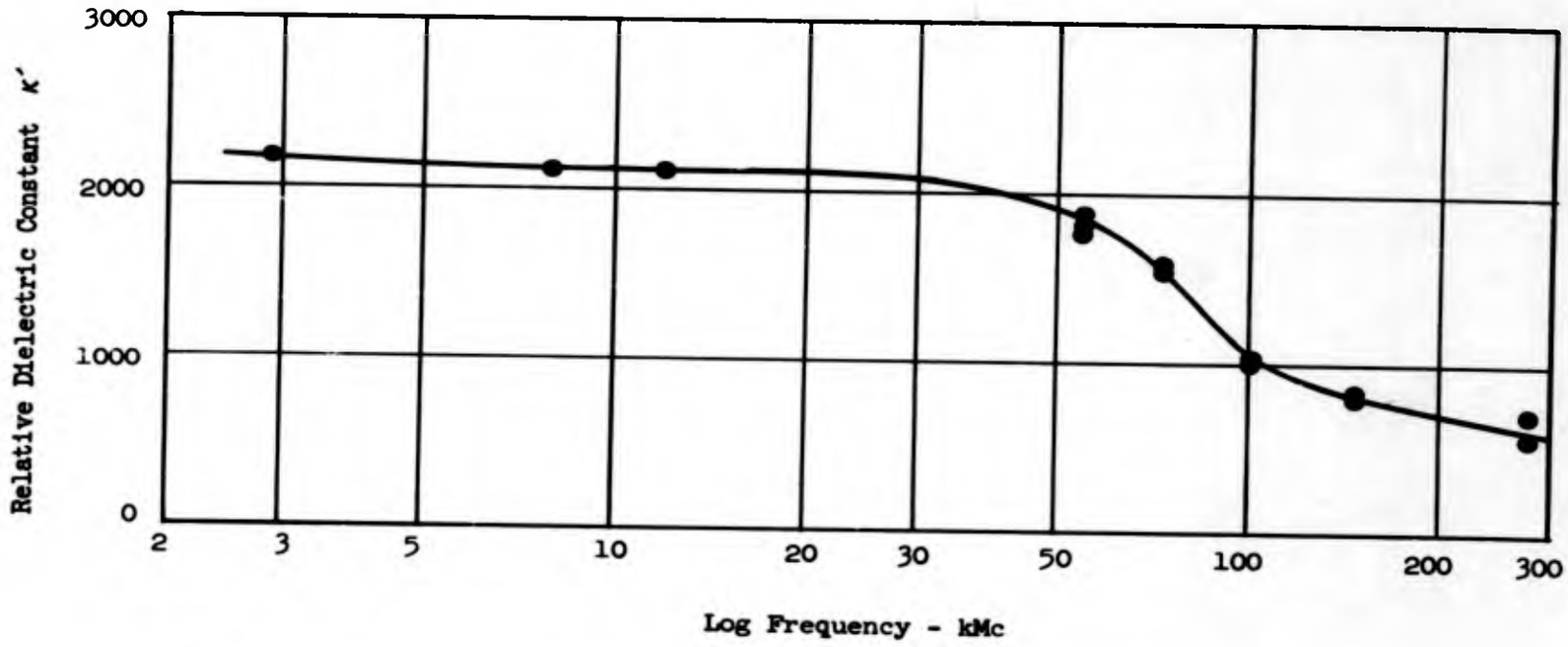

FIG. 2--Relative dielectric constant κ' as a function of frequency for ceramic of 73 per cent $BaTiO_3$ - 27 per cent $SrTiO_3$ at 51°C (After Johnson[1]).

Johnson[1] has made a systematic study of the small signal and large signal microwave characteristics of the ceramic composed of 73 per cent $BaTiO_3$ - 27 per cent $SrTiO_3$ between 3 kMc and 10 kMc. In addition he has measured the small signal dielectric constant of this ceramic for frequencies extending into the millimeter wave region. His measurements were performed on ceramics rather than single crystals since one of the objectives was to obtain design data useful in device applications where ceramic materials are more practical. Compared to single crystals ceramics have the disadvantage of having higher loss tangents. However, the dielectric constants of these materials are not as large as those obtained with single crystals nor do their dielectric properties vary as drastically with temperature. Since it is desirable in device applications to operate the materials above their Curie point where the rf losses are relatively small, and since it is desirable at the same time to have this operating region be near room temperature, it is necessary to dope the $BaTiO_3$ crystal with other elements so as to lower its Curie point. Jackson and Reddish[21] have shown that by replacing the barium ions in the lattice by strontium ions, the Curie point of the (Ba - Sr) TiO_3 composition can be reduced considerably. Hence, the ceramic composition of 73 per cent $BaTiO_3$ - 27 per cent $SrTiO_3$ (which is of interest here) has a Curie point at room temperature ($T_c = 20^oC$) . This is 100^oC lower than the Curie point of pure barium titanate; the ceramic can therefore be operated conveniently as a nonlinear dielectric material near room temperature.

1. Small Signal Characteristics at Millimeter Wavelengths

The curve shown in Fig. 2 of the relative dielectric constant of the nonlinear ceramic referred to above as a function of frequency reveals at a glance the dispersive character of the dielectric constant at microwave frequencies. This curve extends over the greater portion of the microwave spectrum (from 3 to 300 kMc) and illustrates the magnitude and variation of the dielectric constant throughout this part of the spectrum. Furthermore, as discussed below, it indicates over what range of frequencies the dielectric nonlinearity can be used in microwave devices.

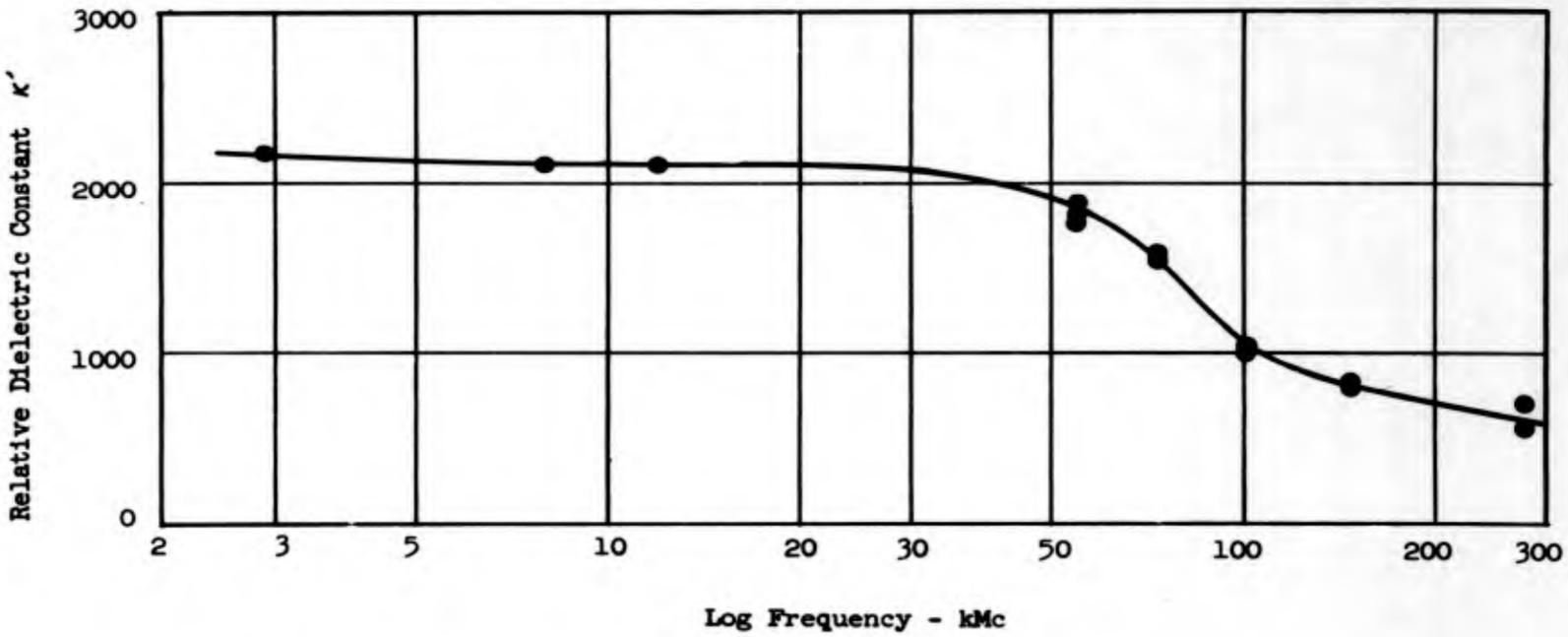

FIG. 2--Relative dielectric constant κ' as a function of frequency for ceramic of 73 per cent $BaTiO_3$ - 27 per cent $SrTiO_3$ at 51°C (After Johnson[1]).

As described in reference 1, such a curve was obtained in the frequency range from 60 kMc to 270 kMc and for various temperatures, by placing a slab of the above mentioned ceramic material in a modified temperature-controlled Fabry-Perot interferometer and noting the shape of the transmission curve through the interferometer. An X-band linear accelerator with a magnetic undulator served as a source of rf power for the experiment. The results of the measurements are shown in Fig. 2 for a temperature of 51°C. The measured data shows that there is little or no dispersion in the dielectric constant from 3 to 40 kMc (these data were obtained from the small signal measurements described below). Between 40 and 150 kMc the dielectric constant drops rapidly to the value of several hundred and remains fairly constant thereafter. The relaxation mechanism giving rise to the dielectric dispersion between 50 and 100 kMc is noted to cause a loss in the temperature sensitivity of the material beyond 100 kMc.[1] This is very strong evidence for believing that the polarization mechanism responsible for the ferroelectric behavior relaxes out between 50 kMc and 100 kMc and that the dc nonlinearity in the dielectric constant, which is thermodynamically related to the temperature dependence of the polarization, is therefore absent at millimeter wavelengths. One can therefore conclude that below 50 kMc the nonlinear properties of the ceramic can be utilized in device work, but that above 50 kMc the degree of nonlinearity should decrease markedly, causing the material to be of little use. It should be noted, however, that the dispersion in the dielectric constant above 50 kMc may find use in filter applications.

2. Small Signal Microwave Characteristics

In the paraelectric phase the microwave dielectric constant and loss tangent of ferroelectric ceramic materials can be controlled by the application of an external dc bias, thus producing a dc nonlinearity in the dielectric properties. The nonlinearities occurring in the paraelectric region are usually strongest for a temperature range of about several tens of degrees above T_c . This is a consequence of the fact that the dielectric nonlinearity is closely related to the large induced polarization which appears in the vicinity of the Curie point. One cause for the nonlinear behavior, which has already been mentioned, is the presence of field-induced phase transitions.[14] The effect that an external field has

on the phase transitions in the material is very similiar to "pulling" the Curie point to higher temperatures and hence to changing the polarization and dielectric constant of the material above T_c . The dielectric nonlinearities in the region above T_c are particularly important for microwave device applications since the rf dielectric losses are smallest in this region.

For small signal microwave applications the dielectric properties of ferroelectric ceramics are best described by giving the variation in the complex dielectric constant defined by

$$\epsilon = \epsilon' - j\,\epsilon'' = \epsilon_0\,(\kappa' - j\,\kappa'') = \epsilon_0\,\kappa'\,(1 - j\,\tan\delta) \qquad (2)$$

as a function of bias, with temperature as a parameter. The terms ϵ'' and/or $\tan\delta = \epsilon''/\epsilon'$ entering in Eq. (2) account for losses and are related to the rf dielectric conductivity σ through the Maxwell equation

$$\nabla \times \vec{H} = \vec{i} + \frac{\partial \vec{D}}{\partial t} \qquad (3)$$

and the constitutive equations

$$\vec{D} = \epsilon'\,\vec{E} \qquad (4)$$

and

$$\vec{i} = \sigma\,\vec{E} \quad . \qquad (5)$$

Assuming that $\vec{E}$ varies as $\exp\,(j\omega t)$, Eqs. (3), (4), and (5) combine to give

$$\nabla \times \vec{H} = \sigma\,\vec{E} + j\omega\epsilon'\,\vec{E} = j\omega\epsilon'\,(1 - j\,\tan\delta)\,\vec{E} \quad , \qquad (6)$$

where $\tan\delta = \sigma/\omega\epsilon' = \epsilon''/\epsilon'$. The rf current density $\vec{i}$ which accounts for the losses in the dielectric via the dielectric conductivity σ is not due to true current flow in the form of conduction currents but to the contributions from the polarization current $\partial\vec{P}/\partial t$. which are in

phase with the applied field $\vec{E}$. Here $\vec{P}$ refers to the induced polarization and is given by $\vec{P} = \vec{D} - \epsilon_0 \vec{E}$ in mks units. Thus, this is a phenomenological macroscopic description of the dielectric properties which can be used conveniently with Maxwell's equations and, moreover, can be extended in a natural way to account for the large signal behavior of the medium.

Figures 3 and 4 give curves of the relative dielectric constant κ' and the loss tangent $\tan \delta$ as a function of dc bias, with temperature as a parameter, for the ceramic composed of 73 per cent $BaTiO_3$ - 27 per cent $SrTiO_3$. These curves are the results of X-band measurements made by Johnson[1] using a transmission technique. They show that the real part of the dielectric constant is extremely high, ranging from 1000 to 3000, and that the quality factor Q of the material, where $Q = 1/\tan \delta$, is moderately high. These results are in general agreement with those obtained by other investigators.[2,4,5]

For design purposes, Figs. 3 and 4 show that a 50 per cent change in κ' is easily achieved with moderate bias fields and that the Q of the material ranges between 7 and 20. The curves given in these figures also show that the temperature sensitivity and dc nonlinearity decrease at higher temperatures, as expected. As a compromise between having a high degree of nonlinearity and small temperature sensitivity, it is generally desirable to operate the ceramic of 73 per cent $BaTiO_3$ - 27 per cent $SrTiO_3$ above $40^{\circ}C$ which is a comparatively low loss region having appreciable nonlinearity.

Finally, it should be mentioned here that the phenomenon of dielectric nonlinearity is most likely to occur in materials with high dielectric constant.[22] It is therefore not surprising from the data given in Fig. 3 that ferroelectrics are strongly nonlinear. In a recent article Diamond[23] has shown that the field-induced variations in the permittivity for perovskite-like polycrystalline substances, such as ferroelectric titanates, may be explained by assuming that the material consists of an ensemble of crystallites whose Curie points obey some statistical distribution. By taking a Gaussian distribution, Diamond has been able to show excellent correlation of experimental curves such as those given in Figs. 3 and 4 with the theory.

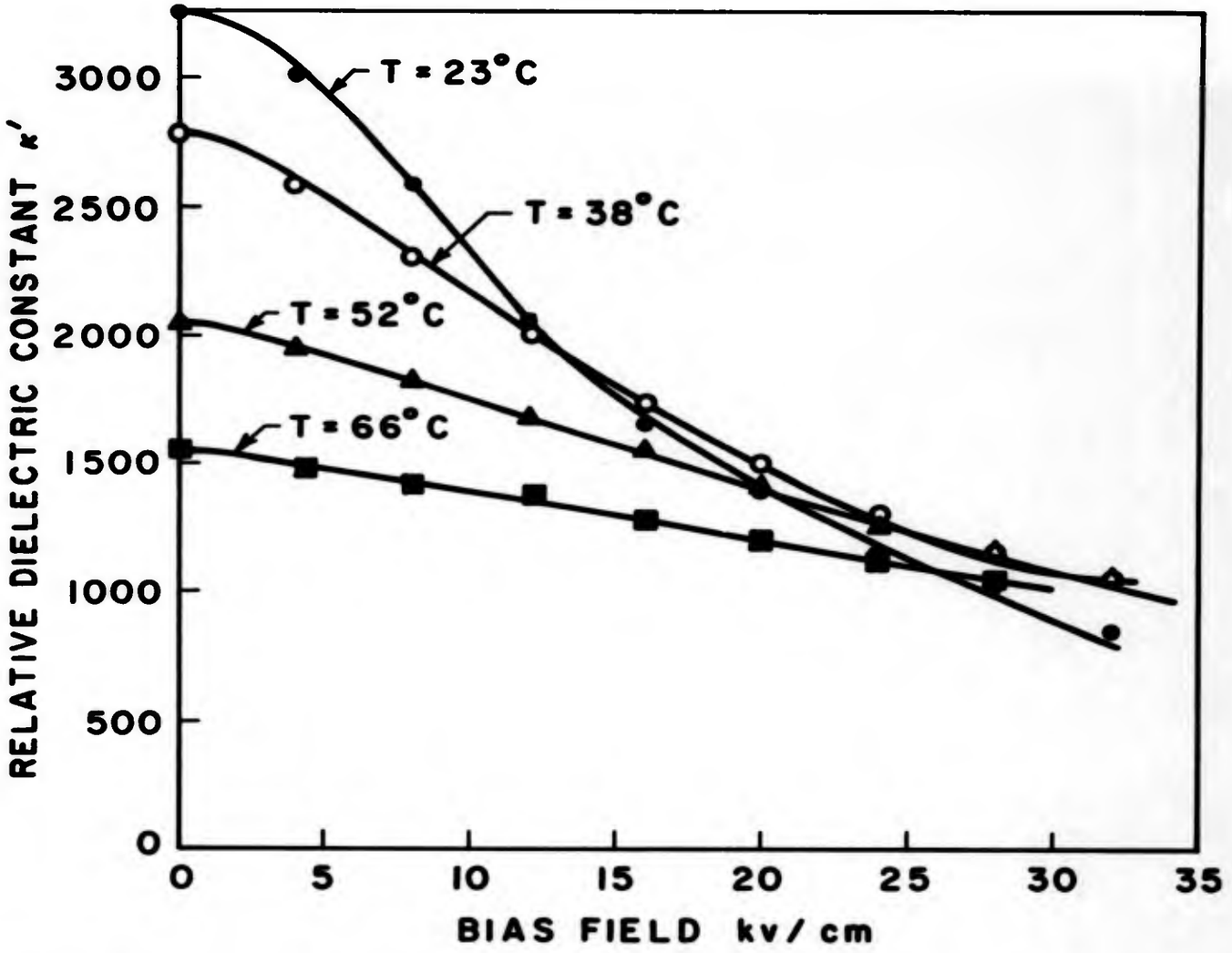

FIG. 3--Relative dielectric constant κ' as a function of dc bias for various temperatures for ceramic of 73 per cent $BaTiO_3$ - 27 per cent $SrTiO_3$.

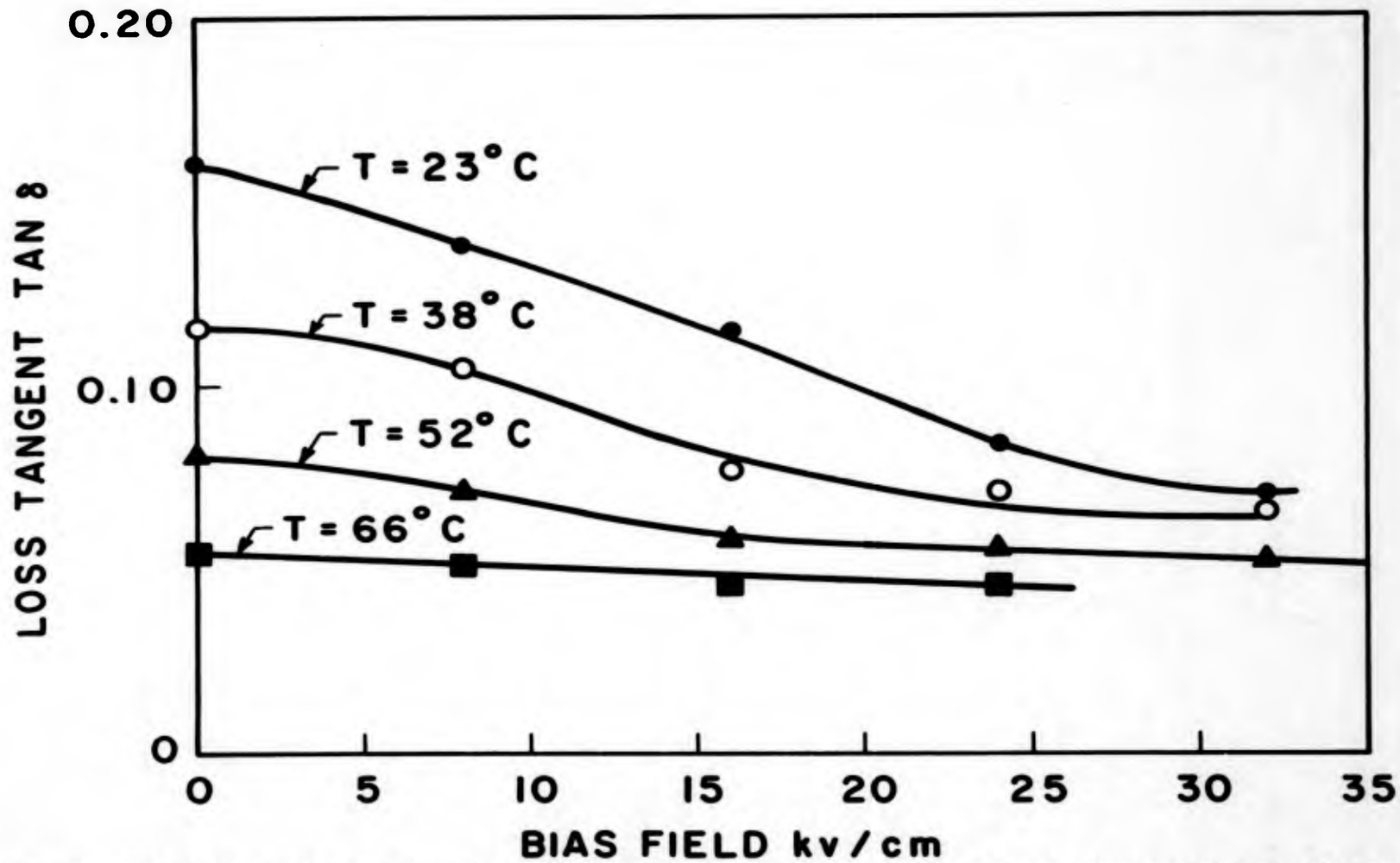

FIG. 4--Loss tangent tan δ as a function of dc bias for various temperatures for ceramic of 73 per cent $BaTiO_3$ - 27 per cent $SrTiO_3$.

3. Large Signal Microwave Characteristics

From the dc nonlinear characteristics shown in Figs. 3 and 4 one would expect that ferroelectrics should exhibit large signal rf nonlinearities. The large signal characteristics of these materials are representative of a true nonlinear dielectric behavior in which both the dielectric constant ϵ' and the dielectric conductivity σ are functions of the instantaneous field intensity within the material. Since the ferroelectric medium exhibits nonlinearity of both the permittivity and conductivity, it represents a generalized nonlinear dielectric. At this point one can distinguish between the small signal and the large signal microwave characteristics of ferroelectric ceramics in the following manner: In the small signal case the dielectric constant can be controlled by an external bias, but for each value of bias the material is linear and the principle of superposition applies. In the large signal case (with or without bias) the material properties change at an rf rate and are functions of the strength of the excitation. Superposition does not apply in this case.

By extending the small signal description of the dielectric properties given in Eqs. (4) and (5), one can arrive at a self-consistent large signal macroscopic description of the dielectric properties of the nonlinear ceramic material. Before giving this description, however, it is worth while to digress and discuss how one can investigate the large signal properties of ferroelectrics from a more fundamental viewpoint and why the description to be given below is of value. Generally, the large signal properties of ferroelectrics can be described by anyone of a number of approaches. Three possible approaches are discussed here.

The first approach, which is the most physical, is to seek simultaneous solutions to Maxwell's equations together with the equations of motion for the polarization of the dielectric medium. This approach has the drawback of requiring one to obtain a nonlinear differential equation for the polarization including the effects of loss in the dielectric. Since very little is known of the physical mechanisms causing nonlinear dielectric polarization,[24] it is usually very difficult to obtain appropriate equations of motion. In addition, very little is known about the origin of microwave losses in ferroelectrics although recently, in the work of Rupprecht and Bell[25] and Silverman,[26] this problem has been investigated from both the experimental and theoretical points of view.

The second approach to the description of the large signal properties invloves integrating the equations of motion to determine the polarization as a nonlinear function of the field and then substituting the resulting expression into the field equations so as to obtain a set of coupled nonlinear differential equations. The difficulty encountered here is in obtaining a solution for the polarization in terms of the field; this is in addition to the problem of determining a suitable set of equations of motion for the polarization in the first place.

The third approach is the one taken here, wherein, for the sake of brevity and in order to eliminate the difficulty of writing equations of motion, it is assumed that the nonlinearities can be incorporated into the Maxwell equation for the curl of $\vec{H}$ by defining phenomenologically a displacement vector $\vec{D}$ which is a nonlinear function of the microwave exciting field $\vec{E}$ and a current density $\vec{I}$ which is likewise a nonlinear function of $\vec{E}$. Thus, in the temperature region above the Curie point, without application of bias, the large signal properties of ferroelectric ceramics may be described by generalizing the constitutive equations [Eqs. (4) and (5)] to

$$\vec{D} = \epsilon' (E) \vec{E} \quad , \tag{7}$$

and

$$\vec{I} = \sigma (E) \vec{E} \quad . \tag{8}$$

Here, $\epsilon' (E)$ and $\sigma (E)$ are the large signal scalar dielectric constant and rf conductivity of the dielectric, respectively; $\sigma (E)$ is a macroscopic loss term which phenomenologically accounts for all of the loss mechanisms occurring in the dielectric. Both of these quantities depend upon the magnitude and not the direction of the electric field since the ceramics, unlike the single crystals, are isotropic. Moreover, since it has been assumed that the dielectric is unbiased and since it is operated above its Curie point where the structure of the material is centrosymmetric on a microscopic scale, $\epsilon' (E)$ and $\sigma (E)$ will consequently be even functions of the instantaneous field intensity E within the ceramic and can be

expanded as a power series in E as follows:

$$\epsilon' (E) = \epsilon_0 \sum_{n=0}^{\infty} \kappa'_{2n+1} E^{2n} \tag{9}$$

and

$$\sigma (E) = \epsilon_0 \sum_{n=0}^{\infty} \kappa''_{2n+1} \bar{\Omega} E^{2n} \quad . \tag{10}$$

The expressions for $\epsilon' (E)$ and $\sigma (E)$ apply in the time domain and it is assumed that over most of the frequency range of interest the effects of dispersion in the coefficients κ'_{2n+1} and κ''_{2n+1} can be neglected. It should be noted that by defining the large signal dielectric properties in this way the physical mechanisms involved in the problem have been somewhat obscured. However, in this formulation one has a set of equations which reduce properly to the small signal description of the dielectric properties and which, from the measurements made herein and in reference 1, permit one to describe the interaction of $\vec{E}$ and $\vec{H}$ fields within the bulk material in a simple manner.

The appearance of the operator $\bar{\Omega}$ in the time domain expression for $\sigma (E)$ given in Eq. (10) can be explained in the following way. In the limit of weak sinusoidal signals one finds that the equivalent rf dielectric conductivity is given by $\sigma = \omega \epsilon_0 \kappa''_1$. It is obvious from this relation that over a limited range of frequencies (which for the ceramic of 73 per cent $BaTiO_3$ - 27 per cent $SrTiO_3$ extends from 3 to 30 kMc) the macroscopic loss term σ is approximately directly proportional to ω in the frequency domain description. Therefore, in order to treat the dispersion appearing in the large signal rf conductivity, which is assumed to have the same frequency dependence in the large signal case as in the small signal case, the operator $\bar{\Omega}$ has been introduced into the time domain expression in Eq. (10) and is defined by the relation

$$\bar{\Omega} \begin{Bmatrix} \sin (\omega_m t + \phi_m) \\ \cos (\omega_m t + \phi_m) \end{Bmatrix} = \omega_m \cdot \begin{Bmatrix} \sin (\omega_m t + \phi_m) \\ \cos (\omega_m t + \phi_m) \end{Bmatrix} \quad . \tag{11}$$

When the large signal rf conductivity operator $\sigma(E)$ is multiplied by $\vec{E}$, one obtains the rf conduction current density $\vec{i}$ in the dielectric which, recall, phenomenologically accounts for all of the loss mechanisms occurring in the material. To evaluate the current density explicitly, the operator $\bar{\Omega}$ must be applied to each spectral component contained in each of the terms $E^{2n}\vec{E}$ entering in the equation for $\vec{i}$. When this is done it is found that because the nonlinearity is an even function of field strength, $\vec{i}$ is made up of a discrete spectrum of the odd harmonics of the fundamental frequency.

By using the description of the large signal characteristics of the ferroelectric ceramic given by Eqs. (9) and (10), it has been shown by measurements made by Johnson[1] and by an independent set of measurements described in Chapter IV of this report that for a ceramic of composition 73 per cent $BaTiO_3$ - 27 per cent $SrTiO_3$,

$$\epsilon'(E) = \epsilon_0 \left[2200 - 7.5 \times 10^{-11} E^2\right] \text{ farad/m} \qquad (12)$$

and

$$\sigma(E) = \epsilon_0 \left[160\,\bar{\Omega} + 29 \times 10^{-12}\,\bar{\Omega}\,E^2\right] \text{ mhos/m}, \qquad (13)$$

where E is in volts per meter. These results apply in the neighborhood of 3 kMc, for field strengths up to $E = 20$ kv/cm, and at temperatures in the range 49-52°C. A discussion of the similarities and differences in the measurement techniques used, as well as a comparison of the results of both experiments has been reported in a recent article.[27] It should be emphasized at this point that the expressions given by Eqs. (12) and (13) are the results of the first experimental measurements of the large signal microwave characteristics of the ferroelectric titanates.

4. Microwave Losses and Skin Effect Phenomena

From the dielectric properties of the ferroelectric ceramic given in Figs. 3 and 4 it can be seen that ferroelectrics have extremely high permittivities and loss tangents. As a consequence, these materials have microwave circuit properties which are intermediate between good dielectrics and poor metals. Typically, low loss dielectrics have rf conductivities

of the order of 10^{-5} mhos/m at centimeter wavelengths and negligible skin effect properties, whereas metals such as copper or silver have rf conductivities in the range of 10^{7} mhos/m and very pronounced skin effect properties. Ferroelectric ceramics, on the other hand, can be expected to have rf conductivities as high as 100 mhos/m and skin depths as great as 0.25 cm in the same frequency range. These characteristics are obviously due to the fact that the equivalent rf dielectric conduction current in the material is not negligible in comparison to the displacement current, which is usually the case for low loss dielectrics. The significance of the finite skin depth in the ferroelectric is two-fold. The first is that it has a direct bearing on the insertion loss through the ceramic; and the second is that in waveguides that are partially filled with the ceramic material the fields will be concentrated on the surface of the dielectric and will rapidly attenuate as one moves into the material. This accordingly has the effect of limiting the volume of material which interacts with the fields.

An equation for the skin depth Δ of ferroelectric ceramics is derived in Appendix A where it is shown that

$$\Delta = \frac{\lambda}{\pi\sqrt{\kappa''\tan\delta}} \quad . \tag{14}$$

Here λ is the free space wavelength of the applied radiation. From Eq. (14) one finds that $\Delta \to \infty$ as $\sqrt{\kappa'}\tan\delta \to 0$, which is the case for low loss dielectrics, and that $\Delta \to 0$ as $\sqrt{\kappa'}\tan\delta \to \infty$, which applies for metals. According to the usual definition, the relation between the power lost in the dielectric P_{lost} and the skin depth Δ may be expressed in terms of the following volume integral:

$$P_{lost} = \frac{\sqrt{\kappa'}}{Z_0\Delta}\int_V |\vec{E}|^2 \, dv \quad , \tag{15}$$

where $Z_0 = 377$ ohms is the impedance of free space. From Eqs. (14) and (15) it is possible to estimate how ferroelectrics affect the losses in waveguide structures. This can be accomplished by, first, estimating the ratio of power lost in the ferroelectric to the power transmitted in the guide, and second, obtaining an approximate expression for the ratio of

the attenuation constant due to losses in the ferroelectric to the attenuation constant due to imperfect walls. By following this procedure it is possible to determine how much power is absorbed in the ferroelectric and what the contribution of wall losses is in comparison with the losses in the dielectric material. In the first of these calculations one finds that since the power transmitted is equal to the product of the group velocity and energy per unit length in the guide, one can represent the ratio of power lost given by Eq. (15) to the power transmitted by the expression $P_{lost}/P_{trans} = K\,(L_f/\Delta)$. The constant K entering in this expression is a geometrical factor which depends upon the frequency of operation and the relative dielectric constant of the ferroelectric; L_f refers to the axial length of the ferroelectric sample. It has been assumed in this analysis that most of the energy is stored in the dielectric due to the fact that κ' is large in the ferroelectric medium. Use has been made of this fact by assuming that the volume integral of $|\vec{E}|^2$ cancels in the numerator and denominator of the ratio P_{lost}/P_{trans}. From the expression $P_{lost}/P_{trans} = K\,(L_f/\Delta)$ and the data given in Figs. 3 and 4, it can be seen that the length of the dielectric is a critical factor in determining the losses in microwave circuits employing ferroelectric materials. This is in contrast, of course, to the case where low loss dielectrics are used and Δ is very large, thus allowing large pieces of dielectric to be employed with negligible absorption of power. In order to compare the losses in ferroelectrics with the wall losses in the guide, a second calculation must be made. This involves finding the ratio of the attenuation constant due to the ferroelectric medium to that due to imperfect walls. Since the attenuation constant α is approximately given by the quotient of the power lost per unit length to twice the power transmitted, one finds that one can write $\alpha_f/\alpha_w = K\,(R_s\,\Delta)^{-1}$. Here α_f is the attenuation constant due to the ferroelectric, α_w is the attenuation constant due to imperfect walls, K is a geometrical factor which depends upon frequency and κ' for the ferroelectric, and R_s is the surface resistivity of the waveguide walls. The same approximations used to obtain the expression for P_{lost}/P_{trans} given above have been used here. By making use of the standard equation for R_s, one finds that at centimeter wavelengths R_s typically has a value which is numerically equal to about one-tenth of Δ. As a general statement, it can therefore be concluded that due to the size of Δ it

is usually possible to omit wall losses completely in comparison to the rf dielectric losses of the ferroelectric. When low loss dielectrics are used (Δ large) , one has the opposite situation, i.e., α_d/α_w is small and wall losses represent the predominant loss mechanism in the guide.

D. COMPARISON WITH OTHER NONLINEAR MATERIALS

Before discussing the small signal and large signal applications of ferroelectric-titanate ceramics, it is of interest to compare these materials with ferrites and variable capacitance diodes from the device standpoint. In relation to both ferrites and diodes the outstanding feature of the ferroelectric titanates is their extremely high permittivity. The fact that κ' typically exceeds 1000 creates unique matching problems when ferroelectrics are incorporated in microwave circuits since the impedance of the ferroelectric sections will normally be of the order of one thirtieth of that corresponding to the air-filled sections. Furthermore, the cutoff frequency in the dielectric loaded sections will likewise be diminished, thus allowing for the possibility of a large number of higher order modes to propagate. Neither ferrites nor diodes present problems of equal complexity in this respect.

The loss characteristics of the materials are also of importance since they not only determine the CW power handling capacity of the materials, but they also determine the insertion loss of the circuits or devices containing the materials. Insofar as losses are concerned, the material having the lowest loss characteristic is the ferrite. In fact, the microwave losses of the poorest ferrite materials are about comparable to the losses in the best ferroelectric materials. The microwave losses (between 3 and 10 kMc) of ferroelectrics and diodes are quite similar, both having material Q's in the neighborhood of 10 to 20. Diodes, however, have the disadvantage that their absorption increases with rf power in the small signal case, whereas in ferroelectrics the absorption is independent of power level when the operating temperature is held constant. Based upon these considerations, one therefore expects that circuits employing ferrites would generally have smaller insertion losses than those utilizing either ferroelectrics or diodes. In addition, since the microwave

losses in ferrites are so much smaller than the losses in ferroelectrics and since the heat capacity of both materials is about 0.2 cal/g.°C, one finds that the increase in temperature, due to the absorption of microwave power, is much smaller in ferrite samples than in ferroelectric samples of comparable volume. Typically it is found that ferrite devices will operate on a CW basis up to about 10-20 watts, that ferroelectrics can carry in the neighborhood of 1-2 watts, and that diodes are limited to approximately 1-10 milliwatts. This assumes, of course, that the ferrite and ferroelectric sample volumes are not very small. A lower limit on the size of the sample volumes is estimated to be of the order of 3-5 cubic millimeters for both cases. It should be noted here that the restriction on the ferrite volume size is not only of significance for determining the rate of increase of temperature in the material, but that, more importantly, it determines the signal field strength at which certain spin waves become unstable and cause anomalous increases in the rf power absorption. The CW power rating of diodes is low compared to both ferrites and ferroelectrics because breakdown across the diode junction is a more important factor than the effects caused by heating.

Upon comparing the nonlinear characteristics of the three elements, it is found that the magnitude of their dc and rf nonlinearities is very similar. With regard to the small signal characteristics, ferroelectrics and diodes have the advantage over ferrites since their dc nonlinearity is controlled by electric fields rather than magnetic fields. This means that the response of their rf properties to changes in the dc field will be fast compared to the response time of ferrites. Moreover, since the dc resistivity of ferroelectric and diode materials is high, the amount of dc control power needed is far less than what is required by ferrites. From the point of view of the large signal characteristics the diode nonlinearity can be excited at comparatively low power levels; both ferroelectrics and ferrites of reasonable size required at least several hundred watts of peak power to cause appreciable nonlinearity. Probably the major difference between the large signal properties of the three materials is that the ferroelectric nonlinearity can easily be excited in the absence of bias, which is not the usual case for ferrites and diodes. Also, ferroelectrics exhibit large signal characteristics of comparable magnitude simultaneously in both the dielectric constant and the rf dielectric conductivity.

Finally, one should mention some of the difficulties encountered in applying ferroelectrics due to the lack of understanding of the physical mechanisms responsible for the behavior of the materials. In the case of other nonlinear materials such as ferrites and semiconductor diodes the material properties can be described with reasonable accuracy from simple physical models. It is therefore possible in many instances to predict and evaluate the behavior of devices utilizing these materials in a purely analytic manner.

For example, in the case of ferromagnetic materials not only can the magnetic properties be understood from a simple dipole model of the solid, but the bulk magnetic properties can also be classically described by considering the gyroscopic nature of the electron spins in the material. Thus one can write a magnetodynamic equation for the magnetization $\vec{M}$ in terms of the applied field $\vec{H}$ [28] as

$$\frac{d\vec{M}}{dt} = \gamma \mu_0 (\vec{M} \times \vec{H}) \quad , \tag{16}$$

where γ is the gyromagnetic ratio given by $\gamma = -1.759 \times 10^{11}$ coulombs per kilogram. By making use of this equation and the Maxwell equations the problem of wave propagation in ferrite media can be analyzed and the general behavior of a number of nonreciprocal devices can be determined.

Even in the case of semiconductor diodes of simple geometry it is possible to predict from fundamental principles the current-voltage and the charge-voltage characteristics of the diode. For a planar P-N junction linearly graded with impurities Shockley[29] has shown that the capacitance of the junction is given by

$$C(V) = \frac{C(0)}{(1 - V/\phi)^{1/3}} \quad , \tag{17}$$

where V is the voltage across the junction and ϕ is the contact potential of the junction. From Eq. (17) it is possible to describe analytically the behavior of a number of diode devices such as parametric amplifiers and harmonic generators.

In the case of ferroelectrics there is no universal model or equation to describe the material properties; however, it is possible to obtain

analytic expressions for the electrical properties from experimental data. The expressions so obtained are empirical and only apply to the macroscopic properties of the material. The accuracy and limitations of the expressions depend, of course, on the accuracy and limitations of the experiments performed in deriving them. Thus, at best, one must resort to a semi-empirical technique for analyzing the behavior of devices that use ferroelectrics as their "active" element. This should not be misconstrued so as to lead one to believe that a semi-empirical method of analysis is disadvantageous. It is evident that any physical theory has certain limitations and the theories resulting in Eqs. (16) and (17) are no exception. In fact, the limitations on the theories are generally greater than those imposed by using empirical data. The advantage of being able to write governing equations such as Eqs. (16) and (17) is that it enables one to make predictions on the behavior of devices without first taking data. It can therefore be seen that the disadvantage of not having an equation or a set of equations to describe the material properties of ferroelectrics is that one must necessarily first measure the electrical properties of the material. Once this has been accomplished the semi-empirical method of analysis is not only accurate, as will be shown in what follows, but also clearly defines the limitations of the solutions obtained.

CHAPTER III

THE SMALL SIGNAL MICROWAVE APPLICATIONS OF FERROELECTRIC CERAMICS

Based upon the discussion given in Chapter II, it is known that in the microwave portion of the spectrum ferroelectric ceramics behave as isotropic nonlinear dielectrics displaying both small signal and large signal nonlinear properties. In the present chapter, the small signal microwave applications of these materials are of concern. Among the possible small signal applications of ferroelectric ceramics are phase shifting, cavity tuning,[30] tunable filtering, attenuating, and switching. The salient feature of the devices constructed for each of these applications is that they are biased with electrostatic fields which can be established with inexpensive, lightweight equipment requiring negligible dc drive power. Generally, the response time of such devices can be expected to be fast, typically better than a microsecond.

The purpose of the work presented here is three-fold. The first objective is to predict theoretically what can be expected of currently available ferroelectric ceramics in a number of representative devices. The second objective is to use these materials in the design and construction of an electrically tunable microwave phase shifter. And the third objective is to compare theoretical predictions with experimental results.

An electrically tunable phase shifter was chosen for investigation since considerable interest has recently been expressed regarding the possibility of using ferroelectric materials in this type of application. One reason for this interest is that devices of this nature may be utilized in the construction of electrically scanned antenna arrays. The materials which are presently available for this kind of application are ferrites[31] and junction diodes,[32] both of which have certain basic disadvantages. The diode, for example, has the undesirable property that its losses

increase with frequency as well as with rf input power, while ferrites have the objectionable feature that they require fairly large amounts of dc drive power to control the phase shift.

A. SMALL SIGNAL BEHAVIOR OF FERROELECTRICS IN WAVEGUIDES AND CAVITIES - GENERAL THEORY

Waveguides and cavities either partially filled or completely filled with dielectric material find use in a number of applications. Such waveguide components as phase shifters, impedance transformers, mode converters, and mode exciters for dielectric rod antennas all depend upon the characteristics of dielectric loaded guides for their operation. The uses of dielectric loaded cavities are more restricted, the most important use being in applications where it is desirable to tune the cavity such as in certain filter applications.

In the general treatment of problems relating to inhomogenously-filled dielectric waveguides, where a cylindrical rod of dielectric of arbitrary cross-section is placed coaxially in an arbitrary cylintrical guide, one usually cannot obtain exact solutions in closed form even for simple configurations. Nevertheless, it is possible to qualitatively describe the important propagation characteristics of these structures without actually solving a specific problem. The most prominent effect of placing a dielectric in a waveguide is to increase the cutoff wavelength of the guide, and to reduce the gain wavelength and impedance. Due to the inherently high permittivity of ferroelectric materials, the changes that they cause in these quantities are appreciable. The presence of a dielectric in a waveguide will also greatly influence the field configuration in the guide by tending to pull the fields into the region of the dielectric. With ferroelectrics this effect is magnified by the size of the permittivity, and in most instances the field configuration is difficult to determine since the permittivity of the material must be treated as being complex. The introduction of a complex dielectric constant into the calculation of the field distribution in the guide accounts for the skin effect phenomenon discussed in Chapter II.

Since it is possible for an unshielded dielectric to support a propagating wave, one further finds that the field (or energy) distribution in inhomogeneous waveguides has the following behavior with respect to frequency: In the region immediately above cutoff, the transverse field distribution can be described by harmonic functions, and one finds that a considerable fraction of the energy per unit length in the guide can be stored outside the dielectric. As the frequency is increased, a crossover point is reached at which total internal reflection takes place at the dielectric air interface. At this point, the energy residing outside the dielectric begins to get trapped more into the dielectric, thereby causing the dielectric to influence the propagation characteristics of the guide more strongly. Beyond the crossover frequency the fields outside the dielectric become exponentially decaying functions. The energy stored per unit length in the guide is therefore concentrated primarily within the dielectric, causing the structure to have the characteristics of a shielded dielectric guide. As far as the modes of propagation are concerned, one finds that in partially filled guides the normal modes are no longer the usual TE or TM modes as in waveguides completely filled with dielectric. Rather, one obtains hybrid modes which are combinations of the TE and TM modes. For dielectric slab-loaded rectangular guides, the normal modes corresponding to the TE and TM modes are the longitudinal section electric (LSE) and longitudinal section magnetic (LSM)[33] modes where in this designation the electric and magnetic fields, respectively, are parallel to the longitudinal dielectric interface. Thus for the LSE modes, for example, the basic modes of propagation are such that the electric field has no component normal to the dielectric interface – the electric field lies safely in the longitudinal interface plane.

It is easily seen from these considerations that the treatment of problems dealing with phase shifters, attenuators, or tunable cavities will generally be very complicated, owing to the complexities involved in characterizing the propteries of dielectric loaded waveguides and cavities. Thus, it is desirable to formulate a general theory for these applications which will allow one to assess the behavior of such devices without regard to any specific waveguide or cavity configuration. It should be noted that although there are a variety of applications for ferroelectric

materials other than these, the phase shifter, attenuator, and tunable cavity or filter under consideration here represent important device applications.

1. Electrically Tunable Phase Shift

Electrically controlled phase shift is usually achieved by varying the dielectric properties of a nonlinear medium in a controllable manner, and can be accomplished by either changing the propagation constant in a propagating circuit or the phase of the reflection coefficient in a reflecting circuit. The former method is employed in the construction of a reciprocal phase shifter and is described in the next section. The problem of finding the change in the propagation constant, in inhomogeneously filled waveguides or in junctions of arbitrary geometry, is usually difficult or impossible to solve exactly. In such cases, where a solution in closed form cannot be obtained easily, perturbation or variational techniques may be used. It is shown in Appendix B that the incremental behavior of an arbitrary phase shifter can be described by

$$\Delta\phi = 0.115 \frac{\Delta \kappa'}{\kappa' \tan \delta} L \text{ rad.} , \qquad (18)$$

where $\Delta\phi$ is the incremental phase shift, $\Delta \kappa'/\kappa'$ is the fractional change in the real part of the dielectric constant of the ferroelectric and L is the insertion loss of the device in db. The original derivation of this equation is due to R. H. Pantell. In the derivation of Eq. (18) it is assumed that the device is well matched, that wall losses are negligible, and that the insertion loss is small (i.e., less than 3 db). The first and third of these restrictions are obviously necessary if the device is to have any practical value; the second is easily justified from the discussion relating to Eqs. (14) and (15). The significance of the phase shift formula is that it is independent of the configuration of the transmission system and of the shape and location of the ferroelectric. As it stands, Eq. (18) only applies to incremental changes in κ' . However, since phase shift is a scalar function, Eq. (18) can be extended to give an equation for the total change in phase shift when the dielectric constant of the ferroelectric is varied between finite limits. This is accomplished by merely dividing the total variation in the dielectric constant into a

number of small increments. Then by evaluating $\Delta\phi$ from Eq. (18) for each incremental change and adding the results, one obtains the desired expression for the total change in phase shift. When this is done it is necessary to include the fact that $\tan\delta$ and L are both functions of κ' .

The primary value of Eq. (18) is that for a given insertion loss one can estimate the incremental phase shift (or variation in total phase shift) in terms of the properties of the ferroelectric material. As an example, suppose that the insertion loss of a phase shifter was limited to $L = 2db$, and that the loss tangent of the material employed was $\tan\delta = 0.05$. For a fractional change in the real part of the dielectric constant of $\Delta\kappa'/\kappa' = 0.05$ the incremental phase shift, computed from Eq. (18), is found to be $\Delta\phi \approx 13^{o}$. This calculation is independent of the configuration of the phase shifter and applies to any geometry having the given variables.

It should be emphasized at this point that an important restriction on the use of Eq. (18) is that the attenuation through the phase shifter or the insertion loss of the device be small. If this condition is not fulfilled the device will behave as an attenuator. It is shown in the following treatment of the problem of electrically tunable attenuation that one can derive an expression similar to Eq. (18) to describe the incremental attenuation characteristics of an arbitrary attenuator. In the derivation of this formula no restrictions are imposed upon the magnitude of the losses of the device.

2. Electrically Tunable Attenuation

Just as it is possible to produce electrically controlled phase shift by varying the phase constant in a waveguide transmission system, so it is possible to produce electrically controlled loss by varying the attenuation constant of the system. From the curves given in Figs. 3 and 4 one finds that in ferroelectric ceramics these effects are not independent. The same problems encountered in computing the phase shift in arbitrary waveguide junctions containing ferroelectrics are also encountered in computing the attenuation or insertion loss. By making use of a perturbation technique similar to the one used in the phase shift calculation, it is shown in Appendix C that the incremental behavior of an arbitrary attenuator is

given by

$$\Delta\eta = \frac{1}{2}\frac{\Delta\epsilon''}{\epsilon''}\frac{P_{lost}}{P_{out}} + \frac{1}{4}\frac{\omega\epsilon''}{P_{out}}\int_{V_f}(\vec{E}\cdot\Delta\vec{E}^{*} + \vec{E}^{*}\cdot\Delta\vec{E})\,dv \quad , \quad (19)$$

where $\Delta\eta$ is the incremental change in attenuation in nepers, $\Delta\epsilon''/\epsilon''$ is the fractional change in the imaginary part of the dielectric constant ($\epsilon'' = \epsilon_0\kappa''$) of the ferroelectric, P_{lost} is the power lost in the ferroelectric, P_{out} is the power transmitted through the device, and $\Delta\vec{E}$ is the change in the fields over the volume of the ferroelectric V_f produced by a change in the complex dielectric constant. In the derivation of Eq. (19) it is assumed that the device is well matched, and that wall losses are negligible. Observe that, if it is desired, the ratio of P_{lost}/P_{out} can be expressed in terms of the insertion loss L by $10^{L/10} - 1$.

Whereas the formula for phase shift given by Eq. (18) is a general expression independent of the boundary value problem under consideration, the formula for attenuation depends explicitly upon the waveguide configuration. It is consequently less general than the equation for the incremental phase shift. To demonstrate that $\Delta\eta$ should depend upon the waveguide geometry and that accordingly no general statement can be made about the integral appearing in Eq. (19), it is only necessary to find two boundary value problems for which $\Delta\eta$ differs. A uniform rectangular guide completely filled with ferroelectric as shown in Fig. 5(a) and the dielectric loaded waveguide given in Fig. 5(b) serve as examples. For the configuration illustrated in Fig. 5(a) it is shown below, in describing the properties of the X-band ferroelectric phase shifter, that the attenuation constant α for the TE_{10} mode is given by

$$\alpha = \frac{1}{2}\,\frac{\omega}{c}\sqrt{\kappa'}\,\tan\delta \qquad (20)$$

where c refers to the velocity of light in free space. The attenuation constant for the TE_{10} - like mode of the dielectric loaded guide shown in Fig. 5(b) is more difficult to derive. The simplest case to consider is where $d/a \ll 1$. In this case it can be shown either by direct calculation

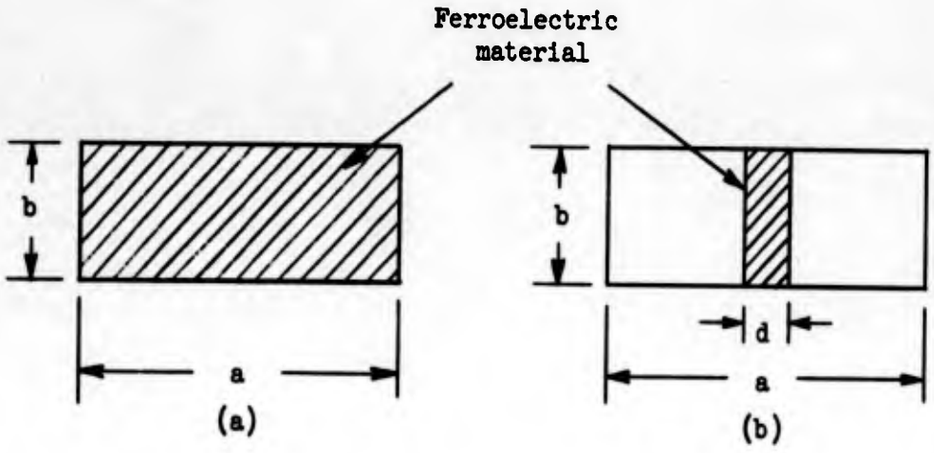

FIG. 5--Dielectric loaded waveguides.

or from the analysis of Vartanian, Ayres, and Helgesson[34] that the resultant expression for the attenuation constant is

$$\alpha = \frac{\omega}{c} \frac{d}{a} \kappa' \tan \delta \quad . \tag{21}$$

The change in attenuation in a guide of length ℓ defined by $\Delta\eta = \Delta\alpha\ell$ may be obtained for each of the configurations given in Fig. 5 from Eqs. (20) and (21). Without further ado it is clear that each equation yields a different relation for $\Delta\eta$. One can therefore conclude that it is impossible to evaluate the integral entering in Eq. (19) independently of the waveguide or junction-geometry. Equation (19) is consequently a general formula which must be applied separately to each boundary value problem under consideration in order to obtain an expression for $\Delta\eta$. Once this is done, however, one can predict the insertion loss characteristics of the attenuator for any nonlinear dielectric material.

As an example of the utility of Eq. (19), suppose that it is desired to make an attenuator with the dielectric filled waveguide depicted in Fig. 5(a). For the case where only the TE_{10} mode propagates one can use

Eq. (19), or more simply Eq. (20), to find $\Delta\eta$. Regardless of which of these equations is used the results are the same, thus demonstrating the validity of Eq. (19). By making use of the relation between insertion loss and attenuation (viz., $L = 8.686\,\eta$) the following expression for the incremental insertion loss is obtained:

$$\Delta L = \left(\frac{1}{2} \frac{\Delta\kappa'}{\kappa'} + \frac{\Delta \tan\delta}{\tan\delta} \right) L \quad . \tag{22}$$

As in the example given above for the phase shifter assume that $L = 2$ db and that $\Delta\kappa'/\kappa' = 0.05$. Then for a fractional change in the loss tangent of $\Delta \tan\delta/\tan\delta = 0.05$ it is found from Eq. (22) that $\Delta L \approx 0.15$ db . One should note that the values chosen for $\Delta\kappa'/\kappa'$ and $\Delta \tan\delta/\tan\delta$ are realistically related. This can be seen by estimating these fractional changes from the curves given in Figs. 3 and 4 for $E \leq 5$ kv/cm . By comparing the values for the change in insertion loss (0.15 db) with the change in phase shift (13°) computed from Eq. (18), it is apparent that for presently available ferroelectrics phase shifting applications are more practical than those concerned with attenuating. This statement is expected to have general validity, since the attenuator configuration considered here is for a waveguide completely filled with ferroelectric. The attenuation due to dielectric losses is obviously greatest in this case.

3. Electrically Tunable Filters

Resonant cavities are used extensively at microwave frequencies as filter elements. In order to have microwave filters with electrically controlled passband characteristics it is necessary to be able to vary the resonant frequencies of the cavities employed in the filters. One way of accomplishing this is to load the cavity with a dielectric material having a permittivity which can be controlled by an external dc bias. Due to the difficulties involved in calculating the resonant frequencies of cavities of complex geometry, it is of interest to be able to predict the change in resonance in a general manner. A formula for the fractional change in resonance $\Delta\omega/\omega$ of an arbitrary cavity is derived in Appendix D where it is shown that

$$\frac{\Delta\omega}{\omega} = -\frac{1}{2} \frac{1}{Q \tan\delta} \frac{\Delta\kappa'}{\kappa'} \quad . \tag{23}$$

In this expression Q is the unloaded Q of the cavity containing the ferroelectric. The original derivation of Eq. (23) is accredited to R. H. Pantell. The assumptions made in deriving Eq. (23) are that the wall losses in the cavity may be neglected compared to the dielectric losses, and that the Q of the dielectric is greater than 10. Equation (23) is a general relation independent of the configuration of the cavity and of the ferroelectric sample. It can therefore be applied to any resonant system. One should emphasize here that the perturbation expression given by Eq. (23) is not restricted to ferroelectric samples of small volume which is the usual restriction imposed upon perturbation expressions for the frequency shift. Equation (23) differs from this case in that it applies for sample volumes of any size, large or small, provided that $\tan \delta \leq 0.10$.

In order to determine the practicality of using ferroelectrics in electrically tuned cavity applications, consider a system having an unloaded Q of 1000 and assume that $\tan \delta = 0.05$ and $\Delta\kappa'/\kappa' = 0.05$. By substituting these values (which can easily be obtained with presently available ferroelectrics) into Eq. (23), one finds that $|\Delta\omega/\omega| \approx 0.5 \times 10^{-3}$. When $Q \tan \delta \gg 1$, the fractional change in resonance is small, since a considerable amount of the energy in the cavity is stored outside the dielectric (in this example $Q \tan \delta = 50$). For a high Q system, i.e., $Q \geq 1000$, this is an obvious necessity. By storing more energy in the dielectric the unloaded Q of the cavity decreases and $|\Delta\omega/\omega|$ increases accordingly. The maximum limit which can be reached is when all of the energy is stored in the dielectric and $Q = 1/\tan \delta$. In the example under consideration here this would occur when $Q = 20$, which is a rather low microwave Q. When this condition is reached, however, it is found from Eq. (23) that $|\Delta\omega/\omega| \approx 25 \times 10^{-3}$. This represents a sizable increase in the change in the resonant frequency of the cavity over the first case where $Q \tan \delta = 50$. Since it is evidently desirable to have $Q \tan \delta = 1$ for maximum tuning, one may conclude that in order to make cavity tuning a practical application it is necessary to have ferroelectric materials with very low loss tangent.

There is one further remark which is germane to this discussion and requires some comment. In applications where it is desirable to tune cavities or resonant circuits, not only is the magnitude of the fractional change in resonance of importance, but it is equally important to know the ratio of $\Delta\omega$ to the bandwidth B (measured in units of angular frequency) of the cavity. That is, the effects of tuning the cavity will be easy to discern if $\Delta\omega \geq B$; however, if the reverse is true $(\Delta\omega \leq B)$, then the change in resonance is of little value, since one cannot distinguish the shift in resonance easily. Stated differently, if $\Delta\omega$ is less than B one cannot filter two signals which differ by $\Delta\omega$ since both signals are in approximately the same passband. By making use of the definition of the cavity Q given by $Q = \omega/B$ one finds that for a given fractional change in resonance [expressed as $|\Delta\omega/\omega| = C$ where C is a constant determined from Eq. (23)] the ratio $\Delta\omega/B$ is simply $\Delta\omega/B = QC$. By using the values given in the example referred to above, one finds that for maximum tuning $(Q \tan \delta = 1$ and $Q = 20)$ $\Delta\omega/B = 0.5$. It is therefore clear that the use of ferroelectrics in electrically tunable filter applications is not very useful. If, on the other hand, the Q of the cavity were much greater or the loss tangent of the ferroelectric much smaller, one would find that it is possible to have $\Delta\omega/B \geq 1$ and that electrically tunable ferroelectric cavities (filters) would be practical.

In order to predict the total change in the resonant frequency of a cavity from Eq. (28) when κ' is varied over a finite range of values, $\Delta\omega$ must be summed up in a manner akin to summing the incremental phase shift $\Delta\phi$ as outlined in the discussion relating to Eq. (18). In this case not only does the resonant frequency of the cavity undergo a finite change but the cavity Q also changes and becoves a function of κ' . The calculation of the change in the cavity Q , ΔQ , can be made in a manner analogous to the calculation of the change in the attenuation given by Eq. (19). However, it is found that this calculation depends upon the configuration of the cavity in the same way that the calculation of $\Delta\eta$ was found to depend upon the configuration of the transmission system. The determination of the formula for ΔQ associated with the change $\Delta\omega$ will not be treated here, although it can be obtained by utilizing the techniques described in Appendix C.

B. AN X-BAND FERROELECTRIC PHASE SHIFTER[35]

The general analysis presented in the preceding section indicates that for currently available ferroelectric ceramics, i.e., ceramics having a material Q between 10 and 20, the electrically tuned phase shifter represents a practical small signal microwave device application of these materials. As a consequence, the design and construction of an X-band electrically controlled phase shifter is discussed in this section. The phase shifter described here consists of a ferroelectric slab completely filling the transverse plane of a rectangular waveguide, with suitable dielectric matching sections placed symmetrically about the slab, thereby forming a band-pass filter. This type of structure is a simple realization of a reciprocal electrically controlled ferroelectric phase shifter; it was chosen as a method of studying the feasibility for using ferroelectrics in this type of device. Among the advantages of this configuration are: simplicity of construction and effectiveness of matching; high power capabilities; ability to describe the device analytically, thus readily permitting a comparison between theory and experiment; and ease of providing bias to control the phase shift. Its disadvantages are common to all small-signal ferroelectric devices, and can be divided into two categories. The first category is concerned with the electrical characteristics of the device. Here one finds that since the loss tangent of the materials employed is in the vicinity of 0.10 to 0.05, the insertion loss, due to power absorbed in the ceramic material, is appreciable. Following the discussion given in section C of Chapter II one might expect at first that this can be minimized by choosing samples of small axial length. However, since the incremental phase shift through the ferroelectric sample is proportional to the insertion loss [see Eq. (18)] it is inconsistent to try to realize an electrically tuned ferroelectric phase shifter having very low loss. Similar statements apply, of course, to other small signal ferroelectric devices; i.e., as the sample volume becomes small the circuit losses also become small but at the same time, one loses the influence of the ferroelectric's nonlinear characteristics. The second category regarding the disadvantages of small signal ferroelectric devices is related to certain practical constructional difficulties. These are: (1) the necessity of providing a means of temperature stabilization and (2) the necessity of

providing a scheme for the prevention of dc breakdown across the ceramic interface at high-bias fields.

1. Phase Shifter Design

A longitudinal section of an X-band transmission-type phase shifter is shown in Fig. 6. The ferroelectric slab shown in the center of the device completely fills the cross section of the rectangular guide. The symmetrically placed low-loss dielectric matching sections also extend throughout the transverse plane and are designed to give the structure a band-pass filter chatacteristic with large bandwidth. Assuming that only the dominant mode propagates, the boundary value problem for such a configuration can be solved exactly, thereby permitting a complete description of its properties.

By controlling the permittivity of the slab with an external dc bias, both the complex propagation constant and the characteristic impedance of the ferroelectric section are varied. Phase shift results from the change in the imaginary part of the propagation constant. By referring to Fig. 6 it can be seen that each dielectric interface or junction presents a discontinuity to an impinging wave. At each of these interfaces the boundary conditions are satisfied by an incident, reflected, and transmitted wave all in the same mode. Therefore by making use of the fact that each waveguide normal mode can be represented by a transmission line of characteristic impedance equal to the wave impedance of the guide,[33] the overall equivalent circuit of the device becomes a series of transmission lines in cascade.

By employing this approach, the properties of the phase shifter can be obtained with a minimum of effort. Since the waveguide is made up of only dielectric discontinuities, it is possible to permit only the TE_{10} mode or the dominant mode of the external waveguide circuitry to propagate within the filter. In accordance with this condition, the propagation constant γ and the wave impedance or characteristic impedance defined by $j\omega\mu_0/\gamma$ can be determined for each waveguide section by[36]

$$\gamma^2 = \left(\frac{\pi}{a}\right)^2 - \frac{\omega^2}{c^2}\,\kappa'\,(1 - j\tan\delta)\ , \qquad (24)$$

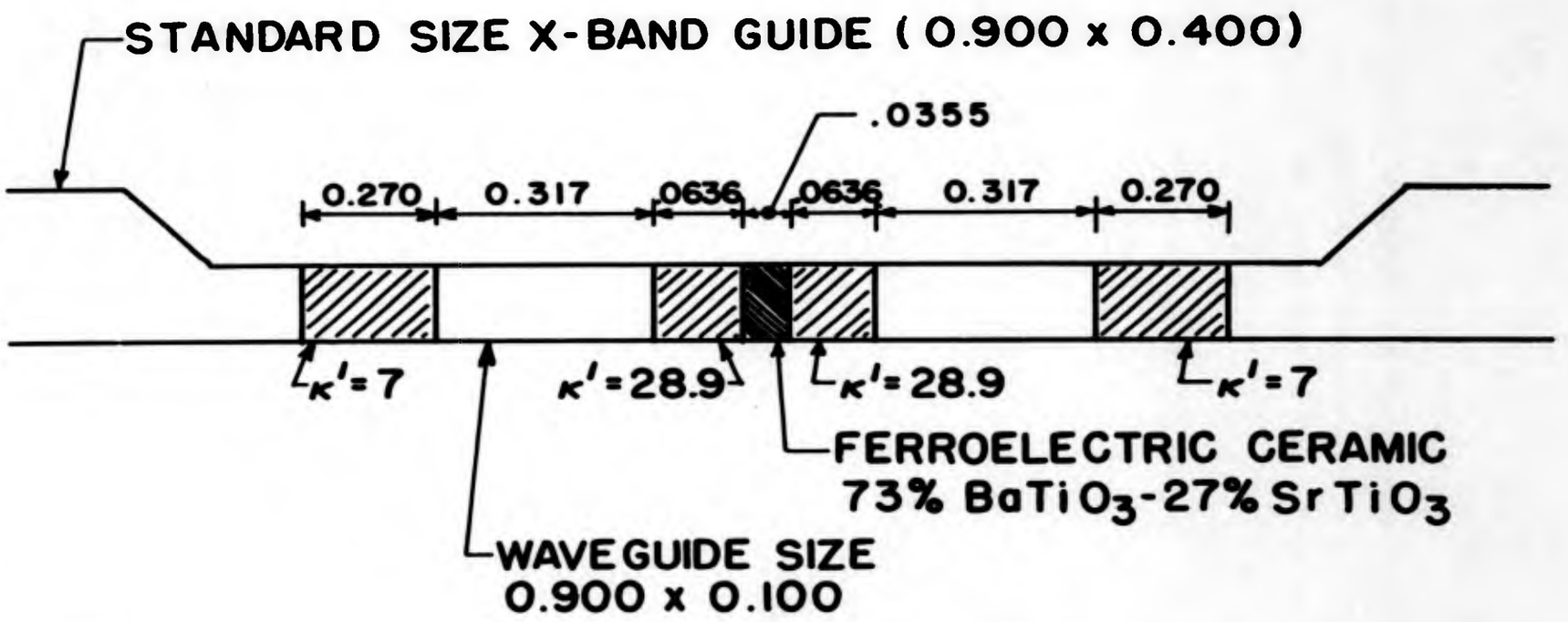

FIG. 6--Longitudinal section of phase shifter. Dielectrics completely fill the transverse plane of the guide.

and

$$Z_0 = j\omega\mu_0 \left[\left(\frac{\pi}{a}\right)^2 - \frac{\omega^2}{c^2} \kappa' (1 - j \tan\delta) \right]^{-1/2} . \quad (25)$$

Here γ and Z_0 are, respectively, the propagation constant and characteristic impedance of each of the equivalent transmission lines of the filter and a is the guide width. In the ferroelectric section where $\kappa' > 1000$ and $\tan\delta < 0.1$ these equations can be simplified to

$$\gamma \approx \frac{\omega}{c} \sqrt{\kappa'} \left(\frac{1}{2} \tan\delta + j\right) , \quad (26)$$

and

$$Z_0 \approx \frac{377}{\sqrt{\kappa'}} . \quad (27)$$

Equations (24) through (27), together with Figs. 3 and 4, form the basis for designing the phase shifter. Assuming lossless matching sections and a perfectly matched system, the insertion loss of the device is the intrinsic loss of the ferroelectric section. The insertion loss L and the total phase shift or phase delay ϕ in traversing the ceramic slab are given by

$$L = 4.343 \frac{\omega}{c} \ell \sqrt{\kappa'} \tan\delta \text{ db} , \quad (28)$$

and

$$\phi = \frac{\omega}{c} \ell \sqrt{\kappa'} \text{ rad} , \quad (29)$$

where ℓ is the length of the ferroelectric slab, and where κ' and $\tan\delta$ refer to the properties of the ferroelectric. Equations (28) and (29) are obtained directly from the real and imaginary parts of Eq. (26).

The incremental phase shift resulting from changes in the permittivity of the ferroelectric is obtained from Eq. (29) by evaluating the total phase shift for two different bias fields and subtracting the results. For a fixed temperature, the values of κ' used in this calculation are

determined from Fig. 3. In this way it is possible to predict how the incremental phase shift through the device varies with bias. Similarly, the behavior of the insertion loss can be determined from Eq. (28) and the curves given in Figs. 3 and 4. It should be noted that, for small changes in the dielectric constant, Eqs. (28) and (29) can be combined to give Eq. (18). Thus the solution of the boundary value problem for the geometrical configuration of Fig. 6 agrees exactly with the general theory, as expected.

Matching into the ferroelectric is achieved by placing low-loss dielectric impedance matching sections symmetrically on each side of the ferroelectric. The combination of the matching sections and the ferroelectric thereby unite to form a band-pass filter. Since the ferroelectric is an integral part of the filter and since its properties are controlled by an external dc bias, the filter characteristics depend upon the bias voltage. The filter is therefore designed for one bias voltage (the average bias) and at some fixed temperature (chosen here to be 52°C). The dielectric constants and lengths of the impedance matching sections, which can be determined from Eqs. (24) and (25), are selected so that the system is perfectly matched at two frequencies f_1 and f_2. Thus, at f_1, the lower frequency, the dielectric section adjacent to the ferroelectric is designed to be a quarter-wave matching transformer while the other dielectric section, furthest removed from the ferroelectric, is chosen to be a half-wave line at this frequency. The dielectric constant and position of this half-wave line can then be determined for matching at f_2, the higher frequency. This last step is most easily carried out on the Smith chart using a trial and error procedure.

The device illustrated in Fig. 6 was designed to operate between 8.7 kMc and 9.3 kMc. Figure 7 shows a comparison of the measured VSWR characteristics and the theoretical predictions. The results show that the measured VSWR is below 2.0 from 0.1 to 9.5 kMc over the complete bias range, giving the phase shifter a 400 Mc operating bandwidth. Generally, the curves tend to agree with the predicted behavior, indicating that this simple matching scheme is an effective one.

2. Experimental Results

A block diagram of the experimental setup used to measure insertion loss and phase shift is shown in Fig. 8. The insertion loss is measured

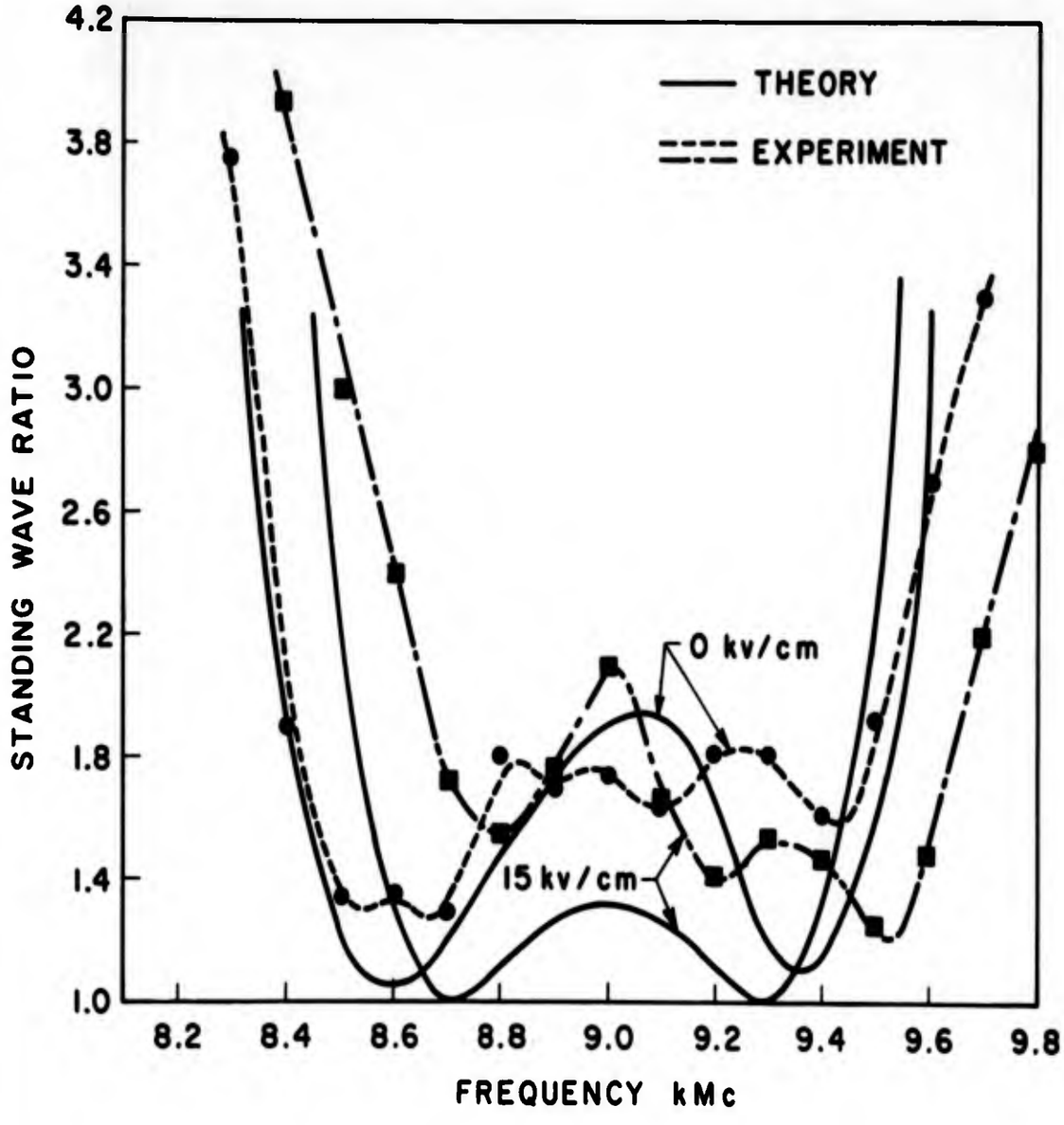

FIG. 7--Measured VSWR characteristics and theoretical predictions.

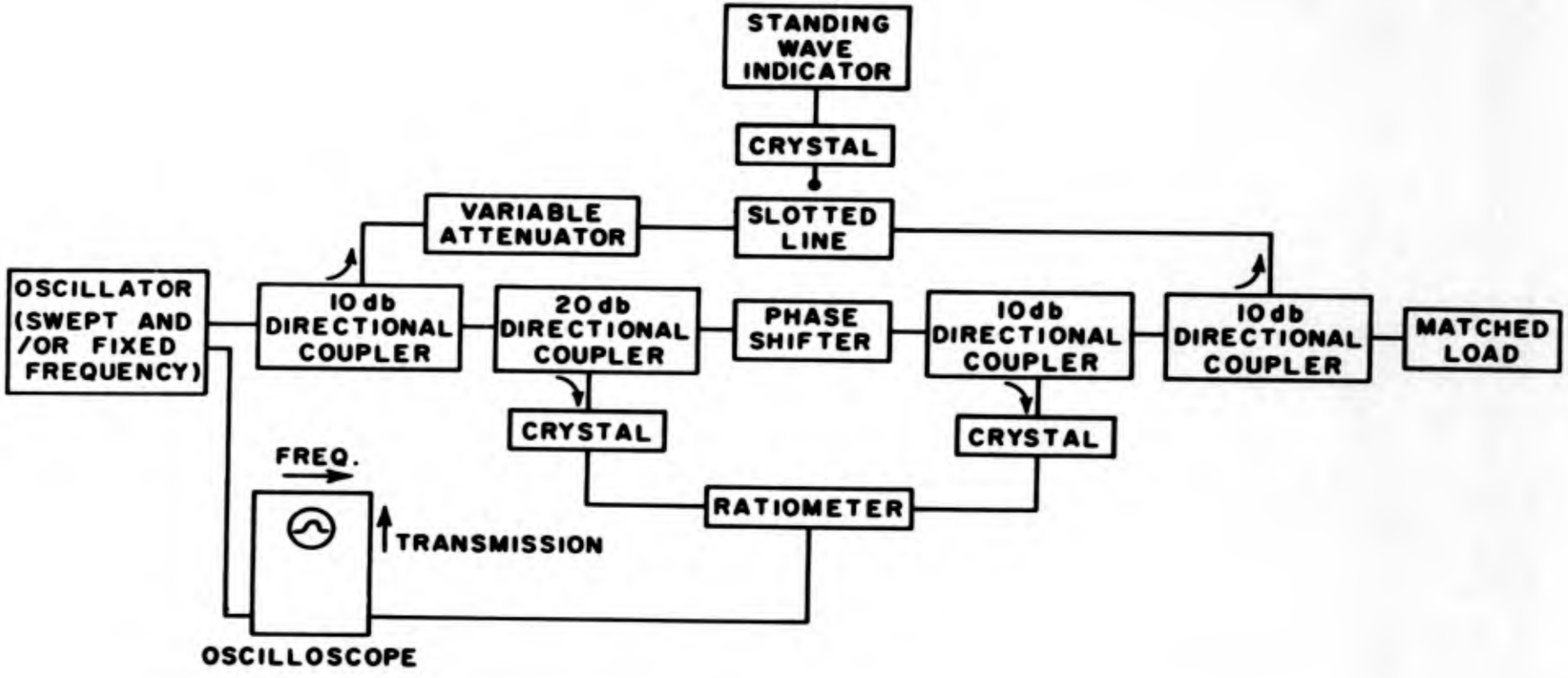

FIG. 8--Block diagram of experimental setup used to measure insertion loss and phase shift.

directly on the ratiometer while the incremental phase shift is obtained by measuring the change in the minimum position on the slotted line due to a change in bias field. In terms of the measured shift in the minimum position on the slotted line Δz one has for $\Delta\phi$

$$\Delta\phi = 2\beta\,\Delta z \text{ radians} \quad , \tag{30}$$

where $\beta = 2\pi/\lambda_g$ is the propagation constant of the slotted line. The accuracy of these measurements is approximately $\pm$ 0.2 db and $\pm 1.0^{\circ}$.

As shown in Figs. 3 and 4, the properties of the ferroelectric material are temperature sensitive and can be varied with dc bias. The practical design of the electrically controlled ferroelectric phase shifter therefore requires a method for controlling the temperature and the bias field. The photograph of the assembled device shown in Fig. 9 illustrates how this is accomplished. To provide temperature stabilization for the ferroelectric ceramic a thermoswitch was mounted in an external metallic heat sink surrounding the waveguide and was connected in series with a Variac and lead-covered heating cable wrapped around the outside of the heat sink. A thermometer was inserted into the heat sink to monitor the temperature. In order to keep the bias voltage below 3000 v, a 0.100-in. waveguide height was used to house the ferroelectric and the matching sections. To further reduce the voltage the ferroelectric slab was divided in half, and a biasing electrode was placed between the two half-sections as illustrated in Fig. 10. A fine wire attached to the biasing electrode was then brought out through the insulated high voltage probe shown in the center of the device in Fig. 9 in the manner indicated in Fig. 10. Arcing was prevented by introducing sulfur hexafluoride gas into the waveguide at atmospheric pressure.

Phase shift was measured in the 400 Mc passband between 9.1 and 9.5 kMc. Figure 11 shows the measured data together with the theoretical behavior at mid-band obtained from Eq. (29). The comparison was made at 66°C rather than 52°C used in the design, since it was found experimentally that the former was the optimum operating temperature; i.e., at 66°C the insertion loss was found to be a minimum and the filter characteristics were observed to behave according to theory (see Fig. 7). An examination

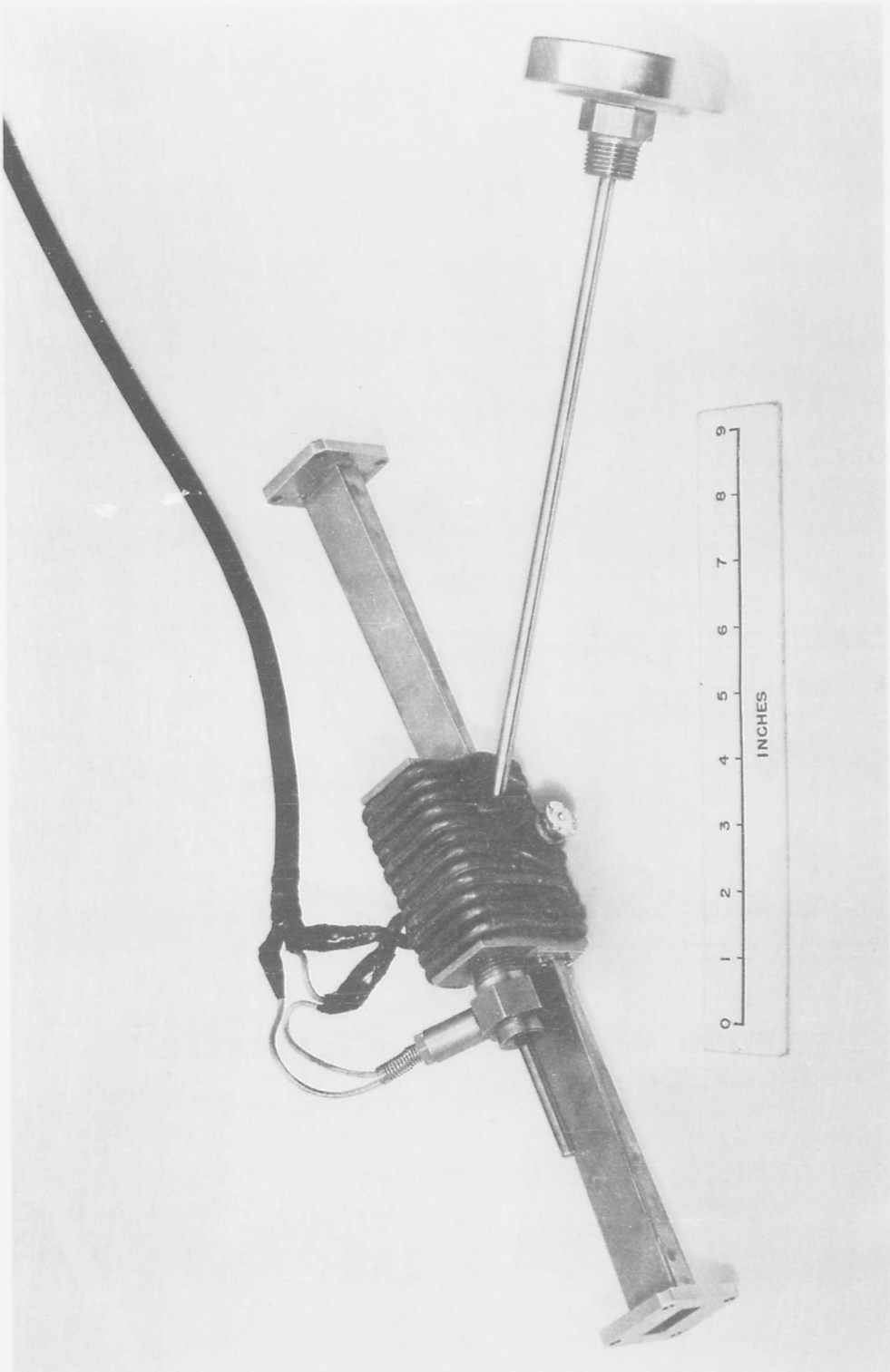

FIG. 9--Photograph of assembled phase shifter.

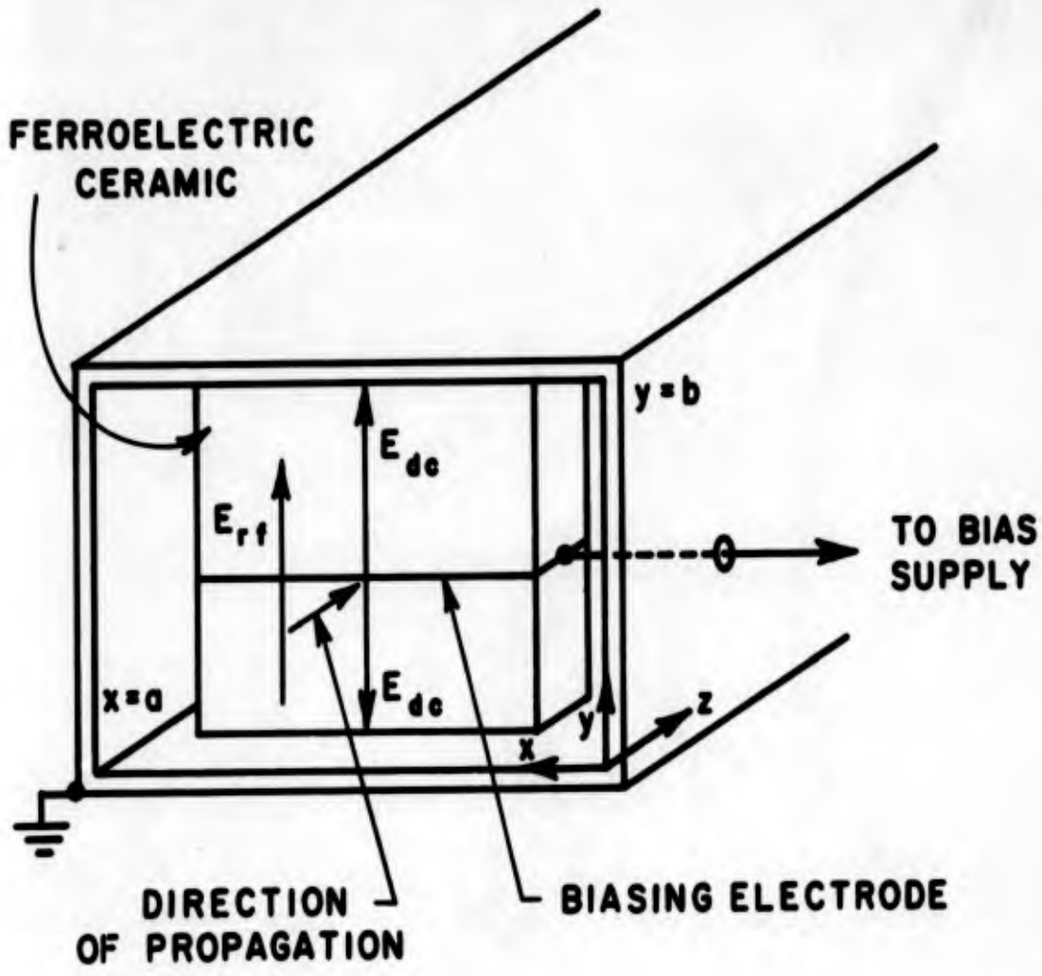

FIG. 10--Configuration of ferroelectric slab in waveguide showing biasing arrangement and representation of rf and dc fields.

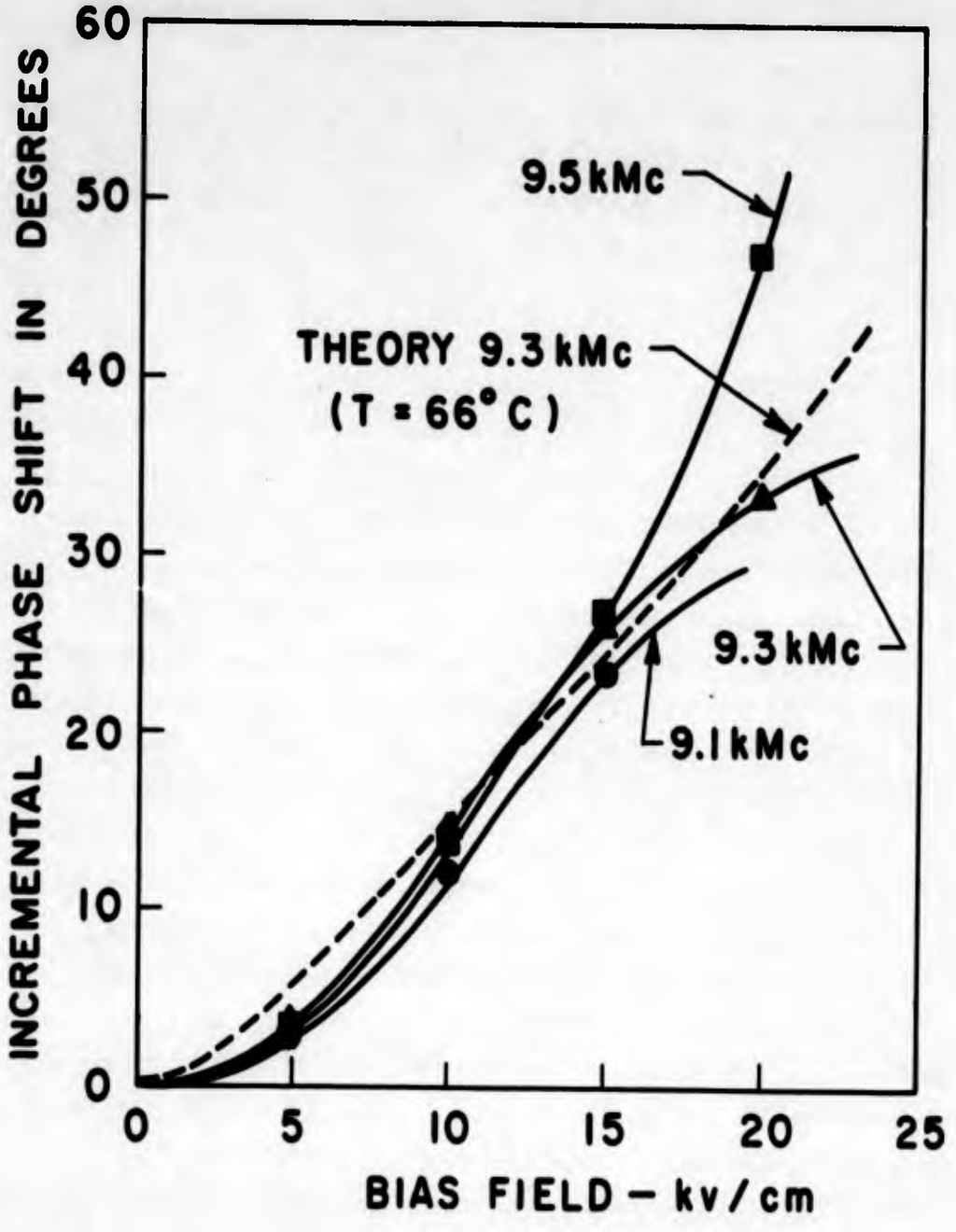

FIG. 11--Measured phase shift and theoretical prediction as a function of dc bias with frequency as a parameter.

of Figs. 3 and 4 reveals the properties of the material are very similar in the temperature range 52°C and 66°C. Since the dielectric constants and lengths of the impedance matching sections are only accurate to within certain tolerances, which vary for different matching sections, one would expect the operating temperature of the device to differ somewhat from the design temperature in order to compensate for the discrepancies. The differences between theory and experiment shown in Fig. 11 may be accounted for by considering the effect of impedance mismatched at the various dielectric interfaces due to changes in the dielectric constant of the ferroelectric section. The theoretical curve determined from Eq. (29) implicitly assumes that the system is perfectly matched internally. Since this condition was not fully realized experimentally, the theoretical curve deviates slightly from the measured results.

The measured insertion loss of the phase shifter and the theoretical prediction, plotted as a function of frequency, are shown in Fig. 12. The theoretical curve was obtained by adding the intrinsic insertion loss computed from Eq. (28) to the experimentally measured reflection loss determined from Fig. 7. The differences between the measured and the predicted behavior are explained by noting that the measurement of insertion loss gives the sum of the dissipation and the reflection loss of the entire device.[37] The dissipation losses in any network are always greater than the intrinsic losses since they take into account the losses due to multiple reflections. In calculating the expected behavior of the phase shifter from Eq. (28), a fundamental assumption was that the ferroelectric slab was perfectly matched internally or that there were no internal resonances giving rise to increased dissipation loss. The difference between the measured and theoretical losses shown in Fig. 12 is therefore a measure of the losses due to internal resonances in the system plus the nonresonant loss in the matching sections. Since the loss tangents of the materials comprising the impedance matching sections were found to be of the order of 10 per cent of the loss tangent of the ferroelectric, the overall losses in the matching sections account for an appreciable fraction of the losses due to internal resonances. Hence, it should be possible to eliminate a considerable portion of the measured losses shown in Fig. 12 by using truly low-loss dielectrics for the filter sections.

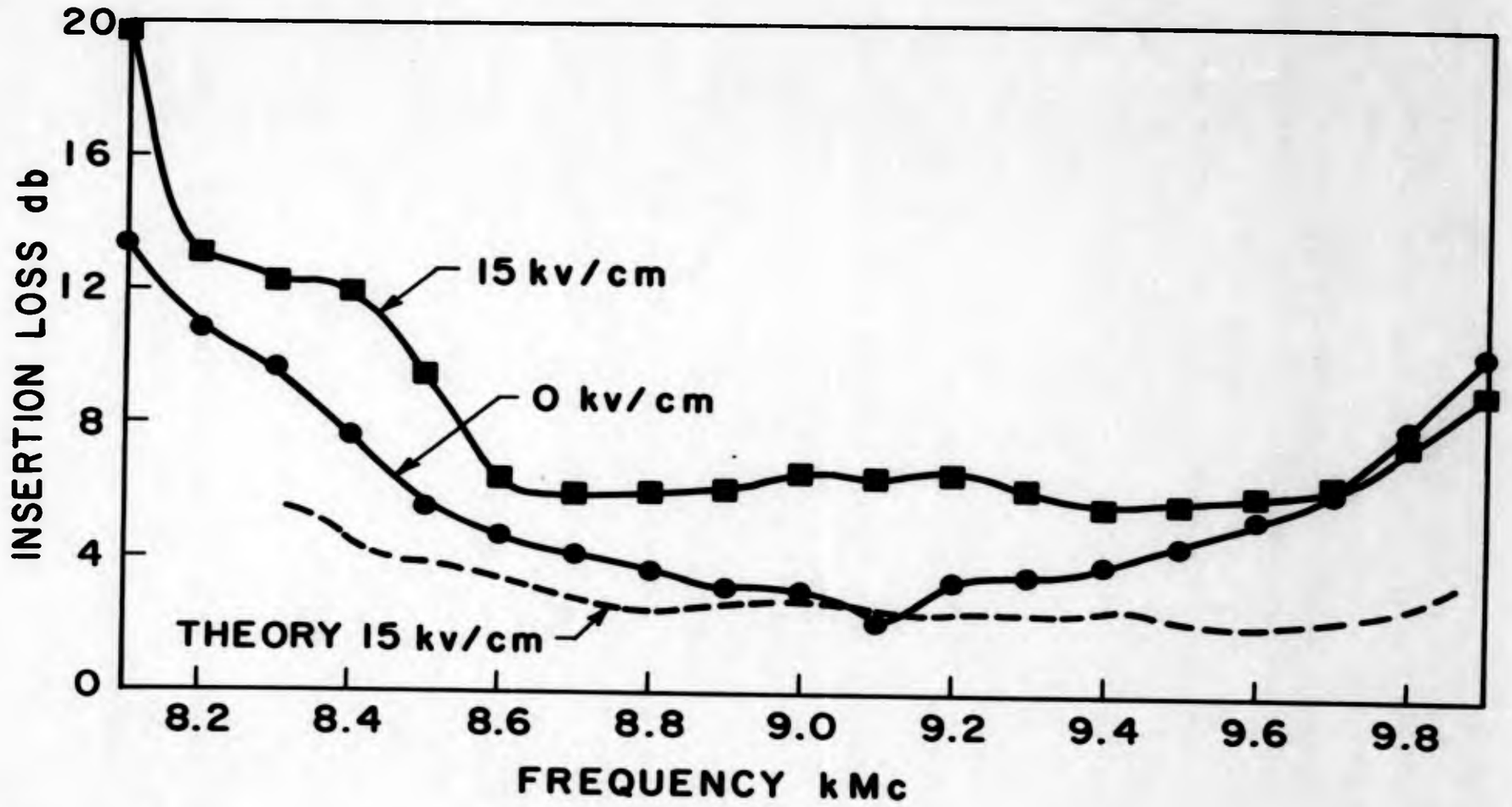

FIG. 12--Measured insertion loss and theoretical prediction as a function of frequency with bias as a parameter.

3. Discussion and Comparison with Ferrite and Diode Phase Shifters

The characteristics of the electrically controlled ferroelectric phase shifter shown in Figs. 7, 11 and 12 indicate that for the configuration given in Fig. 6 incremental phase shifts of 40° to 50° are attainable over reasonable bandwidths with insertion losses averaging about 5 db. These results are in general agreement with those obtained by other investigators working at much lower frequencies with an entirely different geometry.[38] The major disadvantages of the ferroelectric phase shifter are the necessity for temperature control in order to eliminate thermal fluctuations in the characteristics of the device, and the high values of insertion loss due to the losses in the dielectric materials. To estimate the magnitude of the variations in phase shift arising from thermal fluctuations, assume that the temperature of the ferroelectric ceramic varies by $5^{\circ}C$ from the ambient temperature of $66^{\circ}C$. It is then found from Eq. (29) and the curves given in Fig. 3 that for a fixed bias of 10 kv/cm the phase shift can be expected to change by as much as 10° with accompanying small changes in the absorption and the input VSWR.

To determine the relative merit of the ferroelectric phase shifter, a comparison can be made with the behavior of phase shifters which employ other types of nonlinear elements. For example, Reggia and Spencer[31] have utilized ferrites to construct a reciprocal X-band phase shifter. Their findings show that with the proper configuration, phase shifts in excess of several hundred degrees can be obtained with insertion losses in the neighborhood of 0.5 db for rf power levels up to about 25 w. Although these characteristics are superior to those obtained with the ferroelectric device, it should be noted that the ferrite phase shifter requires a longitudinal magnetic field for operation which is generated from a long solenoid. Consequently, the phase shifting control unit is bulky, limits the response time of the device, and requires appreciable amounts of dc control power. To produce 40° to 50° of incremental phase shift in the ferrite device, approximately 50 mw of dc control power is required. The amount of dc control power needed to generate the same phase change in the ferroelectric device is estimated to be about 100 μw which is considerably less than the dc powers necessary to drive the ferrite device. The construction of fast compact-diode phase shifters has been

investigated by Hardin, Downey, and Munushian.[32] They have reported measuring phase changes of 41° at 9 kMc with an insertion loss of 3.9 db. These results are only valid for rf power levels in the vicinity of a few milliwatts due to the fact that the absorption increases with rf power in diodes. The amount of dc control power required to produce the measured phase changes of 41° is very nearly the same as required by the ferroelectric device. From these results it can be seen that the electrically controlled ferroelectric phase shifter is comparable to the diode device in the X-band region. Furthermore, the ferroelectric phase shifter will operate satisfactorily as a CW device for rf powers at the watt level, which is similar to the power handling capabilities of the ferrite device and far superior to those of the diode device.

CHAPTER IV

THE LARGE SIGNAL MICROWAVE APPLICATIONS OF FERROELECTRIC CERAMICS

A. INTRODUCTION

As discussed in the second chapter, very little experimental work has been done toward determining the small signal microwave characteristics of ferroelectric ceramics; and from the material presented in Chapter III it is evident that even less work has been done toward applying them in the design of microwave devices. Insofar as the large signal microwave characteristics of ferroelectric ceramics, or indeed the large signal applications of these materials, are concerned it can truly be said that virtually no experimental or serious theoretical work has been done. An evaluation of the large signal properties of ferroelectric materials is of primary importance in predicting the behavior of nonlinear devices in which these materials are used as mixing elements. Among these devices are harmonic generators, parametric amplifiers, limiters, and modulators. Recently, several investigators[39-42] have proposed using ferroelectrics in such devices; however, in their work they have only considered the reactive nonlinearity of the materials. It is shown here that, as in the small signal case where the incremental complex permittivity is a function of dc bias, consideration should be given not only to the material's nonlinear reactive properties, but also to its nonlinear loss characteristics.

The purpose of this chapter is firstly to describe, both theoretically and experimentally, the properties of ferroelectric harmonic generators employing conventional cavity-type circuits; and secondly, to describe from a theoretical viewpoint the phenomenon of traveling-wave harmonic generation along nonlinear transmission lines which utilize ferroelectric

ceramics for their nonlinear medium. It is shown hereinafter that the results of the harmonic generation experiment can be used to obtain expressions for the dielectric nonlinearity, provided that a sufficiently accurate theory can be developed to describe the behavior of the harmonic generator. This has been done by carrying through a detailed circuit analysis of the device. Most theories dealing with harmonic generation in coupled resonant circuits have been limited to the case where either nonlinear reactance[43-45] or nonlinear resistance[46,47] is employed as the coupling element. The more general case where both effects are present simultaneously, as in ferroelectrics, has received relatively little attention. In the treatment of both the cavity-type device and the traveling-wave-type device both nonlinear mechanisms are included.

Thus far only a limited amount of work has been done towards understanding or utilizing nonlinear distributed systems as a means for harmonic generation. Riley[48] has investigated, by means of the method of characteristics, the growth of harmonics in a wave traveling along a nonlinear transmission line using junction diodes as shunt capacitors. The use of multiphase rectifier circuits to construct a particular kind of traveling-wave harmonic generator has been suggested by Hedderly[49] and Brown.[50] Auld, Shaw, and Winslow[51] have reported on obtaining traveling-wave frequency doubling in ferrites. Their analysis, which applies to a rectangular waveguide uniformly loaded with a thin ferrite slab, has been extended to Bady[52] to the case of frequency doubling in thick ferrite slabs of anisotropic material. The possibility of using the distributed nonlinearity in a finite plasma column to obtain traveling-wave interaction between the fundamental and second harmonic frequencies which propagate as slow waves has been considered by Kino, Pavkovich, and Krenz.[53] Finally, a recent experiment by Franken et al.,[54] demonstrates the feasibility of generating optical harmonics by what is basically a traveling-wave scheme, i.e., by focusing an intense coherent light beam inside an optically nonlinear dielectric. The preceding references show that to date most of the work done on traveling-wave harmonic generation has been restricted to nonlinear systems which may be considered lossless. In the study of traveling-wave harmonic generation in ferroelectric ceramics presented in this chapter, a perturbation solution is developed for determining

the steady-state response of nonlinear TEM transmission lines and nonlinear cylindrical waveguides of arbitrary cross-section where the nonlinear medium comprises both resistive and reactive nonlinearity.

Lastly, it should be mentioned that all theoretical and experimental work has been done for the case of zero bias and at temperatures high enough so that the ferroelectric ceramic operates above its Curie point (the material under consideration is the ceramic of 73 per cent $BaTiO_3$ - 27 per cent $SrTiO_3$ which, recall, has a Curie point at $T_c = 20^oC$). The ceramic can then be viewed simply as an isotropic nonlinear dielectric displaying a nonlinearity which is an even function of field strength, and, accordingly, can be described analytically by Eqs. (9) and (10). Since the dielectric nonlinearity depends only upon even powers of the applied field, ferroelectric ceramics can thus be expected to generate odd harmonics.

B. HARMONIC GENERATION IN CAVITY-TYPE CIRCUITS[27]

This section deals with the theoretical and experimental aspects of harmonic generation in ferroelectric ceramics in coupled resonant circuits. In the theoretical work a detailed circuit analysis of a frequency tripler is presented. This analysis predicts that the first order saturation effects are due to the power consumed by the nonlinear loss mechanisms of the ferroelectric. In the experimental work a successful frequency tripler which operates from 3 kMc to 9 kMc was constructed. The operating characteristics of this device are in excellent agreement with those predicted theoretically.

1. Design and Description of Cavity

Resonant harmonic generators usually consist of two coupled resonant circuits where the coupling is provided by a nonlinear mixing element. One circuit is tuned to the fundamental or pump frequency while the other is tuned to one of the harmonic frequencies. Power is converted directly from the pump frequency f_1 to the harmonic frequency of interest kf_1 through the dynamics of the nonlinear coupling element.

Figure 13 shows a cross-sectional view of an experimental harmonic generator constructed in the form of a coaxial cavity which has been designed to be simultaneously resonant in the TEM mode both at 3 kMc

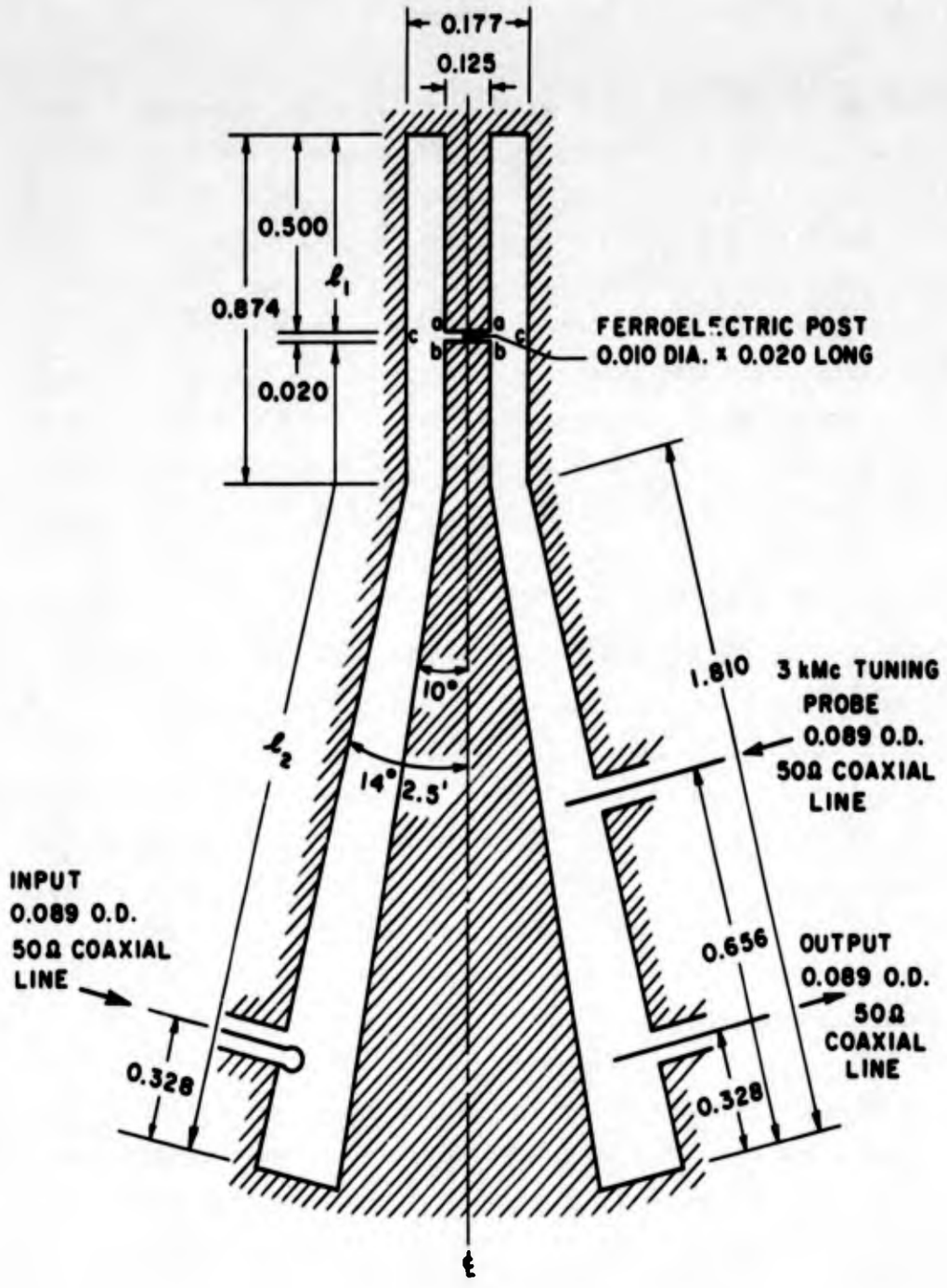

FIG. 13--Cross-sectional view of coaxial cavity used for harmonic generator.

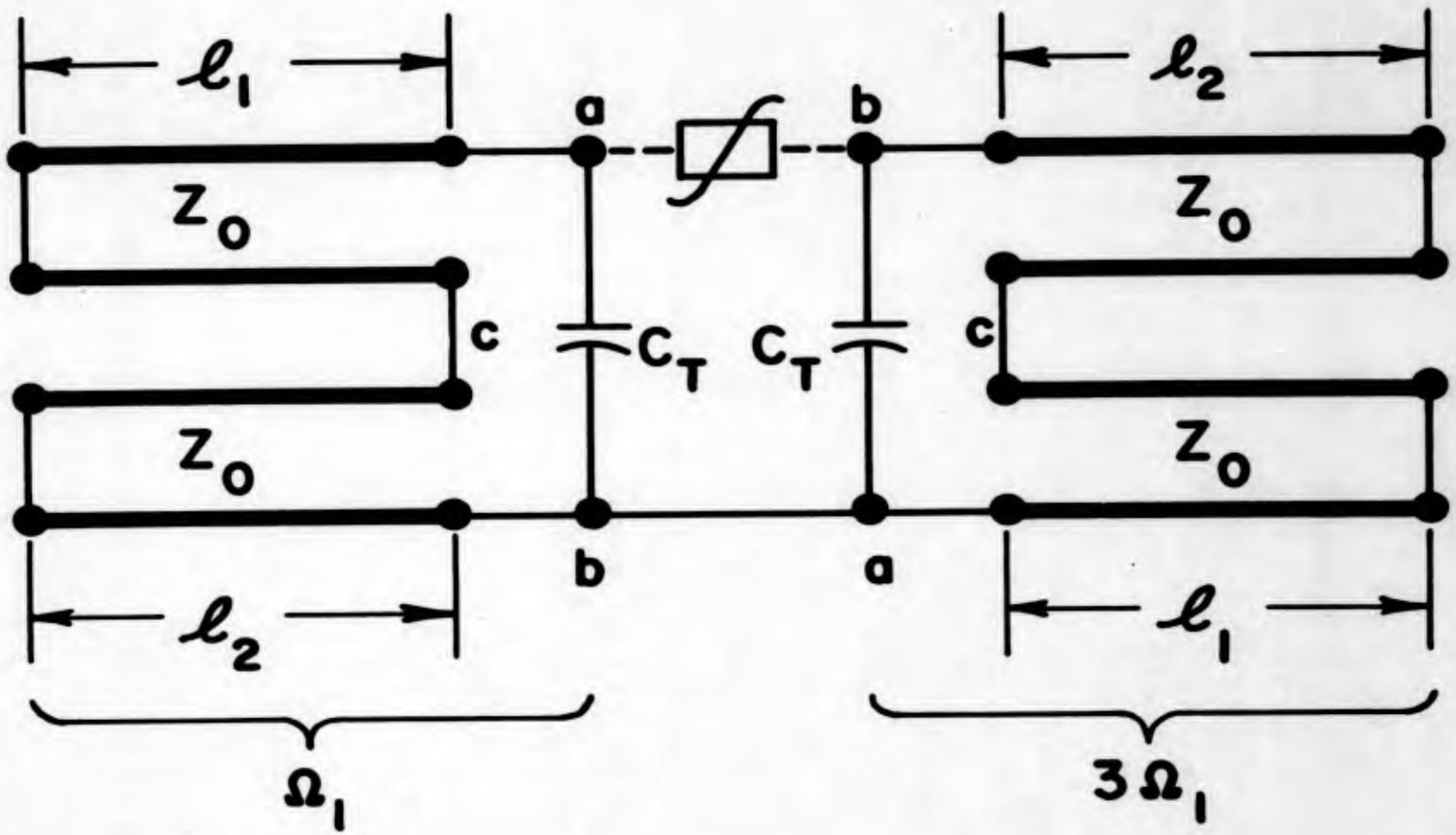

FIG. 14--Transmission line equivalent circuit of the coaxial cavity given in Fig. 13. The circuit resonant at $3\Omega_1$ is a short circuit at frequency Ω_1 and vice versa.

and at 9 kMc. The cavity design is easily understood by referring to the equivalent transmission line circuit given in Fig. 14. Terminals a, b, c refer to the corresponding points indicated in Fig. 13. The schematic nonlinear coupling shown dotted between circuits can be omitted at low power levels in determining the linear resonances at Ω_1 and at $3\Omega_1$. Thus at low power levels, or in the small signal case, the conditions for dual resonance at Ω_1 and $3\Omega_1$ can be obtained by finding a simultaneous solution to the equations describing resonance at Ω_1 and $3\Omega_1$. These conditions are:

$$\tan \beta \ell_1 + \tan \beta \ell_2 = \frac{1}{\Omega_1 Z_0 C_T} \qquad (31)$$

and

$$\tan 3\beta \ell_1 + \tan 3\beta \ell_2 = \frac{1}{3\Omega_1 Z_0 C_T} \quad , \qquad (32)$$

where $\beta = 2\pi/\lambda$ is the propagation constant of the coaxial lines at $\Omega_1 = 2\pi f_1$, ℓ_1 is the length of transmission line above the terminals ac shown in Fig. 13, ℓ_2 is the length of transmission line below the terminals bc shown in Fig. 13, Z_0 is the characteristic impedance of the transmission lines, and C_T is the total capacitance including the dielectric between planes a and b. Equations (31) and (32) do not include the effects of the discontinuity capacitance in the region of the junction between the inner conductors; however, these effects can be made negligible by proper design.

The dielectric used in this experiment was the ceramic composed of 73 per cent barium titanate and 27 per cent strontium titanate. In order to keep the dielectric losses small while retaining a large degree of nonlinearity, the operating temperature was chosen as 49°C. At this temperature, the dielectric constant κ'_1 was found from small signal X-band measurements to be 2000 (see Fig. 3). The high value of dielectric constant required that the dielectric sample be physically small; hence a cylindrical post, 0.020 in. long and 0.010 in. in diameter, was chosen. The small signal capacitance of this post was calculated to be 1.76 μμf.

A micro-photograph of the dielectric post is shown in Fig. 15.[1] Note that the small post length permits setting up high electric field intensities within the dielectric at reasonable power levels.

The dimensions of the cavity were obtained by finding a simultaneous solution to Eqs. (31) and (32) by graphical means when $f_1 = 3$ kMc. An examination of these equations reveals that the cavity dimensions are specified by three unknowns (viz., ℓ_1 , ℓ_2 , and Z_0) . Since there are only two equations for determining the resonances at Ω_1 and $3\Omega_1$, the graphical method of analysis deserves some comment. The resonance conditions given by Eqs. (31) and (32) can be combined to give

$$3 \tan 3\beta\ell_1 - \tan \beta\ell_1 = -3 \tan 3\beta\ell_2 + \tan \beta\ell_2 \quad .$$

By plotting the right and left hand sides of this expression as a function of $3\beta\ell$ (or $\beta\ell$) , one finds from this graph those values of $3\beta\ell_1$ and $3\beta\ell_2$ which make the right and left hand sides equal. From these values together with the known values of Ω_1 and C_T one can plot curves of Z_0 vs $3\beta\ell_1$ from Eqs. (31) and (32). The intersection of these curves determines the characteristic impedance of the cavity Z_0 and $3\beta\ell_1$ (from which $3\beta\ell_2$ can obviously be found). In making use of this technique one can arbitrarily choose the size of the inner conductor (or the outer conductor) of the cavity; the other is determined by the equation for Z_0 . As a matter of convenience, the diameter of the inner conductor of the cavity (Fig. 13) was chosen to be 0.125 in., making the total parallel plane gap capacitance, C_T , be 1.9 $\mu\mu$f . For dual resonance at 3 kMc and at 9 kMc the characteristic impedance of the transmission lines was found to be 20 ohms. Since this corresponds to a ratio of outer conductor to inner conductor diameter that is close to unity, the bottom portion of the cavity was expanded in the form of a biconical coaxial transmission line to allow sufficient space to introduce loops and probes into the cavity. As shown in Fig. 13, a loop was used to couple into the 3 kMc resonance and a probe to couple into the 9 kMc resonance. This coupling scheme was chosen since it permitted selective coupling into each resonance.

---

[1] Details of the sample fabrication can be found in reference 1.

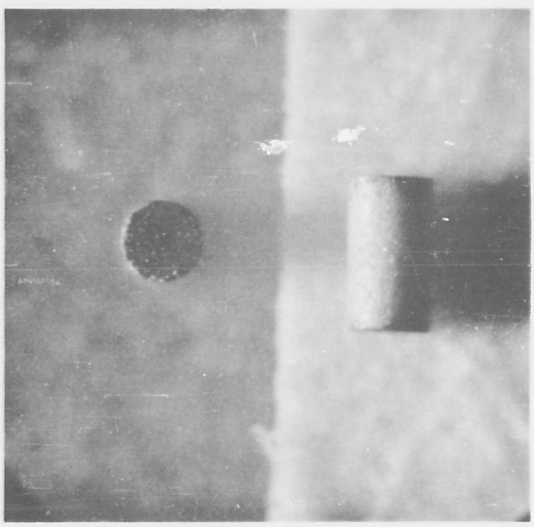

FIG. 15--Microphotograph of ceramic dielectric post. Magnification is 32 × .

2. Equivalent Circuit and Analysis

Since the natural resonances of a cavity may be represented by lumped element resonant circuits, the harmonic generator cavity shown in Fig. 13 can be represented by the equivalent circuit given in Fig. 16 over a narrow band of frequencies. Figure 16(a) shows the complete equivalent circuit. Here the linear elements L'_1 , G'_1 , C'_1 and L'_3 , G'_3 , C'_3 denote the properties of the Ω_1 and $3\Omega_1$ resonances, respectively. The capacitances C'_1 and C'_3 include the linear capacitance of the dielectric post. Transformers T_1 and T_4 are ideal transformers representing the input and output couplings, and the ideal transformers T_2 and T_3 are electrical transformations which account for the nonlinear element possibly not being at a position of maximum electric field. Transformer T_2 applies to the fields at Ω_1 , and transformer T_3 applies to the fields at $3\Omega_1$. The complete equivalent circuit of Fig. 16(a) can be simplified to that of Fig. 16(b) for purposes of analysis. The linear circuit elements L , G_1 , C_1 and L_3 , G_3 , C_3 are obtained by reflecting L'_1 , G'_1 , C'_1 and L'_3 , G'_3 , C'_3 through transformers T_2 and T_3 , respectively. The admittances $n^2 Y_0$ and $m^2 Y_0$ denote the transmission line admittance, $Y_0 = 1/Z_0$, coupled into the cavity on the input and output sides, respectively. In order to carry out this last step the admittance Y_0 must be reflected through transformers T_1 and T_2 on the input side and T_3 and T_4 on the output side. When this is done, one finds that the turns ratios of transformers T_1 and T_2 and T_3 and T_4 can be combined to give the equivalent turns ratios $n = rn'$ and $m = sm'$ used in Fig. 16(b). The constant current generator i_g shown in Fig. 16(b) corresponds to the incident source driving the Ω_1 resonance, and the voltages v_1 and v_3 represent the fundamental and third harmonic cavity fields generated in response to the drive, i_g . It should be noted i_g has been arbitrarily defined as the current source exciting the circuit of the harmonic generator from within the cavity. If it is desired to describe this source in terms of what takes place outside the cavity [i.e., to the left of the terminals of transformer T_1 in Fig. 16(a)], one must divide the current i_g by n , the equivalent input turns ratio of transformers T_1 and T_2 .

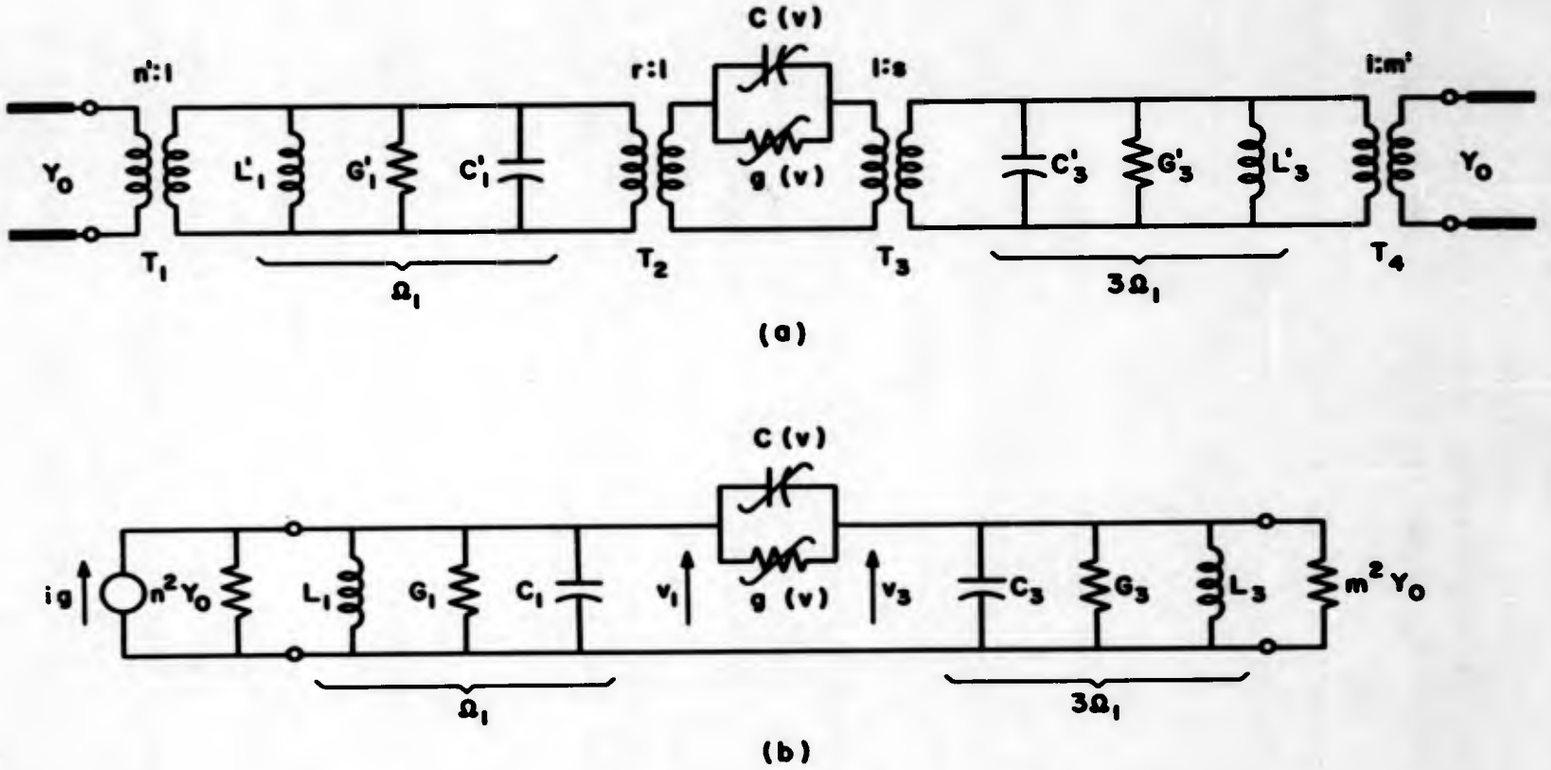

FIG. 16--Equivalent circuit of harmonic generator.

As indicated in Fig. 16, the ferroelectric post may be represented by a nonlinear parallel RC circuit coupling the two resonances. A lumped circuit representation for the nonlinear coupling element is accurate since the longitudinal fields within the dielectric are approximately constant over the diameter of the post. That is, the electric field varies within the post as $J_0 [(2\pi/\lambda)\sqrt{\kappa'}_1 r]$, and the radius of the post, a , has been chosen to be sufficiently small so that $J_0 [(2\pi/\lambda)\sqrt{\kappa'}_1 a] \approx 1$. Thus a lumped nonlinear capacitance and conductance can be defined for the post in the absence of bias by the following expressions:

$$c(v) = \epsilon'(v) \frac{\pi a^2}{\ell} = \sum_{n \text{ even}} c_n v^n \qquad (33)$$

and

$$g(v) = \sigma(v) \frac{\pi a^2}{\ell} = \sum_{n \text{ even}} g_n \bar{\Omega} v^n \quad , \qquad (34)$$

where $v = E\ell$ is the instantaneous voltage across the post, and ℓ is the length of the post. The set of coefficients c_n in the power series expansion describing the nonlinear capacitance $c(v)$ of the post are obtained from Eq. (9), and the set of coefficients g_n in the power series expansion describing the nonlinear rf conductance $g(v)$ of the post are obtained from Eq. (10). The case of most practical interest, and the one considered here, is where $c(v)$ and $g(v)$ can be written approximately as

$$c(v) \approx c_0 + c_2 v^2 \qquad (35)$$

and

$$g(v) \approx \left[g_0 \bar{\Omega} + g_2 \bar{\Omega} v^2\right] \quad . \qquad (36)$$

These equations assume that the terms proportional to the fourth and higher powers of v are always small compared to those proportional to v^2 .

The analysis of the frequency tripler can now be carried out by conventional circuit techniques. The governing equations for the equivalent circuit shown in Fig. 16(b) can be written explicitly as node equations in which current components of each harmonic are equated at the nodes. The resulting set of coupled nonlinear integro-differential equations are

$$i_g = (G_1 + n^2 Y_0)\, v_1 + \frac{1}{L_1}\int v_1\, dt + \left\{ g(v)\, v + \frac{d}{dt}\left[c(v)\, v\right]\right\}\Bigg|_{\omega} \qquad (37)$$

and

$$0 = (G_3 + m^2 Y_0)\, v_3 + \frac{1}{L_3}\int v_3\, dt + \left\{ g(v)\, v + \frac{d}{dt}\left[c(v)\, v\right]\right\}\Bigg|_{3\omega} . \qquad (38)$$

Here ω is the angular driving frequency. The harmonics which are generated arise from the nonlinear terms $g(v)\, v$ and $(d/dt)[c(v)\, v]$ where v is the difference in voltage between nodes. That is, in the nonlinear terms in Eq. (37) v is given by $v_1 - v_3$ and similarly in Eq. (38) v should be replaced by $v_3 - v_1$. The nonlinear terms appearing in the braces in Eqs. (37) and (38) have been written in simplified form so as to eliminate confusion with the functional notation. The voltages v_1 and v_3 , and the current i_g can be written as

$$v_1 = V_1\, e^{j\omega t} + V_1^*\, e^{-j\omega t} \qquad (39)$$

$$v_3 = V_3\, e^{3j\omega t} + V_3^*\, e^{-3j\omega t} \qquad (40)$$

$$i_g = I_g\, e^{j\omega t} + I_g^*\, e^{-j\omega t} \quad , \qquad (41)$$

where $*$ denotes the complex conjugate. By using these expressions together with Eqs. (35) and (36) it can be shown that the governing equations, Eqs. (37) and (38), reduce to the following set of algebraic equations:

$$I_g = (g_{01} + Y_1)\, V_1 + 3\,(g_{21} + j\omega c_2)(V_1^2\, V_1^* + 2\, V_1 V_3 V_3^* - V_1^{*2}\, V_3) \quad , \qquad (42)$$

and

$$0 = (g_{03} + Y_3)\, V_3 - (g_{23} + 3j\omega c_2)(v_1^3 - 6\, V_1 V_1^*\, V_3 - 3\, V_3^2 V_3^*) \quad . \qquad (43)$$

In obtaining these equations the operator $\bar{\Omega}$ appearing in Eq. (36) has been eliminated by applying it to each of the spectral components entering in $g(v)\, v$ in Eqs. (37) and (38). When this is done, it is found that the coefficient relating the spectral components of current and $(\text{voltage})^n$ at $k\omega$ is $k\omega(g_n)$. In writing out Eqs. (42) and (43), which apply in the frequency domain, this has been included by the simplifying notation $k\omega\, g_n \equiv g_{nk}$. Equation (42) applies at the pump frequency ω and Eq. (43) at the third harmonic 3ω . In these equations, Y_1 and Y_3 are the linear circuit admittances of the Ω_1 and $3\Omega_1$ tanks at ω and 3ω , respectively, and are given by the relations

$$Y_1 = n^2 Y_0 + G_1 + j\omega C_1 + \frac{1}{j\omega L_1} \qquad (44)$$

$$Y_3 = m^2 Y_0 + G_3 + 3j\omega C_3 + \frac{1}{3j\omega L_3} \quad , \qquad (45)$$

where n and m are the effective input and output transformer turns ratios. The complex amplitudes V_1 and V_3 represent the responses of the system at ω and 3ω , respectively, to the pump driving function I_g . One can easily relate the amplitude of the drive I_g to the incident power flow P_{inc} in the external transmission line by referring to the circuit of Fig. 17. For the case where $Y_{in,\,\omega} = Y_0$, the transmission line is matched to the cavity input (i.e., $P_{ref} = 0$) and one finds that

$$\left|I_g\right|^2 = 2\, n^2 Y_0\, P_{inc} \quad . \qquad (46)$$

Equations (42) and (43) completely describe the behavior of the frequency tripler when Eqs. (35) and (36) correctly describe $c(v)$ and $g(v)$. They are nonlinear algebraic equations and can be used to obtain the circuit model shown in Fig. 18. The nonlinear coupling admittances Y_{c_1} and Y_{c_3} shown in Fig. 18 analytically describe the reaction of

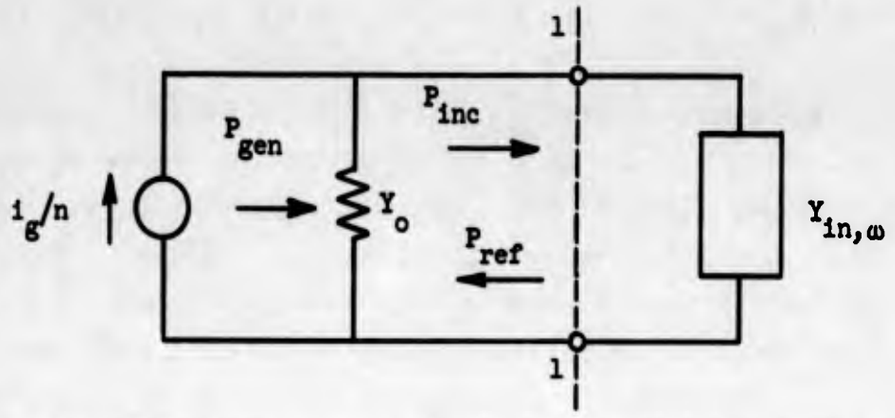

FIG. 17--Equivalent input circuit of the harmonic generator shown in Fig. 16. The admittance $Y_{in,\omega}$ refers to the small signal input admittance at frequency $\omega/2\pi$ and is defined at some suitably chosen reference plane 1 - 1.

the third harmonic fields on the pump fields and vice versa. In addition, due to the fact that each resonant circuit effectively sees a nonlinear parallel RC circuit in shunt [see Fig. 16(b)], the admittances Y_{c_1} and Y_{c_3} take into account the anharmonic voltage dependent detuning effects of the pump fields on the Ω_1 resonance and of the third harmonic fields on the $3\Omega_1$ resonance. It should be noted that the nonlinear coupling admittance Y_{c_3} given in Fig. 18 has a <u>negative conductance</u> term and is therefore the source driving the third harmonic fields. Based upon the fact that nonlinear terms are present in each of the resonant circuits, one would expect that the fundamental and third harmonic response curves should exhibit foldover. This effect can be seen qualitatively in the response of the fundamental circuit, for example, by solving for V_1 from Eqs. (42) and (43) when the inequality $|V_1|>|V_3|$ is satisfied. In this case one finds that V_1 is the solution to a fifth order polynomial. By requiring that V_1 be real, one then finds that the solution to this polynomial (which represents the fundamental circuit response) can either have one, three, or five real roots depending upon the frequency of operation and the drive level I_g . This clearly indicates that the response V_1 will be multivalued over part of the frequency

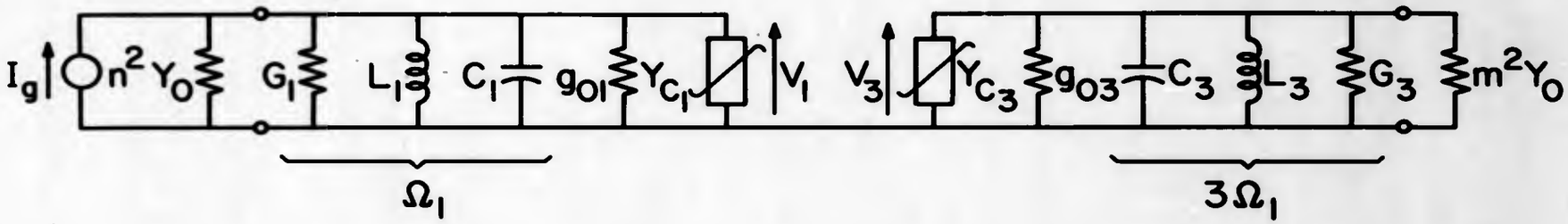

NONLINEAR COUPLING ADMITTANCES:

$$Y_{C_1} = 3(g_{21} + j\omega c_2)\ (V_1 V_1^* + 2V_3 V_3^* - \frac{V_1^{*2} V_3}{V_1})$$

$$Y_{C_3} = -(g_{23} + j\omega c_2)\ (\frac{V_1^3}{V_3} - 6V_1 V_1^* - 3V_3 V_3^*)$$

FIG. 18--Circuit model of frequency tripler.

range and will have two peaks which, of course, fold over. From this discussion one would expect that at high signal levels the response V_1 should exhibit the familiar hysteresis phenomenon with respect to frequency displayed by nonlinear resonant circuits. Here, mention should be made of the fact that the foldover curves obtained from the harmonic generator circuit are analogous to those usually encountered in nonlinear systems which undergo resonance.[55] The one surprising effect observed here is that the foldover curves have two peaks whereas the linear resonances at Ω_1 and $3\Omega_1$ have only one peak. From a physical point of view this behavior can be explained in the following way. As the pump fields are excited more strongly in the cavity, the coupling between the Ω_1 and $3\Omega_1$ resonant circuits increases because of the increased field strength across the nonlinear ceramic post. This in turn causes the third harmonic fields to react more strongly on the pump fields and therefore to have a greater influence on the fundamental circuit response. This behavior is in a sense analogous to varying the coupling between two linear resonant circuits. In this case it is clear that as the coupling increases the natural resonances of each circuit, which are initially degenerate, split into two different resonances which become the natural vibrations of the coupled circuits. In the case of the coupled circuits of the harmonic generator it might at first be thought that this argument is not applicable. However, one should bear in mind that the nonlinear terms coupling the fundamental and third harmonic resonances are capable of converting frequency. It is therefore not surprising that the reaction of the third harmonic fields on the pump fields should be at the fundamental frequency and that the resonant response of the fundamental circuit should accordingly be split into two peaks which fold over. The significance of the foldover effects is that at high power levels they become increasingly important and account, in part, for the saturation of the output by causing the fundamental and third harmonic circuits to detune from the present three to one frequency ratio.

In the case where the efficiency is low one can assume that $|V_1| > |V_3|$ and Eqs. (42) and (43) can be thus linearized with respect to V_3. The resulting equations may then be solved by an iteration process. In this case the products of linear terms are assumed to be much larger than the

products involving nonlinear terms. To second order in I_g the fundamental response V_1 becomes (see Appendix E)

$$V_1 = I_g \left[(g_{01} + Y_1) + 3(g_{21} + j\omega c_2) \frac{|I_g|^2}{|g_{01} + Y_1|^2} \right]^{-1} , \quad (47)$$

and the third harmonic response can be written as

$$V_3 = \frac{(g_{23} + 3j\omega c_2)}{\left[(g_{03} + Y_3) + 6(g_{23} + j\omega c_2) \frac{|I_g|^2}{|g_{01} + Y_1|^2} \right]} V_1^3 . \quad (48)$$

Considering the on-resonance ($\omega = \Omega_1$) high Q ($n^2 Y_0 \gg G_1$ and $m^2 Y_0 \gg G_3$) behavior with the system well matched, the input and output powers and the effective transformer turns ratio n and m are given by

$$P_{in} = P_{inc} \quad (49)$$

$$P_{out} = 2m^2 Y_0 |V_3|^2 \quad (50)$$

and

$$n^2 = g_{01}/Y_0 \quad (51)$$

$$m^2 = g_{03}/Y_0 . \quad (52)$$

Observe that when the unloaded Q of the Ω_1 and $3\Omega_1$ resonances is high, as assumed here, the conductances G_1 and G_3 can be neglected compared with g_{01}, g_{03}, $n^2 Y_0$, and $m^2 Y_0$. Thus in order to match into the cavity one must equate $n^2 Y_0$ and $m^2 Y_0$ to g_{01} and g_{03}, respectively; this has been done in Eqs. (51) and (52). The equations for n and m are therefore only approximate since they omit

the effects of G_1 and G_3 and of the nonlinear conductive terms which appear in Y_{c_1} and Y_{c_3} (Fig. 18). It is shown in Appendix E that, consistent with the approximations used to obtain Eqs. (47) and (48) one can substitute Eq. (48) into Eq. (50) and obtain the following expression for output power when $\omega = \Omega_1$:

$$P_{out} = \frac{3(g_{21}^2 + \Omega_1^2 c_2^2)}{16 g_{01}^4 \left[1 + (15/2)(g_{21}/g_{01}^2) P_{inc}\right]} P_{inc}^3 , \qquad (53)$$

where Eqs. (46), (47), (51), and (52) have been used. Equation (53) is written in terms of pump frequency parameters, and is an absolute expression for output power. It should be noted that the first order saturation effects are due to power consumed in g_{21} , the nonlinear loss term. Finally the conversion efficiency $\eta = (P_{out}/P_{in}) \times 100\%$ may be computed from Eqs. (53) and (49). The resulting expression is

$$\eta = \frac{3(g_{21}^2 + \Omega_1^2 c_2^2)}{16\, g_{01}^4 \left[1 + (15/2)(g_{21}/g_{01}^2) P_{inc}\right]} P_{inc}^2 \times 100\% . \qquad (54)$$

By examining the distribution of power flow in the harmonic generator network, one can formulate an alternative and more general proof to the statement that the power dissipation in g_{21} is responsible for the first order saturation between input and output power. It is shown in Appendix F that by starting with the nonlinear algebraic circuit equations given by Eqs. (42) and (43), one can derive an expression for the power absorbed P_{abs} at frequencies ω and 3ω in the nonlinear parallel RC circuit coupling the two resonant tanks (see Fig. 16). The resultant expression shows that there is no power absorbed in the nonlinear capacitance and that the power absorbed in the nonlinear conductance is given by

$$P_{abs} = 6\, g_{21} \left[|V_1|^4 + 3\,|V_3|^4 + 8\,|V_1|^2\,|V_3|^2 - (V_1^{*3} V_3 + V_1^3 V_3^*)\right] . \qquad (55)$$

Based upon this equation and the previous discussion pertaining to fold-over, it is found that the behavior of the frequency tripler may be

described in the following manner. At low power levels, the output power is proportional to the cube of the input power, as expected from Eq. (53). As the input power level increases, the power absorbed in g_{21} becomes appreciable [see Eq. (55)] and the output power follows a square law relation with respect to the input power [see Eq. (53)]. For still higher input powers one enters the high power region where the reaction of the third harmonic fields upon the fundamental frequency fields (and vice versa) becomes significant and produces detuning between the two resonant circuits due to the foldover effects. In accordance with this one finds that in the high power region the output power saturates to the point where it is directly proportional to the input power.

3. Experimental Results

A block diagram of the instrumentation used to perform the harmonic generation experiment is shown in Fig. 19. All measurements were made with a pulsed source since high peak power with low average power was required to drive the harmonic generator. The source was triggered 10 times per second and yielded a 2.3 μsec pulse. The low duty cycle of 2.3×10^{-5} was chosen to minimize the heating of the dielectric during the "on" time of the pulse. For the ceramic post shown in Fig. 15 and for power levels of the order of a few kilowatts, the rate of increase of temperature within the post is approximately $\Delta T/t \approx 9.5^{\circ}C/\mu sec$. Therefore, to keep ΔT small, a short pulse was used, and to permit the temperature of the ceramic to relax back to the ambient temperature of the cavity, a long period between pulses was employed.

The apparatus shown in Fig. 19 was used to measure the power flow and to observe the pulse shapes. The incidental power was monitored through a 20 db directional coupler with a thermistor and power meter and was controlled by means of the variable attenuator. The incident power was also sampled by a 20 db directional coupler and put through a transmission-type wavemeter, a crystal, and onto vertical channel A on the oscilloscope for observation. The third harmonic output power from the cavity was sampled with a 3 db directional coupler and broad-band crystal; the power level at the crystal was amplified and fed to vertical channel B on the oscilloscope. Reflected power at the fundamental frequency was monitored in the same manner as the third harmonic

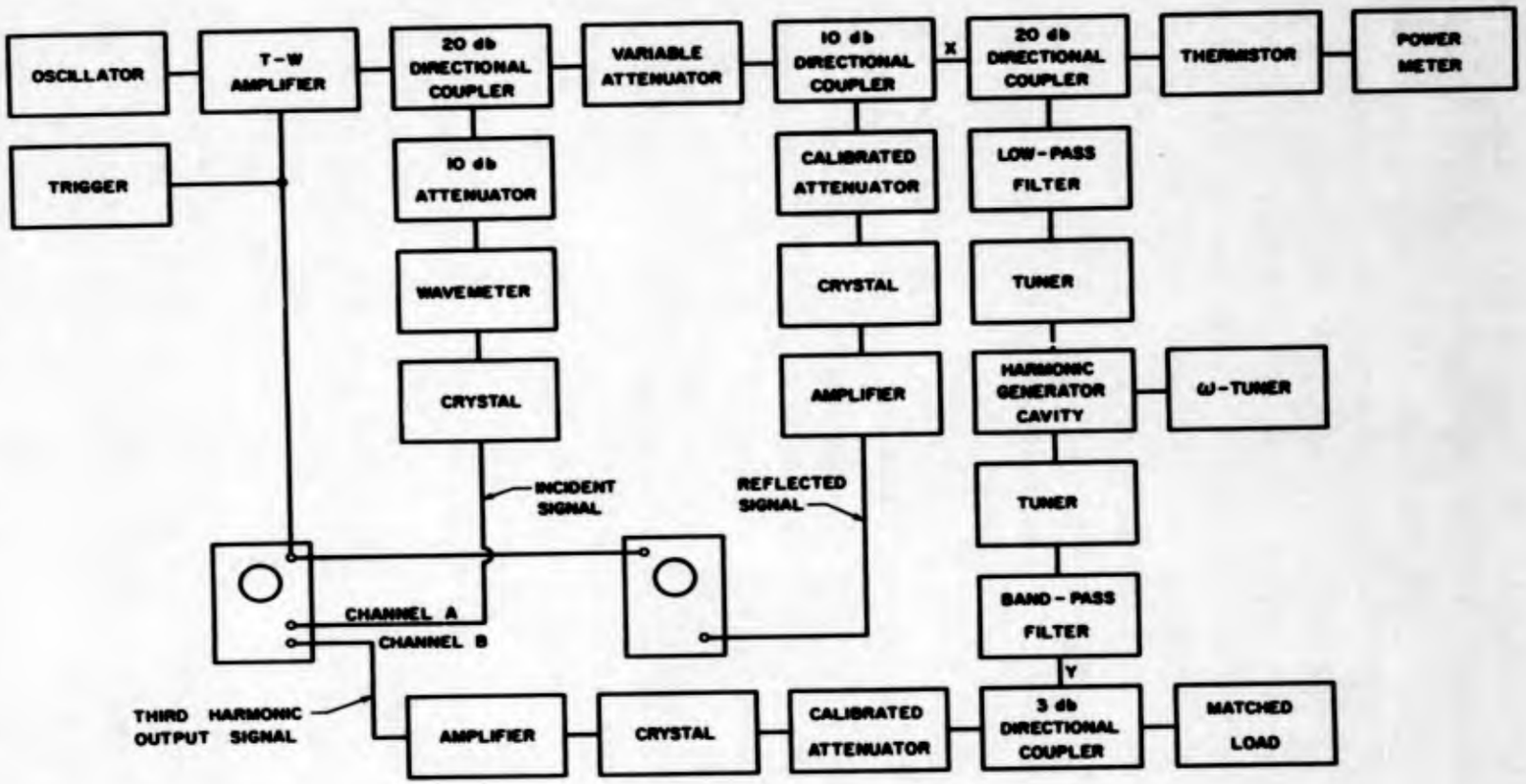

FIG. 19--Block diagram of instrumentation used to perform harmonic generation experiment.

output with a 10 db directional coupler and a second oscilloscope. In each case the precision attenuators were used to obtain a fixed vertical deflection of 2 cm on the oscilloscope. The peak output and reflected powers were then measured by noting the change in the attenuator readings from the calibration level which was obtained by feeding a known amount of power into points X and Y shown in Fig. 19. Appropriate low-pass and band-pass filters were utilized, as shown in Fig. 19, to separate the fundamental and third harmonic signals.

To control the wall temperature of the cavity, a thermoswitch was mounted in the external metallic heat sink surrounding the cavity and was connected in series with a Variac and lead-covered heating cable wrapped around the outside of the heat sink. A thermometer was also inserted in the heat sink to monitor the temperature. Sulfur hexafloride gas was fed into the cavity at atmospheric pressure through a hole drilled in the center of the tapered inner conductor of the cavity as shown in the simplified assembly drawing of the device given in Fig. 20. This served two purposes. The first was to partially cool the dielectric, and the second was to act as an insulator for the prevention of breakdown.

The experimental characteristics of the harmonic generator are given in Figs. 21 and 22. As indicated previously, the ferroelectric material used in this experiment was a ceramic of 73 per cent $BaTiO_3$ - 27 per cent $SrTiO_3$. The equilibrium temperature of the cavity was held at $49^{\circ}C$. The device was observed to triple from 3.010 kMc to 9.030 kMc with the measured conversion efficiency shown in Fig. 21. Figure 22 is a plot of the same data given in Fig. 21, but in a form which demonstrates the dependence of output power upon input power. The experimental results shown in these figures were obtained by adjusting the tuners on the output and input side of the harmonic generator for a match. Viewed together, Figs. 21 and 22 show that output power is proportional to the cube of input power in the region between 0 and 350 w where the conversion efficiency is below 1.5%. Between 350 w and 1000 w the first order saturation effects due to g_{21} occur [see Eq. (53)] and the output power becomes proportional to the square of the input power. In this region the conversion efficiency rises linearly to about 6.5%. Beyond 1000 w of input power, higher order saturation effects apparently

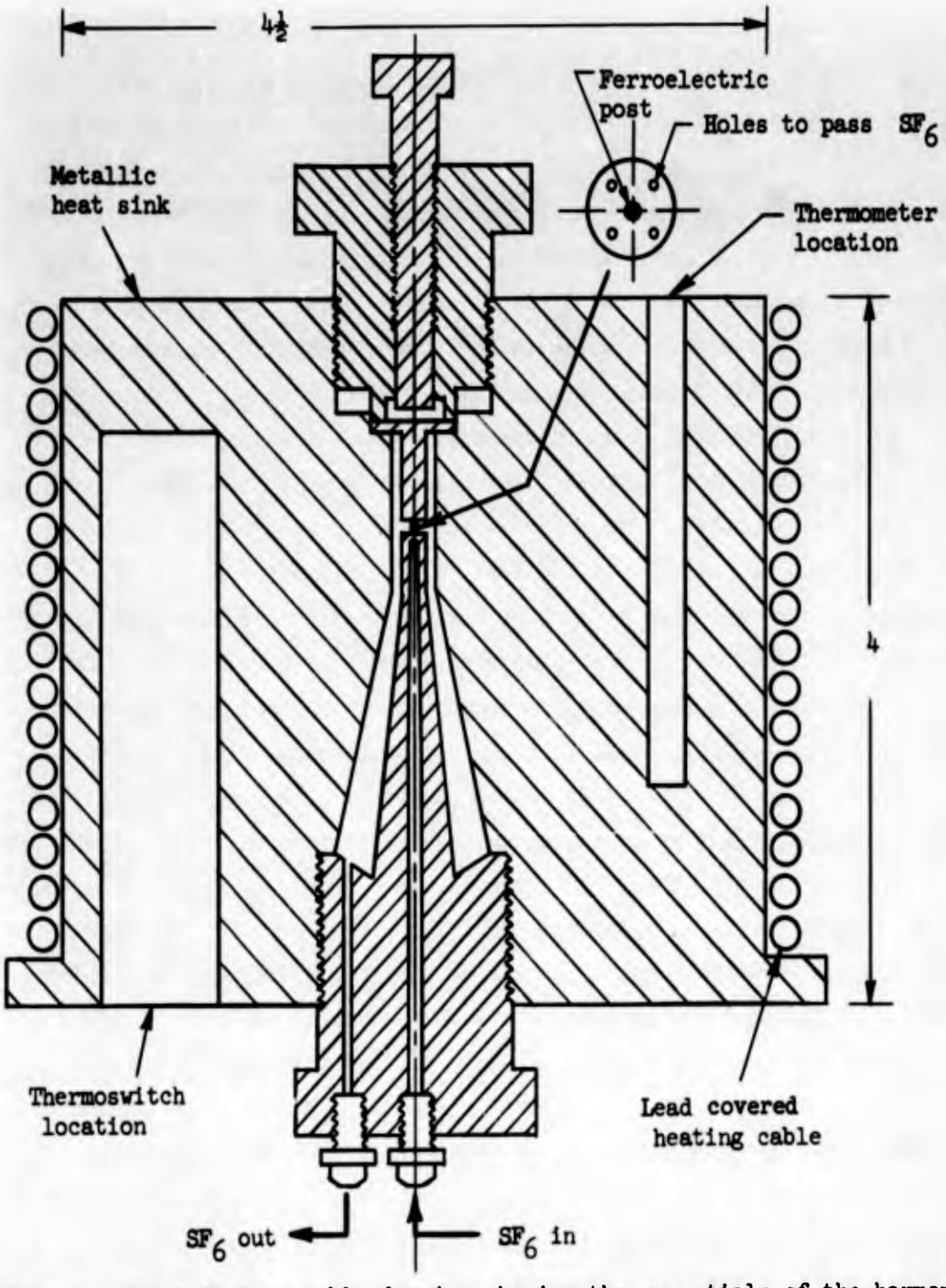

FIG. 20--Simplified assembly drawing showing the essentials of the harmonic generator. The internal cavity dimensions together with the coupling loop locations (not shown here) are given in Fig. 13. The external dimensions given here are included to indicate the overall size of the device; the dimensions of the other parts, external to the cavity, have been omitted since they are not critical. The enlarged drawing of the inner conductor of the cavity shown in the upper right hand portion of the device gives the details of the sample mounting and the arrangement for introducing the sulfur hexafluoride gas (SF_6) into the cavity.

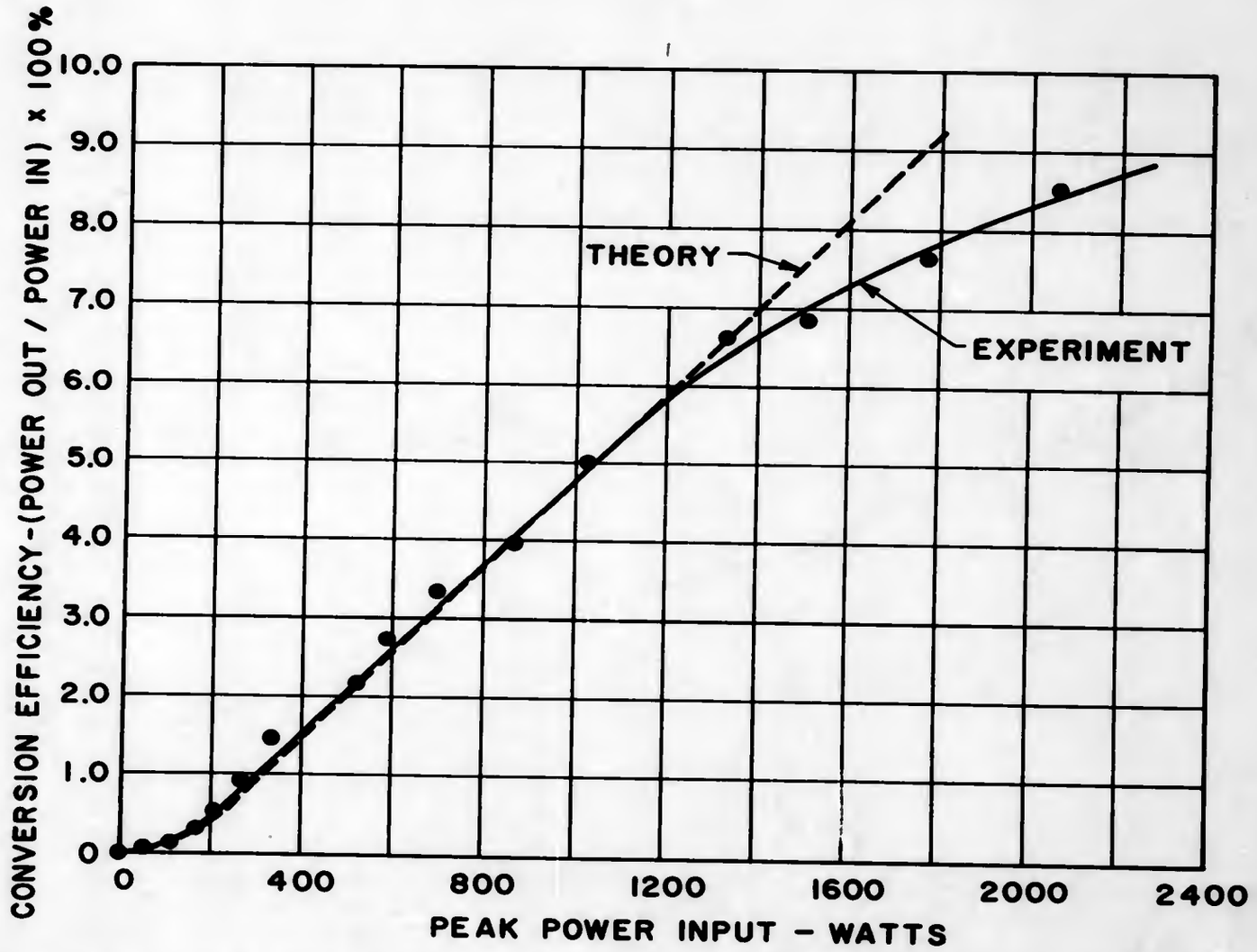

FIG. 21--Measured conversion efficiency of harmonic generator as a function of input power together with theoretical comparison.

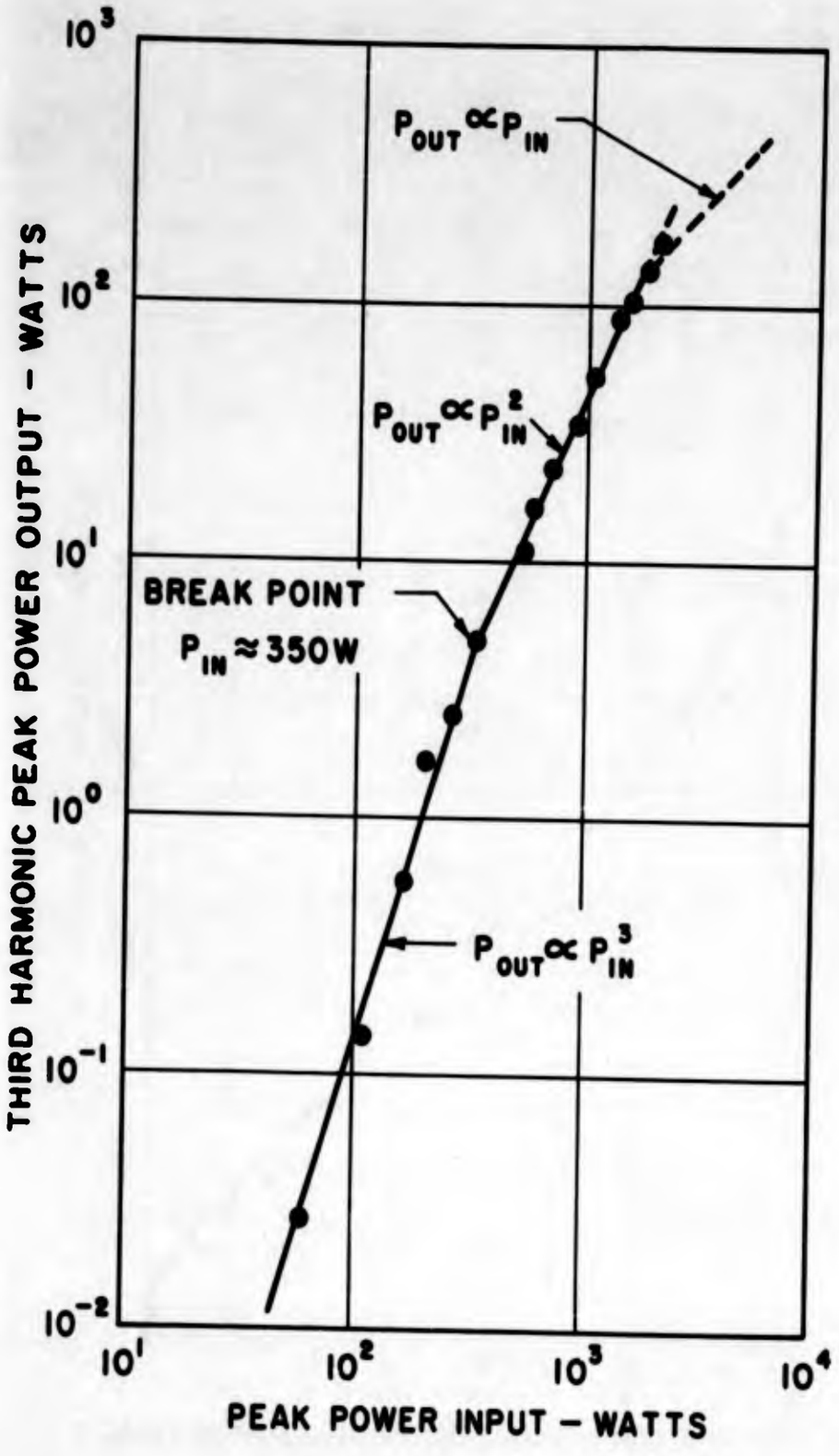

FIG. 22--Third harmonic output power as a function of input power. The slopes of the lines show how output power depends upon input power.

begin to occur and the linear relation between conversion efficiency and input power is no longer realized. The conversion efficiency in this region reaches 8.5% for an input of 2100 w and approaches an extrapolated saturation level of 10% at about 3000 w. Data were taken only up to input powers of 2100 w because breakdown was observed to occur beyond 2200 w.

The theoretical efficiency curve shown in Fig. 21 was derived by matching Eq. (54) to the experimental curve. From the known constants Ω_1 , P_{inc} , and g_{01} the nonlinear coefficients c_2 and g_{21} were determined and were found to have the following values:

$$c_2 = - 2.98 \times 10^{-7} \ \mu\mu f/v^2$$

$$g_{21} = + 1.62 \times 10^{-9} \ \text{mhos}/v^2 \quad .$$

For the case under consideration the value of the linear loss term g_{01} was found to be 2.65×10^{-3} mhos . This value was computed from the small signal X-band value of κ''_1 ($\kappa''_1 = 160$) obtained by other means.[56] The results given in Fig. 21 illustrate two significant points. The first is that the theoretical curve does not deviate from the measured curve up to efficiencies which are greater than half of the extrapolated saturation level; the second is that the experimentally determined values of c_2 and g_{21} are in excellent agreement with those obtained from independent large signal measurements.[1,27] It can therefore be concluded that the theoretical expressions given by either Eq. (53) or Eq. (54) represent an accurate description of the power flow in the harmonic generator when both nonlinear reactive terms and nonlinear loss terms are present simultaneously, as denoted by Eqs. (35) and (36).

The discussion of the heating effects occurring in the dielectric indicates that during the time of the pulse, the temperature of the ceramic post can be expected to increase. Figure 23 shows how these thermal effects distort the pulse shapes. Figure 23(a) is a typical oscilloscope trace photograph of the "on" resonance behavior when $200 < P_{in} < 2000$ w . The 3 kMc incident pulse is 2.3 μsec long and is reasonably square; however, the 9 kMc output pulse and the 3 kMc reflected pulse show considerable distortion. The point to be noted here is that where the output pulse is a maximum, the reflected pulse is a minimum,

which is the condition that one would expect. Figure 23(b) gives typical oscilloscope trace photographs of the 3 kMc incident pulse and the 9 kMc output pulse as functions of frequency when $200 < P_{in} < 2000$ w for a 5 μsec incident pulse. The distortion of the pulses shown here can be explained qualitatively in terms of the heating of the ceramic. During the time of the pulse, the heating of the ceramic causes its small signal dielectric constant to decrease (see Fig. 3). This in turn causes the resonant frequency of the cavity to increase. As a consequence, the output pulse does not reproduce the square-wave shape of the input pulse. It is of interest to note that at high power levels the thermal effects limit the effective pulse width of the third harmonic signal to about 1 μsec and produce time delays of as much as several microseconds between the start of the input pulse and the peak of the output pulse.

Figure 24 gives the measured frequency response of the third harmonic for various incident power levels. The differences in slopes above and below resonance are a direct consequence of the temperature rise in the dielectric just discussed. The extra resonant hump appearing in the upper two curves at $f \approx 3.02$ kMc is due to the nonlinear effects appearing in the coupled circuits of the harmonic generator.

4. Discussion and Determination of the Large Signal Characteristics of the Ferroelectric Ceramic

It is evident from the results of the experiment described in the foregoing paragraphs and the correlation obtained between theory and experiment that at microwave frequencies ferroelectric ceramics exhibit large signal nonlinear characteristics in both the dielectric constant and rf conductivity. The nonlinear behavior of the ceramic of 73 per cent $BaTiO_3$ - 27 per cent $SrTiO_3$ has been used successfully to construct an efficient frequency tripler operating from 3 kMc to 9 kMc. Efficiencies of nearly 10% have been realized with input power levels of 2-3 kw. These performance characteristics are generally much better than what can be expected of diode devices operating in the same frequency range. In addition, the ferroelectric harmonic generator is a high power device capable of generating hundreds of watts of peak power.

The first order nonlinear properties of the 73 per cent barium titanate - 27 per cent strontium titanate ferroelectric ceramic have also been found by fitting the theoretical expression for the conversion

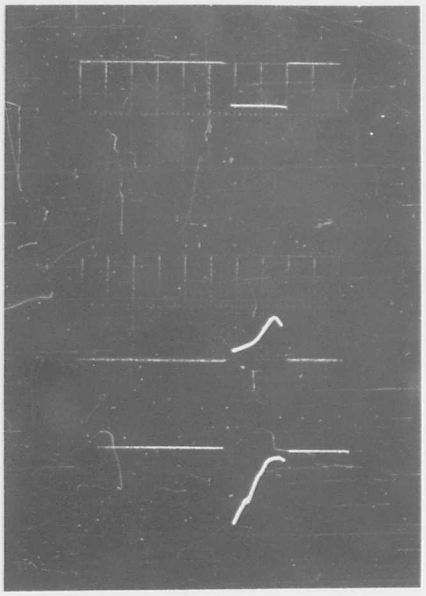

Incident pulse

Output pulse

Reflected pulse

← Time (μ sec/cm)
(a)

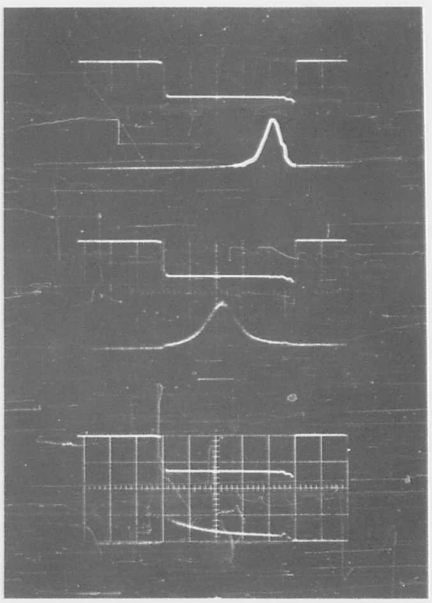

On or below resonance

Above resonance

Far above resonance

← Time (μ sec/cm)
(b)

FIG. 23--Typical pulse shapes observed for harmonic generator. These pulses occur for input powers in the range $200 < P_{in} < 2000$ w .

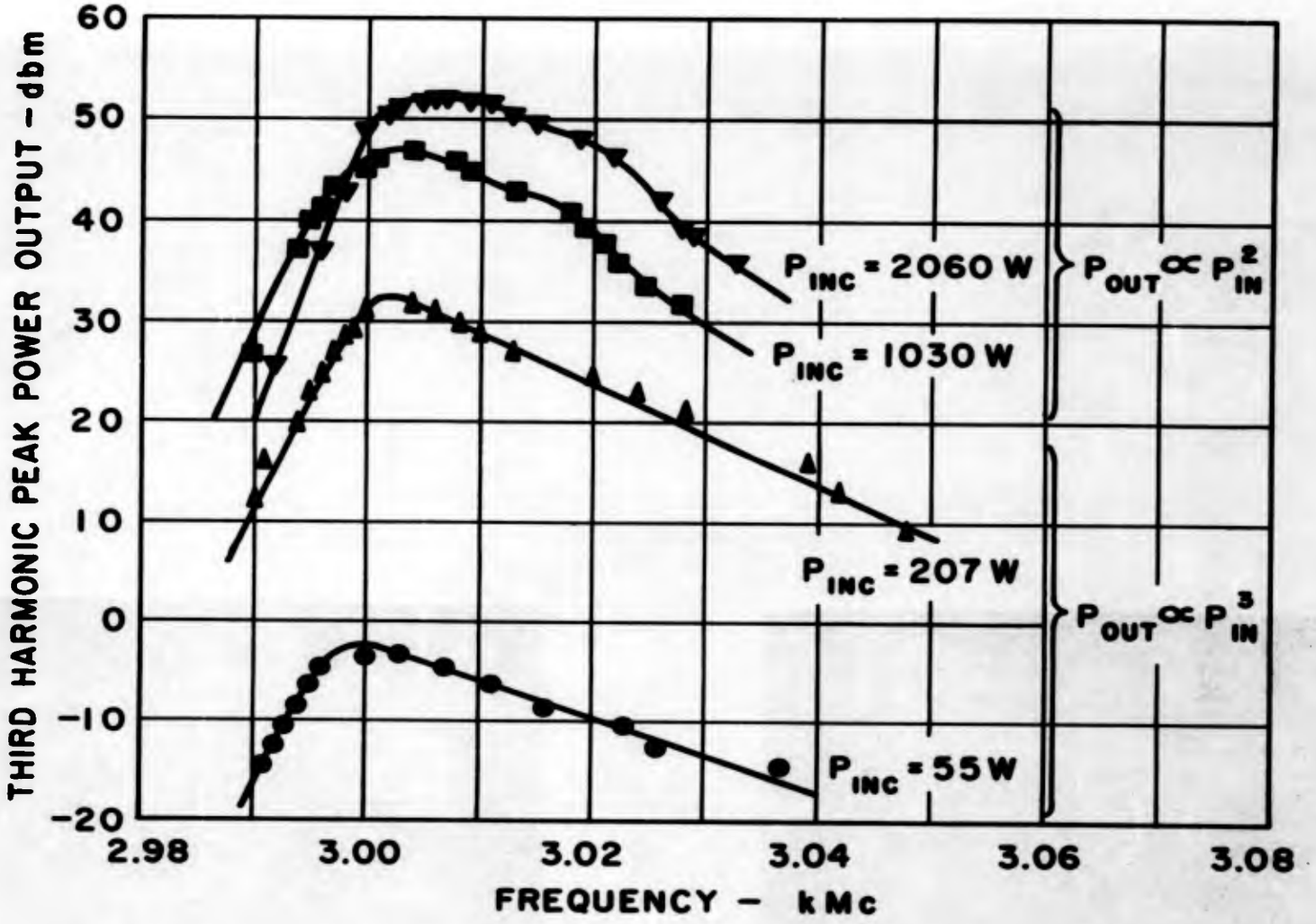

FIG. 24--Third harmonic output power as a function of pump frequency.

efficiency [Eq. (54)] to the measured curve (see Fig. 21). The values so obtained for the nonlinear coefficients c_2 and g_{21} have been used to determine the constants κ'_3 and κ''_3 entering in Eqs. (9) and (10). This has been done by utilizing the expressions for the nonlinear capacitance and conductance given by Eqs. (33) and (34). The resulting values for κ'_3 and κ''_3 are compared in Table I with the values obtained by Johnson[1] from independent large signal measurements. It is clear from this comparison that the results of both experiments are in excellent agreement. This not only demonstrates that the values for the coefficients listed in Table I are correct, but also shows that the circuit analysis of the harmonic generator culminating in Eqs. (53) and (54) accurately describes the behavior of the device. By using the average values of κ'_3 and κ''_3 the large signal nonlinear properties of the ferroelectric titanate ceramic may be cast in the notation of Eqs. (9) and (10) and may be written as

$$\epsilon'(E) = \epsilon_0 \left[2200 - 7.5 \times 10^{-11} E^2\right] \text{ farads/m}$$

$$\sigma(E) = \epsilon_0 \left[160\,\bar{\Omega} + 29 \times 10^{-12}\,\bar{\Omega}\, E^2\right] \text{ mhos/m} \quad ,$$

where E is in volts per meter. The linear terms $\kappa'_1 = 2200$ and $\kappa''_1 = 160$ used in these expressions have been determined from small signal measurements (for details see reference 1). The resultant expressions for $\epsilon'(E)$ and $\sigma(E)$ apply in the temperature range $49 - 52^{\circ}C$ and for field strengths up to $E = 20$ kv/cm . Since the results of the two experiments are in close agreement, it is felt that they accurately describe the first order nonlinear behavior of the ferroelectric ceramic when operated above its Curie point. Since it appears that there is little or no dispersion in the properties of the material in the neighborhood of 3 kMc, these results are considered to be accurate at frequencies somewhat higher and lower than 3 kMc.

Finally, it should be noted that for such device applications as parametric amplification and parametric limiting, the material must be biased in order to have a first order nonlinearity. In this case the nonlinear coefficients will also be functions of bias and may be measured either by using the techniques described herein or by using those described in reference 1.

TABLE I

Comparison of nonlinear coefficients κ'_3 and κ''_3 obtained from harmonic generation and large-signal experiments for ferroelectric ceramic of 73 per cent $BaTiO_3$ - 27 per cent $SrTiO_3$.

Nonlinear Coefficient	Harmonic Generation Experiment	Large-Signal Measurements
κ'_3	-8.4×10^{-11}	-6.5×10^{-11}
κ''_3	$+25 \times 10^{-12}$	$+34 \times 10^{-12}$

C. HARMONIC GENERATION ALONG NONLINEAR TRANSMISSION LINES[57]

The propagation of waves of large amplitude in nonlinear media leads to the progressive distortion of the waves as a function of distance, due to the fact that the different parts of the waves travel with different characteristic phase velocities. This phenomenon, which has long been recognized in mechanical systems, as in the case of finite amplitude sound waves,[58,59] has recently become of interest in electrical systems. When the losses in the nonlinear medium are small, the distortion of the waves will eventually result in the formation of shock waves. Since the process of deforming the wave is accompanied by the generation of harmonic frequencies, such a scheme may be employed as a method for constructing traveling wave frequency multipliers. Devices of this nature would have the advantage over conventional harmonic generators of being extremely wide-band due to the absence of resonant circuits and also of being very simple to fabricate. Moreover, such devices could easily be constructed for frequencies ranging into the optical portion of the spectrum.

The objectives of the present section are to obtain analytic expressions for the power flow in the first few harmonics along nonlinear transmission lines and nonlinear waveguides that are excited by sinusoidal

signals. The analysis of these systems is carried out by conventional perturbation theory, taking as the nonlinear medium a generalized dielectric material having a nonlinear dielectric constant as well as a nonlinear dielectric conductivity. The physical embodiment of such a medium is the ferroelectric ceramic composed of 73 per cent $BaTiO_3$ - 27 per cent $SrTiO_3$ operated above its Curie point (20°C). This material is used throughout to illustrate quantitatively what can be expected of distributed systems comprised of both nonlinear reactance and nonlinear resistance.

At this point it is important to emphasize that in this work both nonlinear reactive and nonlinear loss mechanisms are taken into account in analyzing the deformation of the wave as a function of distance along the line. This is in contrast to the calculations which are usually made concerning shock wave formation in nonlinear dissipative media. It is customary in these calculations to neglect loss terms and higher order nonlinear terms when analyzing the deformation of the wave shape and determining the position of shock formation. When a shock forms there is an equilibrium set up between nonlinear reactive and loss processes and the shape of the front becomes very nearly stationary. In the usual analysis of nonlinear propagation, loss and higher order nonlinear terms are introduced into the calculation only for the purpose of determining the shape of the stationary profile. By making use of this technique, it has been shown that the width of the shock front in ferroelectrics[60] and ferrites[61] is related to the relaxation times of the respective media. A more general theory of shock wave formation along nonlinear transmission lines, with particular emphasis placed on the possibility of using such lines as harmonic generators and as saw-tooth voltage generators, has been given by Khokhlov.[62] His analysis, which applies to nondispersive nonlinear media, treats the case in which linear losses are taken into account during the process of deforming the wave.

The analysis presented herein is limited to the case of weak nonlinearities and to the case where dispersion is absent in the lossless nonlinear terms. The latter restriction implies that the resulting wave form will have high harmonic content and that the harmonics generated along the line will interact strongly with one another. From the results of the analysis of the nonlinear transmission line and the known nonlinear properties of the ferroelectric ceramic a calculation is made of the

expected performance of a rectangular waveguide filled with this nonlinear material, used as a traveling-wave harmonic generator. The general treatment of the waveguide problem shows how the model used in this example must be modified to account for the presence of simultaneous frequency and mode conversion. Lastly, by using the experimental results obtained from the cavity-type ferroelectric harmonic generator, a comparison is made of the relative merit of the cavity vs the traveling-wave device. The comparison brings out the superiority of the resonant system and indicates ways of improving the distributed system.

1. Nonlinear Transmission Lines Utilizing Ferroelectric Ceramics

As a realization of a nonlinear transmission line loaded uniformly with a ferroelectric ceramic, consider a line with distributed linear inductance ℓ per unit length in the series branches and nonlinear distributed shunt capacitance $c(v)$ and conductance $g(v)$ per unit length as illustrated in Fig. 25. Since the voltage and current are uniquely defined on a TEM transmission line and since the electric field intensity E is proportional to the voltage v on the line, the distributed nonlinear capacitance and conductance per unit length can be found from Eqs. (9) and (10) and may be written as

$$c(v) = \sum_{n \text{ even}} c_n v^n \quad , \tag{56}$$

and

$$g(v) = \sum_{n \text{ even}} g_n \bar{\Omega} v^n \quad , \tag{57}$$

where $v = v(z,t)$ is the transmission line voltage. Equations (56) and (57) are functionally identical with Eqs. (33) and (34). The only difference between the two sets of equations is that in this representation $c(v)$ and $g(v)$ refer to the distributed capacitance and conductance per unit length, whereas in Eqs. (33) and (34) they refer to total lumped capacitance and conductance.

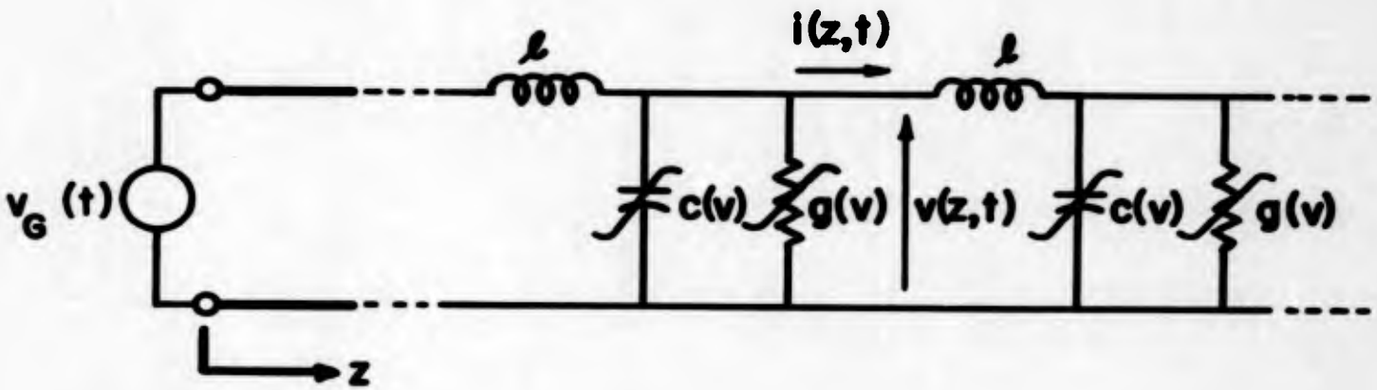

FIG. 25--Circuit model for a nonlinear TEM transmission line using a ferroelectric medium.

The differential equations describing the propagation of TEM waves along the transmission line given in Fig. 25 are

$$\frac{\partial v}{\partial z} = - \ell \frac{\partial i}{\partial t} \tag{58}$$

and

$$\frac{\partial i}{\partial z} = - g(v)\, v - \frac{\partial}{\partial t} [c(v)\, v] \quad . \tag{59}$$

This system of equations constitutes a set of nonlinear hyperbolic differential equations. Calculations of how simple waves, governed by these equations, distort with distance may be obtained by using the method of characteristics which essentially allows one to follow the trajectories of points of constant voltage down the line and thereby follow the progressive deformation of the wave. Riley[48] and Landauer[41,63] have both made use of this method to investigate some of the properties of electromagnetic shock waves occurring in one-dimensional isotropic nonlinear media. The ensuing analysis is concerned with the way in which the amplitudes of the harmonic frequencies grow with distance in response to the distortion of the wave arising from the nonlinearity of the ferroelectric medium. Solutions describing this process of traveling-wave harmonic generation are obtained by developing the line voltage, $v(z\ ,\ t)$, in a perturbation expansion in a manner similar to the one given by Auld[64] for the propagation of finite amplitude waves in gyromagnetic media.

2. Perturbation Solutions

The nonlinear wave equation describing the behavior of the voltage $v(z\ ,\ t)$ along the transmission line illustrated in Fig. 25 can be obtained by eliminating the current $i\ (z\ ,\ t)$ between Eqs. (58) and (59). The resulting equation is

$$\frac{\partial^2 v}{\partial z^2} = \ell c(v) \frac{\partial^2 v}{\partial t^2} + \ell \left[g(v) + 2 \frac{\partial c(v)}{\partial t} \right] \frac{\partial v}{\partial t} + \ell \left[\frac{\partial g(v)}{\partial t} + \frac{\partial^2 c(v)}{\partial t^2} \right] v \ . \tag{60}$$

By making use of the power series expansions for $c(v)$ and $g(v)$ given in Eqs. (56) and (57), it is possible to express Eq. (60) explicitly in

terms of the known nonlinear coefficients c_n and g_n . By assuming that the amplitude of the signal is limited to the case where the inequalities $|c_0| \gg |c_2 v^2|$ and $|g_0| \gg |g_2 v^2|$ hold, and neglecting the higher order nonlinear terms, Eq. (60) becomes

$$\frac{\partial^2 v}{\partial z^2} = \ell c_0 \frac{\partial^2 v}{\partial t^2} + \ell g_0 \bar{\Omega} \left(\frac{\partial v}{\partial t}\right) + 3\ell c_2 \left[v^2 \frac{\partial^2 v}{\partial t^2} + 2v \left(\frac{\partial v}{\partial t}\right)^2 + \frac{g_2}{c_2} \bar{\Omega} \left(v^2 \frac{\partial v}{\partial t} \right) \right] . \quad (61)$$

It is then apparent that the nonlinear terms appearing in this equation are small in comparison to the linear terms and can therefore be treated as a perturbation. This represents the case of most practical interest for ferroelectric materials.

Steady-state solutions to Eq. (61) are sought for the case where the transmission line is excited by a sinusoidal source with angular frequency ω . These solutions can be obtained by noting that at each point along the line the voltage is a periodic function of time, with the fundamental period equal to the period of the forcing function. Accordingly, the voltage can be expressed as a Fourier time series in which the Fourier coefficients are allowed to vary with distance to account for the progressive deformation of the wave. To determine the growth of the harmonic amplitudes with distance, the Fourier coefficients can be expanded as a power series in the parameter $\xi = 3\ell c_2$. The transmission line voltage $v(z, t)$ can therefore be written as

$$v(z, t) = \sum_{k=-\infty}^{\infty} \sum_{p=0}^{\infty} \xi^p V_k^{(p)}(z) \, e^{jk\omega t} , \quad (62)$$

where $V_k^{(p)*}$ is equal to $V_{-k}^{(p)}$ in order to have $v(z, t)$ be a real quantity.

It is now possible to reduce the problem to the solution of a set of linear ordinary differential equations by substituting Eq. (62) into Eq. (61). By performing this substitution and equating equal powers of ξ and invoking the orthogonality relations for the terms $\exp(jk\omega t)$,

one obtains the following system of inhomogeneous equations:

$$\frac{d^2 V_k^{(0)}}{dz^2} - \gamma_k^2 V_k^{(0)} = 0 \tag{63a}$$

$$\frac{d^2 V_k^{(p)}}{dz^2} - \gamma_k^2 V_k^{(p)} = \sum_{m,n=-\infty}^{\infty} \sum_{s=0}^{p-1} \sum_{r=0}^{s} \left\{ \left[\omega^2 (m-n)^2 + 2\omega^2 (k-m)\, n - j\omega (m-n)\, \xi_k \right] V_{k-m}^{(r)} V_n^{(s-r)} V_{m-n}^{(p-1-s)} \right\} , \tag{63b}$$

where $\xi_k = g_{2k}/c_2$ has been introduced for convenience, and γ_k^2 is the square of the complex propagation constant of the k^{th} harmonic along the linearized line and is given by

$$\gamma_k^2 = - k^2 \omega^2 \ell c_0 + jk\omega g_{0k} \quad . \tag{64}$$

The system of inhomogeneous differential equations given by Eqs. (63) applies in the frequency domain. In obtaining these equations the operator $\bar{\Omega}$ appearing in Eq. (61) has been eliminated by applying it to each of the spectral components included in the terms $\partial v/\partial t$ and $v^2 (\partial v/\partial t)$ where v is given by Eq. (62). When this is one, one finds in a manner exactly analogous to the discussion following Eqs. (42) and (43) that the coefficient g_n is multiplied by $k\omega$. In Eqs. (63) and (64) use has been made of this fact by introducing for the sake of brevity the notation $g_{nk} \equiv k\omega g_n$.

The governing equations describing the propagation of a wave in a generalized nonlinear dielectric medium containing both nonlinear reactive and nonlinear resistive components are given by Eqs. (63) and (64). Since the nonlinearity of the dielectric material is an even function of voltage, it is easily seen that a sinusoidal excitation at the fundamental frequency $\omega/2\pi$ will only generate odd harmonic frequency $k\omega/2\pi$ along the line.

Equations (63) can be integrated successively to any order in p to obtain approximate solutions. By assuming that the transmission line

is infinite and that the generator voltage is given by

$$v_G(t) = \tfrac{1}{2} V_G \left(e^{j\omega t} + e^{-j\omega t}\right) \quad , \tag{65}$$

the boundary conditions at the two ends of the line can be written as

$$V_{\pm 1}^{(0)}(0) = \tfrac{1}{2} V_G \; ; \; V_{\pm 1}^{(p)}(0) = 0 \quad \text{for} \quad p \geq 1 \quad , \tag{66}$$

$$V_k^{(p)}(0) = 0 \quad \text{for} \quad |k| \neq 1 \quad ,$$

and

$$V_k^{(p)}(z) \quad \text{satisfies a radiation condition as } z \to \infty \quad . \tag{67}$$

The relations $V_k^{(p)}(0) = 0$ for $|k| \neq 1$ given in Eq. (66) imply that at the input end of the nonlinear line provisions are made to filter out all of the harmonic frequencies by providing a parallel arrangement of ideal filters, the k^{th} filter having zero impedance at the k^{th} harmonic and infinite impedance at all other frequencies. This is shown schematically in Fig. 26. It should also be noted that the relation $V_{\pm 1}^{(0)}(0) = V_G/2$

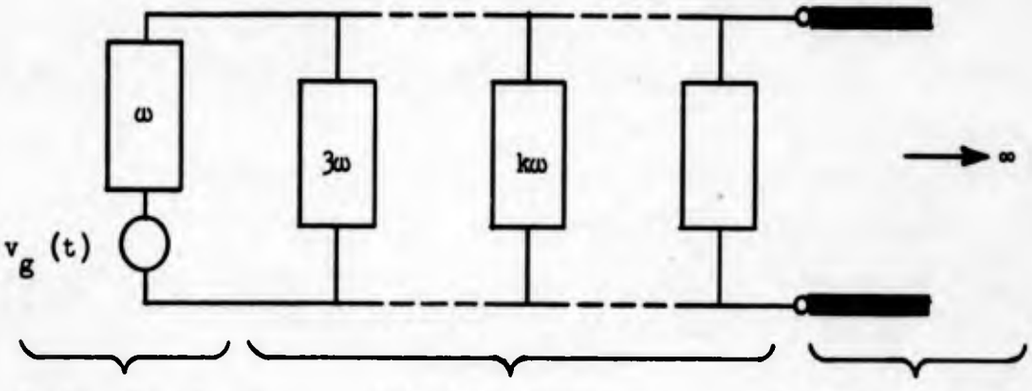

FIG. 26--Illustrative circuit showing the input circuit of the nonlinear transmission line. This circuit arrangement physically provides the desired boundary conditions given by Eq. (66).

given in Eq. (66) implies that the voltage source at the input end of the line is in series with an ideal filter which only passes the fundamental, and that this series combination is in parallel with the harmonic filters (Fig. 26). Solutions to Eqs. (63) can be obtained in a simple and direct manner by using, for example, Laplace transforms. Approximate solutions for the fundamental, third, and fifth harmonic frequencies have been found by carrying through the analysis to second order using this technique. The resulting expressions which describe the behavior of the harmonic amplitudes $v_k(z\ ,\ t)$ can be conveniently written as

$$v_k\ (z\ ,\ t) = A_k(z) \cos\ (k\omega t - \beta_k z) + B_k(z) \sin\ (k\omega t - \beta_k z) \quad , \qquad (68)$$

where β_k is the phase constant of the k^{th} harmonic determined from Eq. (64). The response functions $A_k(z)$ and $B_k(z)$ are listed in Appendix G for $k = 1, 3, 5,$ as Eqs. (G. 1) through (G. 6). The superposition of the harmonic amplitudes given in Eq. (68) analytically describes the progressive distortion of the wave launched on the nonlinear transmission line.

The power transfer on the line can be computed from the relation

$$P(z) = \frac{1}{2\pi} \int_0^{2\pi} i(z\ ,\ \omega t)\ v\ (z\ ,\ \omega t)\ d\ (\omega t) \quad , \qquad (69)$$

where the voltage, $v(z\ ,\ \omega t)$, is given by

$$v(z\ ,\ \omega t) = \sum_{k=1}^{\infty} v_k(z\ ,\ k\omega t) \quad , \qquad (70)$$

and the current, $i(z\ ,\ \omega t)$, is found by integrating Eq. (58):

$$i(z\ ,\ \omega t) = -\frac{1}{\omega t} \int \frac{\partial v(z\ ,\ \omega t)}{\partial z}\ d\ (\omega t) \quad . \qquad (71)$$

The static contribution has been omitted from Eq. (71) since it does not contribute to the power flow. By making use of the orthogonality relations for the sine and cosine terms it can be shown that Eqs. (69), (70) and (71) reduce to

$$P(z) = \sum_{k=1}^{\infty} P_k(z) \quad , \qquad (72)$$

where $P_k(z)$ is the power flow in the k^{th} harmonic and is given by

$$P_k(z) = \frac{1}{2Z_0}\left[A_k^2(z) + B_k^2(z)\right] + \frac{1}{2\beta_k Z_0}\left[A_k(z)\frac{\partial B_k(z)}{dz} - B_k(z)\frac{\partial A_k(z)}{\partial z}\right]. \quad (73)$$

In the derivation of this formula it has been assumed that the linear losses in the system are small enough that the approximation $\beta_k \approx k\omega\sqrt{\ell c_0}$ can be made. The parameter Z_0 used here refers to the characteristic impedance of the transmission line $(Z_0 = \sqrt{\ell/c_0})$.

An examination of the functions $A_k(z)$ and $B_k(z)$ reveals that the expressions for the power flow in the harmonic frequencies depend explicitly upon the amplitude of the generator voltage V_G . At microwave frequencies, it is desirable to relate these expressions to the power delivered by the generator P_G which is directly amenable to measurement. This can be accomplished by noting that at $z = 0$, $P_G = P(z)$. From Eqs. (G. 1) through (G. 6) for $A_k(z)$ and $B_k(z)$ and Eqs. (72) and (73) it is easily shown that

$$P_G = \frac{1}{2Z_0} V_G^2 + \frac{3}{16}\frac{\omega^2 Z_0 c_0 c_2}{\beta_1^2} V_G^4 \quad , \quad (74)$$

and that the power in the harmonics vanishes at $z = 0$. The first term appearing on the right hand side of Eq. (74) gives the power transfer on an infinite linear line while the second term represents the effect of the distributed nonlinearity.

The results of the preceding perturbation analysis show that the power flow along the nonlinear transmission line is divided among the propagating harmonics, as one would expect. Due to the presence of loss, the power transfer in the harmonics initially grows with distance, reaches a maximum, and rapidly attenuates thereafter. As a consequence, when the losses are moderately large, the amplitudes of the harmonics will not be sufficient to cause shock wave formation.

3. An Example

Based upon the results given in Eqs. (73) and (74) and the approximate solutions listed in Eqs. (G.1) through (G.6), the performance of a traveling-wave harmonic generator utilizing the ferroelectric ceramic of 73 per cent $BaTiO_3$ - 27 per cent $SrTiO_3$ will now be discussed. As a specific example, consider the case of a rectangular waveguide completely filled with this material as shown in Fig. 27(a). The waveguide illustrated in section A-A of this figure is assumed to be excited in the TE_{10} mode at the fundamental frequency $f = 3$ kMc via the standard size S-band guide (inside dimensions 7.214×3.404 cm). The waveguide height has been reduced in the ferroelectric section in order to build up the field strength and hence the voltage at the center of the guide for a given amount of input power. In the example considered here the waveguide height has been chosen to be $b = 0.5$ cm. To eliminate reflection losses at the ferroelectric interface it is assumed that suitably designed impedance matching sections are placed on the input and output sides of the ferroelectric section. For matching at one frequency these can take the form of simple quarter-wave transformers or for matching over a band of frequencies more elaborate schemes may be employed such as discussed in Chapter III regarding the X-band phase shifter. It should be noted that in this example the transverse variations in fields are not taken into account. However, in the general nonlinear transmission line problem these field variations must be included since they introduce mode conversion. This effect is treated in the next section.

An approximate equivalent transmission line circuit for the waveguide can be obtained by equating the transmission line characteristic impedance $(Z_0 = \sqrt{z/y})$ to the impedance of the TE_{10} mode defined on a power-voltage basis,[65] and by equating the transmission line propagation constant $(\gamma = \sqrt{zy})$ to the propagation constant of the TE_{10} mode. Here z and y are, respectively, the series impedance per unit length and the shunt admittance per unit length of the transmission line. The resulting equivalent transmission line circuit is illustrated in Fig. 27(b). The linear shunt inductance $(a/2b)(a^2/\pi^2)\,\mu_0$ per unit length which accounts for the dispersion characteristics of the TE_{10} mode has been drawn dotted since the susceptance of this element is negligible in comparison to the linear susceptance of the shunt capacitance due to the extremely high

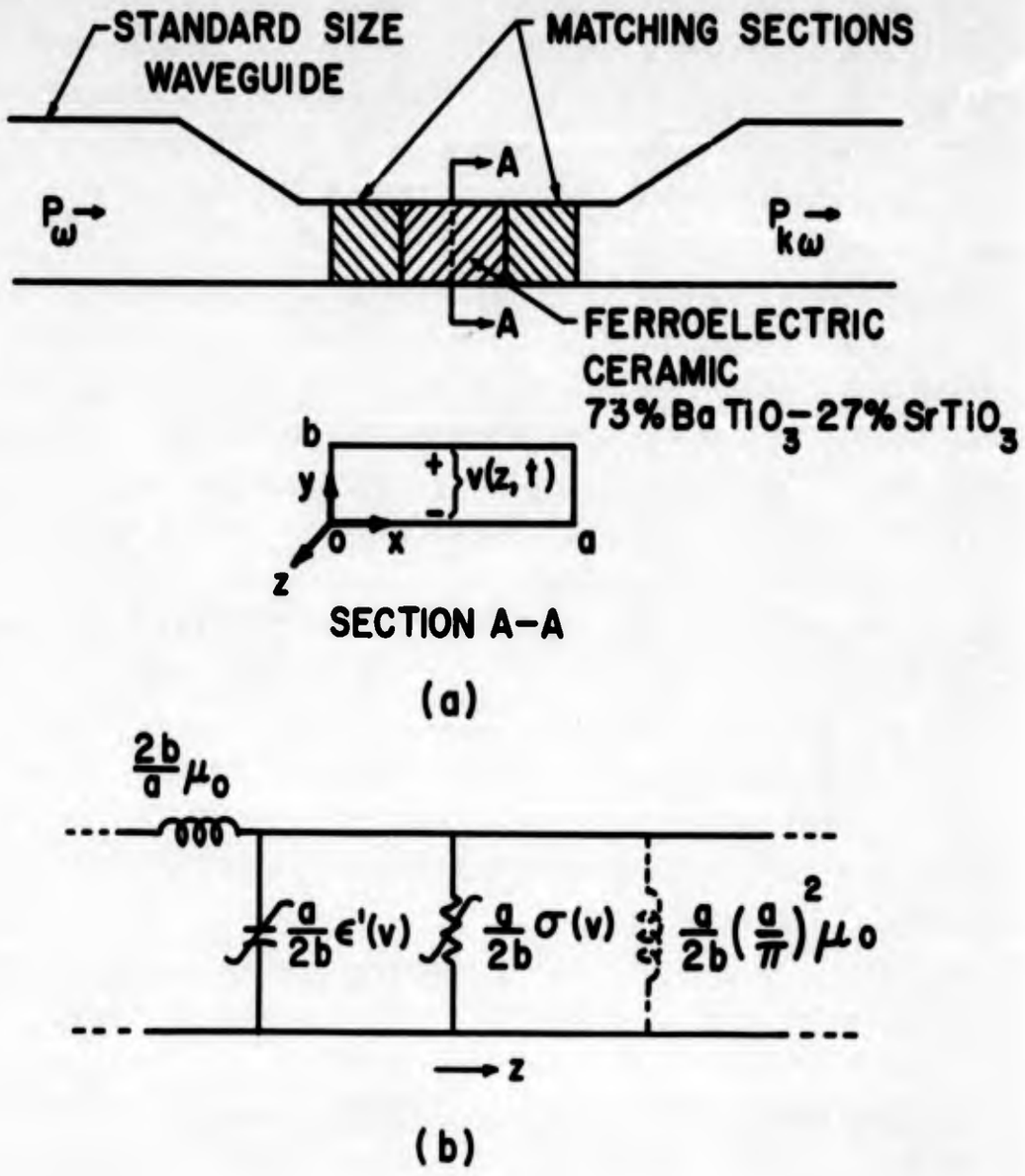

FIG. 27--Waveguide version of a ferroelectric traveling-wave harmonic generator: (a) longitudinal section, (b) equivalent circuit.

permittivity of the ferroelectric. At the fundamental frequency of 3 kMc, the equivalent circuit therefore approaches that of a TEM transmission line. Accordingly, assuming that provisions are made for the suppression of higher order modes, the uniform waveguide structure becomes a simple realization of a nonlinear transmission line propagating a TEM-like wave at microwave frequencies, and will serve to demonstrate the behavior of the functions derived above.

The large signal microwave characteristics of the ferroelectric ceramic of 73 per cent $BaTiO_3$ - 27 per cent $SrTiO_3$ are known in the temperature range 49 - 52° [see Eqs. (12) and (13)]. Since the voltage and field strength at the center of the guide are related by $v = E\,b$, one can compute the parameters entering in the functions $A_k(z)$ and $B_k(z)$. Then, by using Eq. (74) to determine V_G , the power flow in the various frequencies can be computed from Eqs. (73) and (G. 1) through (G. 6). The results of the computations for the present example are shown in Fig. 28 for generator powers [equal to P_ω in Fig. 27(a)] of 10^6 and 10^7 watts. These power levels give field strengths of 3 kv/cm and 9.5 kv/cm , respectively, at the center of the guide, and are consistent with the conditions required for the perturbation solution to be valid. It is evident from these considerations that for experimental purposes it would be necessary to drive the system shown in Fig. 27(a) from a pulsed source.

The curves shown in Fig. 28 clearly demonstrate the effects of the losses in the nonlinear transmission line. The linear loss terms present a certain attenuation to each frequency component generated along the line, while the nonlinear loss terms not only provide attenuation but at the same time are partly responsible for the conversion of energy to higher harmonics. The net effect of the reactive and the resistive frequency conversion mechanisms and the overall losses in the system is to cause the power flow in the harmonic frequencies to initially build up in a manner analogous to what takes place on the lossless line, to reach a maximum which does not necessarily occur at the same position for each harmonic, and to attenuate for large distances.

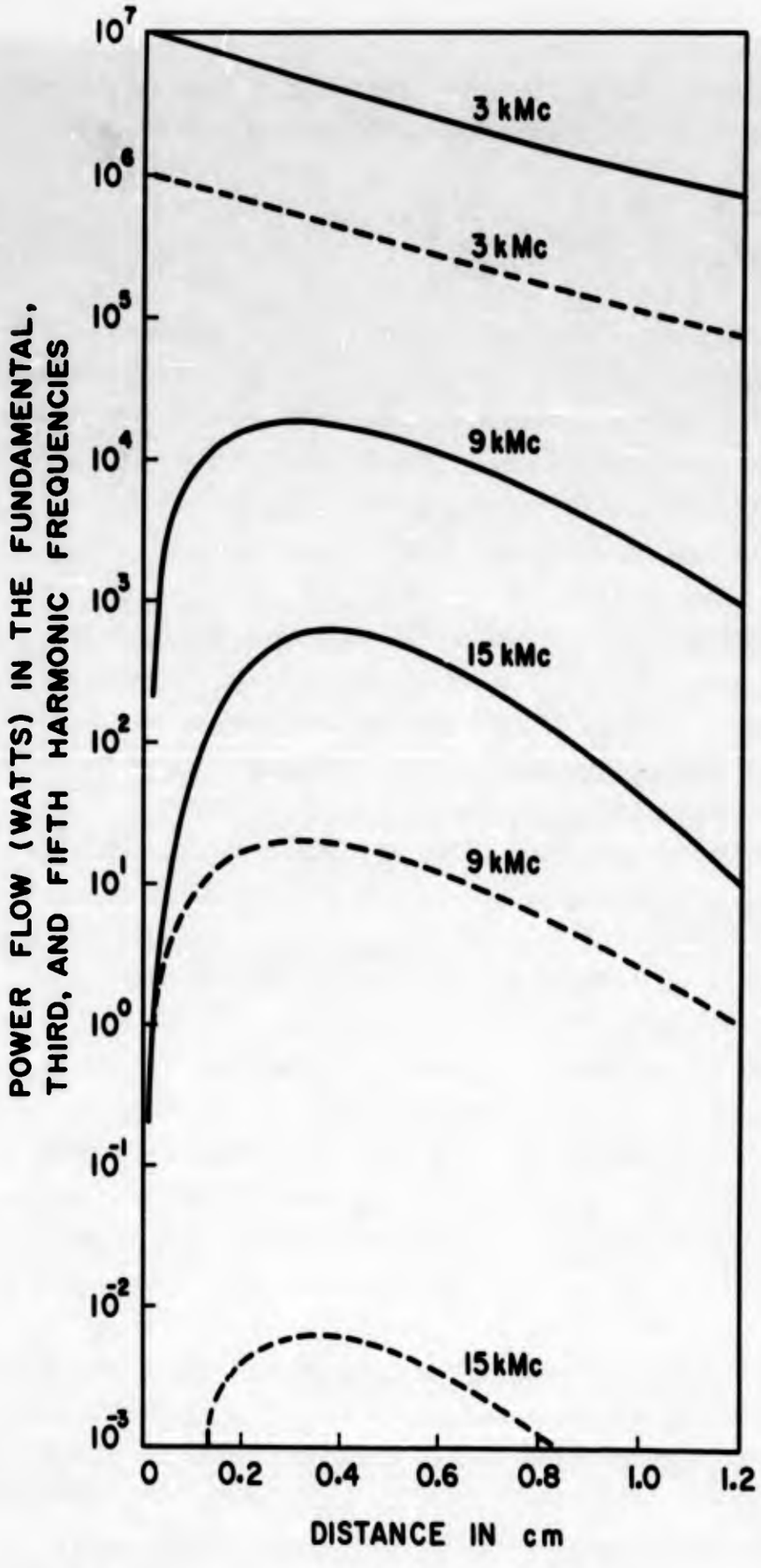

FIG. 28--Calculated power flow in the fundamental, third, and fifth harmonic frequencies. The dashed curves apply for 10^6 watts while the solid curves apply for 10^7 watts.

The conversion efficiency $\eta_k(z)$ for the k^{th} harmonic generated along the nonlinear transmission line may be defined by the relation

$$\eta_k(z) = \frac{P_k(z)}{P_1} \times 100\% \quad , \tag{75}$$

where $P_1 = P_G$ is the net power transferred into the nonlinear section at the fundamental frequency. The conversion efficiency is plotted in Fig. 29 for the third and fifth harmonics for an input power of 10^7 watts. Since power is lost at the fundamental frequency due to circuit losses as well as to conversion losses, there exists a critical length z_{crit}, over which the power level is high enough to cause appreciable frequency conversion. From the curves given in Fig. 29 it can be seen that, for obtaining optimum traveling-wave interaction between fundamental and third harmonic frequencies, $z_{crit} \approx 0.3$ cm . For $z > z_{crit}$ the attenuation of the fundamental signal is great enough to decrease the nonlinear coupling to the point where all frequencies effectively propagate approximately independently along the lossy line.

The results given in Figs. 28 and 29 show that it is possible to generate considerable harmonic power with the traveling-wave scheme, but with low conversion efficiency. By comparing this device with the cavity-type device one might expect that the distribtuted system would require about Q times the drive power necessary for the lumped system. In addition, due to the lower circuit impedance of the distributed system and to the loss of energy to undesired higher harmonics, one might further expect that the conversion efficiency of the distributed system would be much less than what is obtainable from the lumped system. The cavity-type ferroelectric frequency tripler operating from 3 kMc to 9 kMc discussed above serves to illustrate these points. This device was observed to give a third harmonic conversion efficiency of 8.5 per cent for a peak input power of 2000 watts. By comparing the input powers of 10^6 - 10^7 and 2200 watts required to drive the traveling-wave and cavity-type devices, respectively, it becomes apparent that these input powers are essentially related by the Q of the cavity which was approximately 1000. Furthermore, the measured conversion efficiency of 8.5 per cent is about 40 times better than the theoretical prediction for the traveling-wave device.

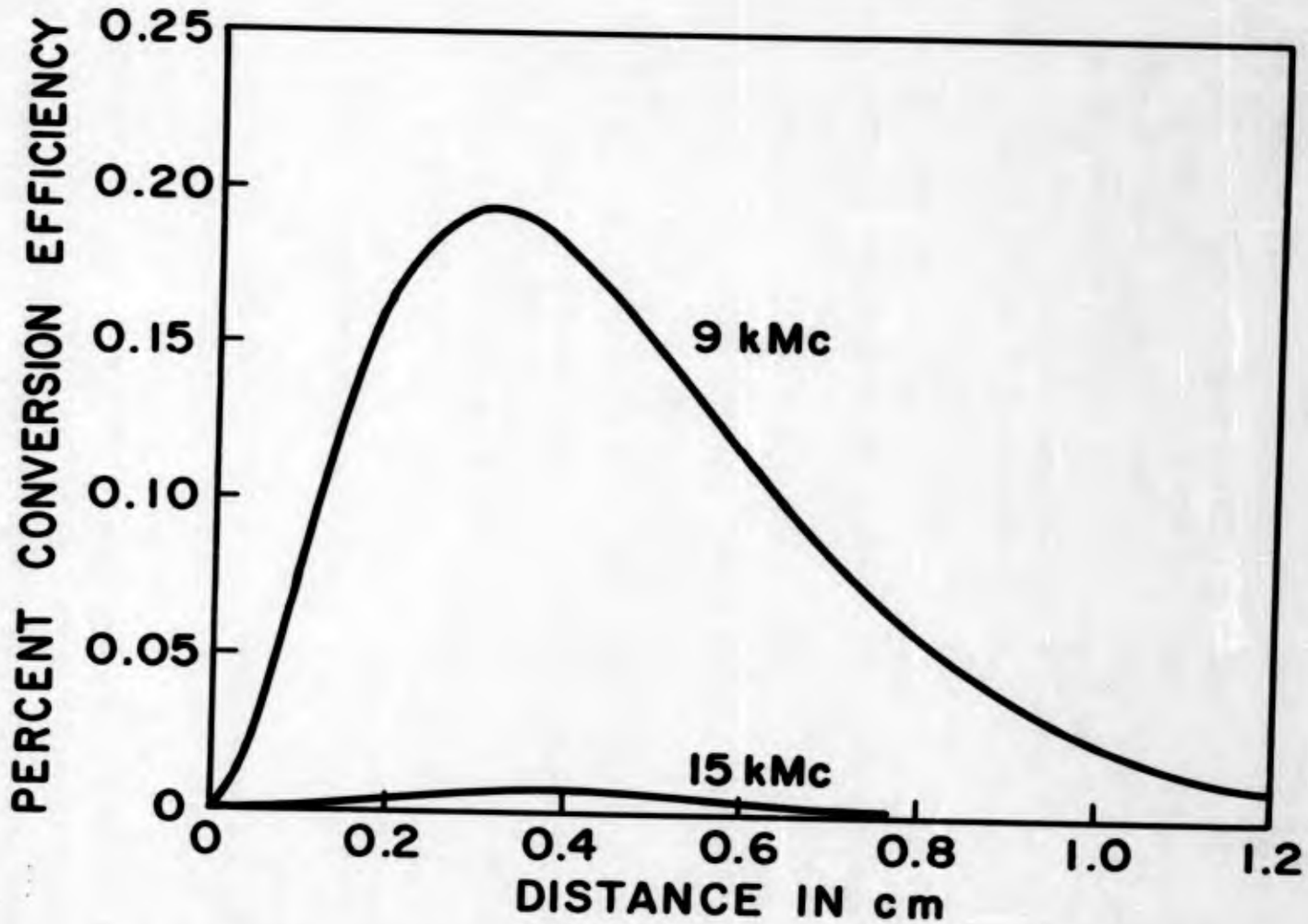

FIG. 29--Conversion efficiency from fundamental to third and fifth harmonics.

The contrast between these devices clearly demonstrates the superiority of the lumped system. It should be noted, however, that it may be possible to construct efficient traveling-wave harmonic generators by using circuits which have distributed filter characteristics such as periodic structures. Circuits of this nature have two highly desirable features. The first is that they have a much higher impedance level than uniform transmission lines, and the second is that they can be designed to suppress the unwanted harmonics by filtering them out. Both of these properties directly contribute to improving the conversion efficiency of traveling-wave systems. As an application of these principles, it has been shown[66] that high efficiency frequency doubling can be obtained by using a dispersive distributed circuit having a low-pass filter characteristic which cuts off between the second and third harmonics. Aside from the considerations concerned with conversion efficiency, it should be emphasized that harmonic generators employing distributed circuits have the advantage over lumped circuits of being broadband or of being able to generate harmonic power over a wide range of frequencies.

D. HARMONIC GENERATION IN NONLINEAR WAVEGUIDES

The problem treated in the preceding section dealt specifically with a nonlinear TEM transmission line where voltage and current are uniquely defined and have the same value throughout the entire transverse plane. In the more general waveguide problem this is not the case since the variations in the transverse fields must be taken into account. Thus, treating the waveguide as a TEM structure, as discussed above, is only an approximation which allows one to estimate the process of traveling-wave harmonic generation in ferroelectric ceramics at microwave frequencies. Due to the nonlinearity of the dielectric medium and the transverse variations in the fields, a different value of permittivity is associated with each point in the transverse plane of the waveguide. These transverse variations in permittivity are of considerable importance since they are responsible for the presence of mode conversion in nonlinear waveguides. The effect that the transverse variations in permittivity have upon the propagation of a wave may be seen qualitatively by noting that it is possible to derive distributed constant networks for field problems by

using finite difference techniques.[67,68] As an example, consider the two-dimensional transmission line network representing the TE_{h0} modes in a uniform rectangular waveguide filled with a lossless nonlinear dielectric as shown in Fig. 30.[1] From this network representation it is apparent that, in contrast to the linear problem, when the dielectric medium is nonlinear, the phase velocity of the wave is different for each point in the transverse plane since each of the component longitudinal lines has a different relative excitation level due to the properties of the mode distribution. Thus in the nonlinear waveguide the variations in the transverse fields cause the mode distribution of the wave to be progressively deformed or, what is essentially the same, cause the propagation of a wave in one mode to be broken up into a set of normal modes. Similarly, the longitudinal variations of the wave cause progressive distortion of the wave as a function of distance and the simultaneous generation of harmonic frequencies.

To analyze the nonlinear waveguide problem, consider a cylindrical waveguide of arbitrary cross-section completely filled with ferroelectric for $z > 0$ as shown in Fig. 31. Assume that the guide is illuminated by an incident wave in one mode, i.e., in the region $z < 0$ let

$$\vec{E}(\vec{r}, t) = a\,[\vec{e}_i(\vec{\rho}) \exp(j\omega t - \gamma_i z) + c.c.]$$
$$\vec{H}(\vec{r}, t) = a\,[\vec{h}_i(\vec{\rho}) \exp(j\omega t - \gamma_i z) + c.c.] \quad , \tag{76}$$

where $\vec{\rho}$ is the transverse position vector, a is the amplitude of the signal, the subscript i refers to the incident mode, and c.c. denotes the complex conjugate. At each point within the waveguide the fields must satisfy Maxwell's equations,

$$\nabla \times \vec{E} = -\frac{\partial \vec{B}}{\partial t}$$
$$\nabla \times \vec{H} = \vec{I} + \frac{\partial \vec{D}}{\partial t} \quad , \tag{77}$$

---

[1] It is evident from this equivalent circuit that, for the case of plane wave (or TEM wave) propagation, the transverse coupling vanishes; hence, the two-dimensional transmission line network reduces to a degenerate set of ordinary one-dimensional transmission lines.

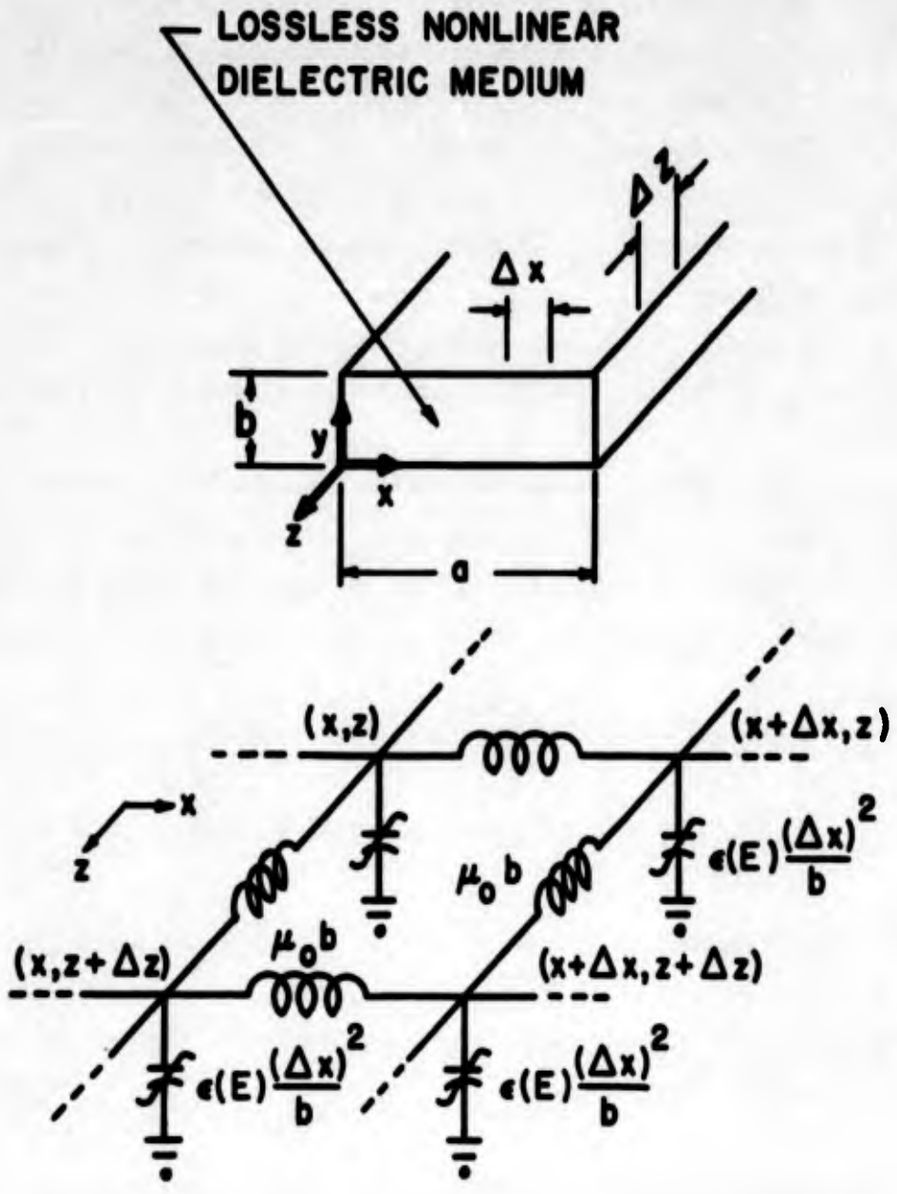

FIG. 30--Two-dimensional transmission line network representing the TE_{n0} modes in a uniform rectangular waveguide filled with a lossless nonlinear dielectric medium. This circuit applies when $\Delta x = \Delta z$.

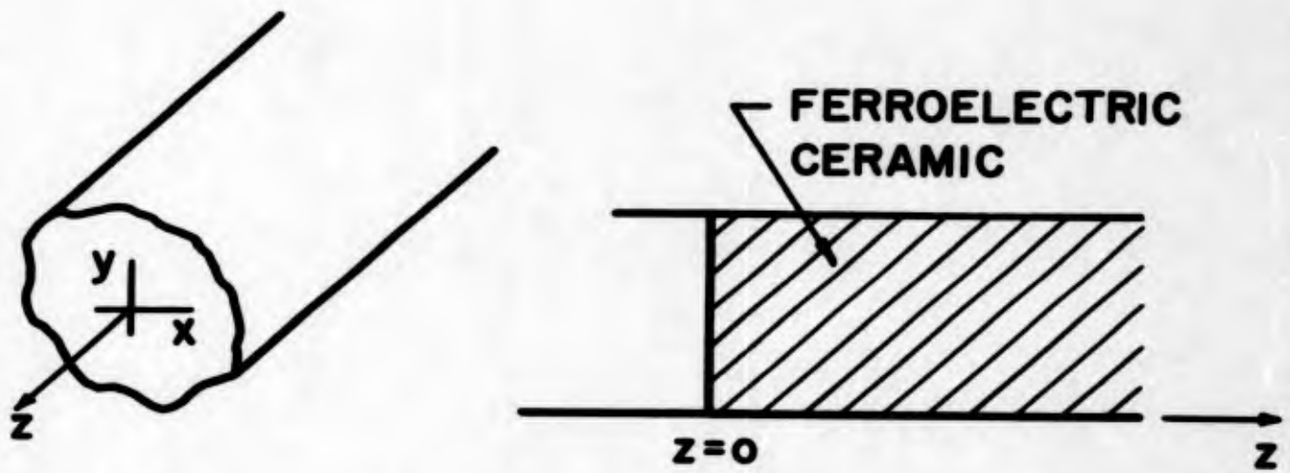

FIG. 31--Arbitrary cylindrical waveguide completely filled with ferroelectric ceramic medium in the region $z > 0$.

where $\vec{D}$ and $\vec{I}$ are given by Eqs. (9) and (10), respectively. As discussed above in connection with Eq. (62), steady-state solutions to Eqs. (77) are sought in the form of a Fourier time series, and, since the response is a function of the strength of the excitation, they are also sought as a power series in the amplitude a of the drive. Thus, one can write

$$\vec{E}(\vec{r}\,, t) = \sum_{k=-\infty}^{\infty} \sum_{p=1}^{\infty} a^p \vec{E}_k^{(p)}(\vec{r})\, e^{jk\omega t} \tag{78a}$$

and

$$\vec{H}(\vec{r}\,, t) = \sum_{k=-\infty}^{\infty} \sum_{p=1}^{\infty} a^p \vec{H}_k^{(p)}(\vec{r})\, e^{jk\omega t}\,, \tag{78b}$$

where $\vec{E}_k^{(p)*} = \vec{E}_{-k}^{(p)}$, and $\vec{H}_k^{(p)*} = \vec{H}_{-k}^{(p)}$. The perturbation scheme used here is somewhat different from the one used in the solution of the transmission line problem, where the Fourier coefficients were expanded as a power series in the parameter multiplying the nonlinear terms in the differential equation [see Eqs. (61) and (62)]. The choice of the present perturbation method is dictated by the fact that when one is dealing with a set of nonlinear vector equations as given by Eqs. (77) this technique allows one to obtain solutions more conveniently. After substituting Eqs. (78) into Eqs. (77) and employing Eqs. (9) and (10), it can be shown [by using the orthogonality of the $\exp(j\omega t)$ terms and equating terms with the same power of p] that the following set of linear inhomogeneous boundary value problems results:

$$\nabla \times \vec{E}_k^{(p)} = -jk\omega\mu_0 \vec{H}_k^{(p)} \tag{79a}$$

$$\nabla \times \vec{H}_k^{(p)} = jk\omega\epsilon_0(\kappa'_1 - j\kappa''_1)\vec{E}_k^{(p)} + \sum_{m,n=-\infty}^{\infty} \sum_{s=1}^{p-1} \sum_{r=1}^{p-s-1} jk\omega\epsilon_0(\kappa'_3 - j\kappa''_3)\left[\vec{E}_{m-n}^{(r)} \cdot \vec{E}_n^{(p-s-r)}\right]\vec{E}_{k-m}^{(s)}\,. \tag{79b}$$

In deriving these equations the amplitude of the signal has been restricted to the case where only the first two terms in the power series expansions given by Eqs. (9) and (10) are of significance. Equations (79a) and (79b) represent the three-dimensional generalization of Eqs. (63a) and (63b).

Equations (79) can be integrated successively to obtain solutions to any order in p. The boundary conditions which must be imposed on these equations are the usual conditions on the waveguide walls together with the continuity relations at $z = 0$ given by

$$\vec{E}_{\pm 1}^{(1)}(\vec{\rho}) = (1 + \Gamma)\,\vec{e}_i(\vec{\rho}) \quad ; \quad \vec{E}_{\pm 1}^{(p)}(\vec{\rho}) = 0 \quad \text{for} \quad p = 2,3,4 \ldots$$

$$\vec{H}_{\pm 1}^{(1)}(\vec{\rho}) = (1 - \Gamma)\,\vec{h}_i(\vec{\rho}) \quad ; \quad \vec{H}_{\pm 1}^{(p)}(\vec{\rho}) = 0 \quad \text{for} \quad p = 2,3,4 \ldots \qquad (80)$$

$$\vec{E}_k^{(p)}(\vec{\rho}) = 0 \quad ; \quad \vec{H}_k^{(p)}(\vec{\rho}) = 0 \quad \text{for} \quad |k| = 2,3,4 \ldots$$

and a radiation condition as $z \to \infty$. Here Γ is the reflection coefficient for the fundamental owing to the discontinuity at $z = 0$, and it is assumed, as discussed above in connection with Fig. 26, that all harmonics are short-circuited at $z = 0$. In the process of successively integrating Eqs. (79) to build up approximate solutions, it should be noted that for each value of p the inhomogeneous terms appearing in these equations constitute a known distribution of sources which can be expanded in the normal modes of the problem under consideration. Thus the inhomogeneous terms analytically describe the generation of higher order modes within the waveguide. The significance of these higher order mode solutions is that a finite number of them will not be cut off in the diclectric loaded guide. Hence, the power flow in the guide will not only exist in a series of harmonic frequencies but also in a finite set of propagating modes. If provisions are not made to extract the power in all of the existing modes at any one frequency, the efficiency of harmonic generation will be greatly reduced from the case of the nonlinear transmission line propagating a single TEM mode. The power transfer in the k^{th} harmonic and the n^{th} mode, $P_{k,n}(z)$, can be computed from Poynting's theorem and the orthogonality relations for the modes. The conversion efficiency from the fundamental to the k^{th} harmonic and n^{th} mode, $\eta_{k,n}(z)$, may be written

as

$$\eta_{k,n}(z) = \frac{P_{k,n}(z)}{P_{in}} \times 100\% \quad , \tag{81}$$

where P_{in} is the net power input at $z = 0$.

The solutions to the waveguide problem represented by Eqs. (78), (79), and (80) may now be applied to the example of the rectangular waveguide excited in the TE_{10} mode discussed above. From the form of the nonlinearity and the symmetry of the problem one would expect that odd harmonics will be generated as well as all TE_{n0} modes where n is an odd integer. The calculation outlined in Appendix H shows that this is indeed the case. Equation (H. 10) of Appendix H is an expression for the electric field generated within the ferroelectric medium. It can be seen from this equation, which is correct to third order, that both third harmonic fields are generated as well as higher order modes (e.g., the TE_{30} mode). Thus, one can generally expect the power flow in the guide to be split into a large number of propagating modes and harmonics. By comparing the solutions in Appendices G and H, it is apparent that the growth of the harmonic amplitudes (in each mode) is very similar to the transmission line response functions $A_k(z)$ and $B_k(z)$. In addition, the mode conversion properties of the system have the same analytic form as the frequency conversion properties. One can therefore conclude that the power generated in the TE_{10} mode at the third harmonic given in Fig. 28 is less than the values predicted due to the power lost in the other propagating modes, especially the TE_{30} mode.

E. CONCLUSIONS

The material presented in this chapter has been concerned with harmonic generation in ferroelectric ceramics. The cavity-type harmonic generator described in detail in section B represents the first successful large signal microwave device application of ferroelectric ceramics. Moreover, in the analytic description of the device it has been found possible to explain the causes for saturation in the input - output characteristics of the device. It is of interest to compare the efficiency of third

harmonic generation obtained here with that obtained by other investigators using different nonlinear materials. Chang[44] has experimented with germanium point contact diodes and has reported measuring third harmonic conversion efficiencies of about 2 per cent for tripling at 6.6 kMc. This should be compared to the conversion efficiency of 8.5 per cent measured with the ceramic of 73 per cent $BaTiO_3$ - 27 per cent $SrTiO_3$. Ferrites also find considerable use as harmonic generators; however, these materials are used primarily in frequency doubling applications. As frequency doublers ferrites usually give conversion efficiencies somewhat less than 10 per cent, although Melchor, Ayres, and Vartanian[69] have reported measuring efficiencies as high as 25 per cent. Based upon these considerations, it appears that from the device standpoint ferroelectrics are certainly competitive with diodes and ferrites in applications dealing with frequency multiplication.

The problem of wave propagation in nonlinear dielectric media comprising nonlinearities in both the dielectric constant and the dielectric conductivity has also been treated in this chapter. By using perturbation techniques the steady-state response of nonlinear TEM transmission lines and nonlinear cylindrical waveguides of arbitrary cross-section has been obtained. For nonlinear lossy dielectric media the perturbation method of developing solutions represents a simple and direct way of treating the propagation problem. Basically, the solutions found for the amplitudes of the harmonic fields generated along the line describe how the progressive deformation of a wave may be synthesized by Fourier series. The results of the solutions for the nonlinear transmission line have been applied to the problem of traveling-wave harmonic generation, where quantitative results have been obtained by using the known large signal characteristics of a ferroelectric ceramic of 73 per cent $BaTiO_3$ - 27 per cent $SrTiO_3$ as a model of the nonlinear dielectric. These results not only predict what can be expected of traveling-wave harmonic generators utilizing ferroelectric ceramics, but also describe the analytic behavior of the functions derived herein.

Generally speaking, traveling-wave harmonic generators are not as efficient as cavity-type devices, and require significantly more drive power due to the absence of the resonant circuits. The lower efficiencies obtained from the traveling-wave devices are primarily due to the existence of a large number of undesired harmonic frequencies and a finite number of

higher order propagating modes, each of which extracts available power from the harmonic (and mode) of interest. In addition, the impedance level of traveling-wave devices is to a great extent the controlling factor in determining the amount of harmonic power generated, and since it is relatively low for uniform transmission lines it causes the conversion efficiency for devices of this nature to be poor. As a consequence, it is necessary to employ dispersive distributed circuits which reactively filter out the unwanted frequencies and modes in a manner akin to the behavior of resonant circuits, and at the same time have impedance levels which are favorable for the process of harmonic generation. The major advantages of the traveling-wave device are the possibility of having broadband interaction and the relative simplicity of construction which is especially attractive in the millimeter wave and optical regions.

CHAPTER V

SUMMARY AND CONCLUSIONS

The prevailing objective of this report has been to describe through both analysis and experimentation how ferroelectric ceramics can be used in microwave device applications. To this end the work has been divided into three parts. The first part, comprising Chapter II, deals specifically with the current known microwave properties of the ferroelectric titanates as well as with a brief description of the outstanding physical characteristics of these materials. The titanate material discussed most extensively and used throughout the course of this investigation is the ceramic composition of 73 per cent $BaTiO_3$ - 27 per cent $SrTiO_3$.

The major portion of the work reported herein is devoted to the remaining two parts which constitute Chapters III and IV. Chapter III deals with the small signal microwave applications of ferroelectric ceramics. In the first portion of this chapter the general incremental behavior of phase shifters, attneuators, and tunable cavities is given in considerable detail. The incremental formulas expressed as Eqs. (18), (19), and (23) are all independent of the specific ferroelectric material and of the configuration of the device in which it is incorporated. On the experimental side, the latter portion of the chapter describes the design and construction of an X-band ferroelectric phase shifter. Although the performance of this device is at best marginal (see Figs. 7, 11, and 12), it clearly demonstrates the limitations of ferroelectrics in small signal devices and further shows what important design considerations are made for a typical application.

Lastly, the material of Chapter IV treats in some detail the problems of harmonic generation in ferroelectric ceramics in cavity-type devices and along nonlinear transmission lines. These analyses are novel in the sense that they include provisions for both nonlinear reactive and nonlinear

resistive mechanisms for frequency multiplication, and in addition, each analysis gives a rather complete circuit description of the behavior of the device. Most other studies of harmonic generation reported in the literature have avoided analyzing a particular circuit configuration in detail. As a consequence, these analyses have usually been incapable of predicting saturation phenomena. Moreover, studies of traveling-wave harmonic generation have not given due consideration to the process of mode conversion in nonlinear waveguides which accompanies the process of frequency conversion.

From the results of the experiments performed on the ferroelectric frequency tripler (see Figs. 21, 22, and 24) it appears that the most promising application of ferroelectrics is in large signal devices. This is based upon the fact that with presently available ferroelectrics, which are far from ideal from the microwave standpoint, third harmonic conversion efficiencies of nearly 10 per cent can be realized.

At the present time, the general use of ferroelectrics in microwave devices appears to be impractical, except in certain specialized cases. This is due to the low material Q (typically between 10 and 20) and to the extremely high dielectric constant (typically between 1000 and 2000) of these materials. Nevertheless, ferroelectrics do have the potential of replacing ferrites in a variety of applications such as phase shifting, cavity tuning, parametric amplification, and harmonic generation. In each of these applications the materials could be used up to wavelengths of 3 to 6 millimeters and would be biased with <u>electric</u> rather than magnetic fields. This is not meant to infer that ferroelectrics can replace ferrites in all types of microwave devices. For example, ferrites have the unique property of being gyromagnetic which makes such nonreciprocal devices as isolators, circulators, and gyrators possible.

Finally, it seems justified that further work should be done on investigating the large signal characteristics of the materials in the presence of dc bias. By applying a bias to the material, the nonlinearity becomes directly proportional to the rf field and becomes a function of dc bias. From these large signal characteristics one could evaluate the possibility of using ferroelectrics in device applications involving parametric amplification, parametric limiting, and frequency doubling.

It would also be of interest to continue the work on traveling-wave harmonic generation by performing some experiments to test the theory of Chapter IV and by doing additional work on distributed nonlinear filter circuits. A very graphic illustration of why this work on traveling-wave harmonics is of interest can be found by referring to Fig. 24 which demonstrates just how narrow-band the cavity-type harmonic generators are. The traveling-wave device has the obvious advantage of being wide-band. As a final observation one should note, above all, that since any device is as good as the materials of which it is comprised, much important work in the future will be directed toward understanding and improving the microwave characteristics of ferroelectric materials.

APPENDIX A

SKIN EFFECT PROPERTIES OF FERROELECTRIC CERAMICS

In the steady state, when all field quantities vary as $\exp(j\omega t)$, the fields within the ferroelectric ceramic are governed by Maxwell's equations

$$\nabla \times \vec{E} = - j\omega \mu_0 \vec{H} \quad , \tag{A. 1}$$

and

$$\nabla \times \vec{H} = j\omega \epsilon_0 \kappa' (1 - j \tan \delta) \vec{E} \quad . \tag{A. 2}$$

By making use of Ohm's law $\vec{i} = \sigma \vec{E}$ and by eliminating $\vec{H}$ between Eqs. (A. 1) and (A. 2), one obtains the wave equation for the rf current density $\vec{i}$ in the dielectric medium

$$\nabla^2 \vec{i} + \left(\frac{\omega}{c}\right)^2 \kappa' (1 - j \tan \delta) \vec{i} = 0 \quad , \tag{A. 3}$$

where c is the velocity of light in free space.

To determine the skin depth in the ceramic, consider a semi-infinite slab of material in which $\vec{i}$ varies with the depth of penetration (taken to be the x-direction). By assuming that the current flow is limited to the z-direction or is parallel to the surface of the slab, Eq. (A. 3) becomes

$$\frac{d^2 i_z}{dx^2} + \left(\frac{\omega}{c}\right)^2 \kappa' (1 - j \tan \delta) i_z = 0 \quad . \tag{A. 4}$$

The solution to this equation which vanishes at $x = \infty$ may be written as

$$i_z = i_0 e^{- px} \quad , \tag{A. 5}$$

where $p^2 = -\left(\frac{\omega}{c}\right)^2 \kappa' (1 - j \tan \delta)$ and i_0 is the current density at $x = 0$. Since $\kappa' > 1000$ and $\tan \delta < 0.1$, one finds from the expression for p^2 that the factor which determines the decay of current in the dielectric is $\exp\left[-\frac{1}{2} \left(\frac{\omega}{c}\right) \sqrt{\kappa'} \tan \delta \, x\right]$. Finally, by defining the skin depth Δ as the distance at which the current density is attenuated by a factor of e^{-1} of its value at the surface, one has

$$\Delta = \frac{2}{\left(\frac{\omega}{c}\right) \sqrt{\kappa'} \tan \delta} \quad . \qquad \text{(A. 6)}$$

APPENDIX B

THE INCREMENTAL BEHAVIOR OF ELECTRICALLY TUNABLE PHASE SHIFTERS

In order to determine the general incremental behavior of ferroelectric phase shifters, consider the arbitrary waveguide configuration shown in Fig. B. 1, where reference planes 1 and 2 are chosen sufficiently far from the junction so that all higher order modes are vanishingly small at these points.

It is desired to find the incremental change in phase shift $\Delta\phi$ for an incremental change in complex permittivity $\Delta\epsilon$ of the nonlinear ceramic. The system is assumed to be well matched so that reflection losses can be neglected. In addition, wall losses are taken to be negligible in comparison to the losses occurring within the ferroelectric.

Within the volume bounded by reference planes 1 and 2 the fields must satisfy Maxwell's equations:

$$\begin{aligned} \nabla \times \vec{E} &= -j\omega\mu_0 \vec{H} & \nabla \times \vec{E}' &= -j\omega\mu_0 \vec{H}' \\ \nabla \times \vec{H} &= j\omega\epsilon \vec{E} & \nabla \times \vec{H}' &= j\omega(\epsilon + \Delta\epsilon)\vec{E}', \end{aligned} \tag{B. 1}$$

where the primed quantities refer to the conditions existing after ϵ has been changed to $\epsilon + \Delta\epsilon$. Assume that the fields at reference plane 2 can be represented in terms of the fields at reference plane 1 by

$$\begin{aligned} \vec{E}_2 &= \vec{E}_1 e^{-\eta - j\phi} & \vec{E}_2' &= \vec{E}_2' = \vec{E}_1' e^{-\eta' - j\phi'} \\ \vec{H}_2 &= \vec{H}_1 e^{-\eta - j\phi} & \vec{H}_2' &= \vec{H}_1' e^{-\eta' - j\phi'} \end{aligned}$$

where ϕ is the phase shift through the device, and η is the attenuation of the signal at reference plane 2 relative to reference plane 1. For small

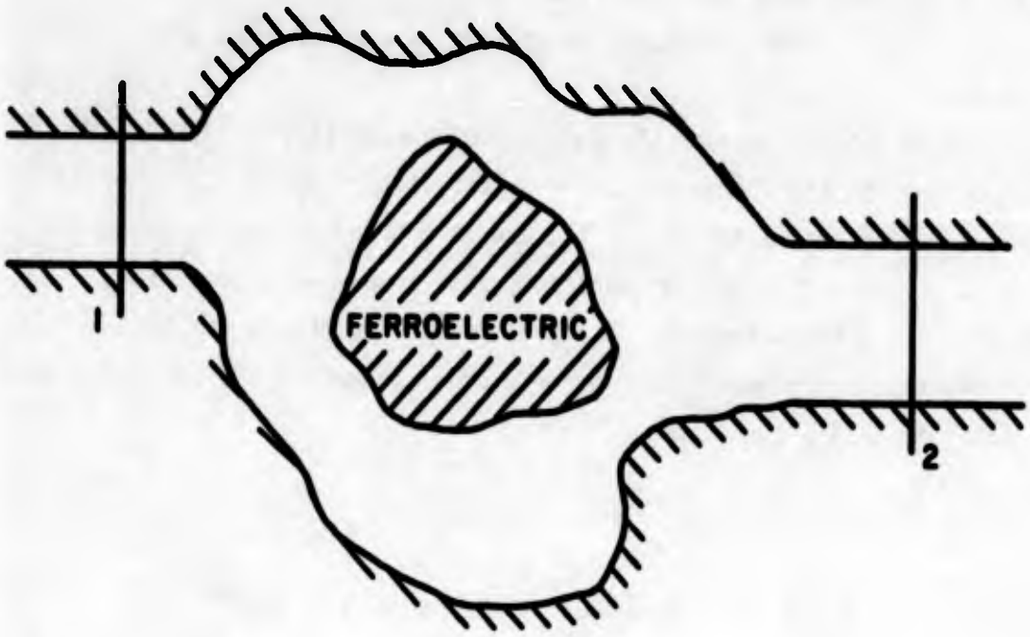

FIG. B. 1--Arbitrary waveguide configuration with ferroelectric.

changes in ϵ , one can write

$$\vec{E}' = \vec{E} + \Delta\vec{E}$$
$$\vec{H}' = \vec{H} + \Delta\vec{H} \qquad \text{(B. 3a)}$$

and

$$\phi' = \phi + \Delta\phi$$
$$\eta' = \eta + \Delta\eta \quad , \qquad \text{(B. 3b)}$$

where $\Delta\vec{E}$ and $\Delta\vec{H}$ represent the changes in the fields due to the change in ϵ and $\Delta\phi$ and $\Delta\eta$ are, respectively, the change in phase shift and attenuation.

The incremental phase shift $\Delta\phi$ can be computed by considering the vector identity

$$\nabla \cdot (\vec{E} \times \vec{H}'^* - \vec{E}' \times \vec{H}^*) = \vec{H}'^* \cdot (\nabla \times \vec{E}) - \vec{H}^* \cdot (\nabla \times \vec{E}')$$
$$- \vec{E} \cdot (\nabla \times \vec{H}'^*) + \vec{E}' \cdot (\nabla \times \vec{H}^*) \quad , \qquad \text{(B. 4)}$$

where * denotes the complex conjugate. By taking the volume integral of Eq. (B. 4) over the volume V enclosed between reference planes 1 and 2 and by converting the volume integral on the left hand side to a surface integral, one obtains the relation

$$\oint_S (\vec{E} \times \vec{H}'^* - \vec{E}' \times \vec{H}^*) \cdot d\vec{a}$$
$$= j\omega\mu_0 \int_V (\vec{H}' \cdot \vec{H}^* - \vec{H}'^* \cdot \vec{H})\, dv$$
$$+ j\omega\epsilon_0 \int_{V-V_f} (\vec{E}'^* \cdot \vec{E} - \vec{E}' \cdot \vec{E}^*)\, dv$$
$$+ j\omega\epsilon^* \int_{V_f} (\vec{E}'^* \cdot \vec{E} - \vec{E}' \cdot \vec{E}^*)\, dv$$
$$+ j\,\omega\Delta\epsilon^* \int_{V_f} \vec{E}'^* \cdot \vec{E}\, dv \quad , \qquad \text{(B. 5)}$$

where use has been made of Eq. (B. 1). In deriving this equation, the volume integral containing terms in ϵ has been broken up into an integral over the volume of the ferroelectric V_f (the only place where the permittivity is complex and can undergo a change) and an integral over the remaining volume $V - V_f$ enclosed by the surface S. Due to the boundary conditions on the waveguide walls the surface integral vanishes everywhere except at the two reference planes S_1 and S_2. For a constant input signal at reference plane 1 (i.e., $\vec{E}_1' = \vec{E}_1$ and $\vec{H}_1' = \vec{H}_1$) it is found, by substituting Eqs. (B. 2) and (B. 3b) into Eq. (B. 5), that

$$
\begin{aligned}
&2j \sin \Delta\phi \, e^{-2\eta - \Delta\eta} \int_{S_2} (\vec{E}_1 \times \vec{H}_1^*) \cdot d\vec{a} \\
&= 2\omega\mu_0 \int_V \mathrm{Im}\,(\vec{H}' \cdot \vec{H}^*)\, dv - 2\omega\epsilon_0 \int_{V-V_f} \mathrm{Im}\,(\vec{E}'^* \cdot \vec{E})\, dv \\
&- 2\omega\epsilon^* \int_{V_f} \mathrm{Im}\,(\vec{E}'^* \cdot \vec{E})\, dv + j\,\omega\Delta\epsilon' \int_{V_f} (\vec{E}'^* \cdot \vec{E})\, dv \quad , \qquad \text{(B. 6)}
\end{aligned}
$$

where Im denotes the imaginary part. By equating the imaginary terms in Eq. (B. 6) and assuming small losses (viz., $\epsilon'' \ll \epsilon'$) one obtains, to first order in Δ,

$$
\begin{aligned}
&2\,\Delta\phi\, e^{-2\eta}\, \mathrm{Re}\left[\int_{S_2} (\vec{E}_1 \times \vec{H}_1^*) \cdot d\vec{a}\right] \\
&= \omega\,\Delta\epsilon' \int_{V_f} |\vec{E}|^2\, dv \quad .
\end{aligned}
\qquad \text{(B. 7)}
$$

By making use of the relations for the output power P_{out} and the power lost in the dielectric P_{lost} given by

$$
\frac{1}{2}\, e^{-2\eta}\, \mathrm{Re}\left[\int_{S_2} (\vec{E}_1 \times \vec{H}_1^*) \cdot d\vec{a}\right] = P_{out} \quad , \qquad \text{(B. 8)}
$$

and

$$
\frac{1}{2}\,\omega\epsilon' \tan\delta \int_{V_f} |\vec{E}|^2\, dv = P_{lost} \quad , \qquad \text{(B. 9)}
$$

Eq. (B. 7) reduces to

$$\Delta\phi = \frac{1}{2} \frac{\Delta\epsilon'}{\epsilon' \tan\delta} \frac{P_{lost}}{P_{out}} \quad . \tag{B. 10}$$

For small losses the insertion loss of the device is approximately given by

$$L \approx \frac{1}{0.23} \frac{P_{lost}}{P_{out}} \text{ db} \quad . \tag{B. 11}$$

Hence, by combining Eqs. (B. 10) and (B. 11) and noting that $\epsilon' = \epsilon_0 K'$, one obtains the formula for the incremental phase shift

$$\Delta\phi = 0.115 \frac{\Delta K'}{K' \tan\delta} \text{ L radians} \quad . \tag{B. 12}$$

APPENDIX C

THE INCREMENTAL BEHAVIOR OF ELECTRICALLY TUNABLE ATTENUATORS

In reference to Fig. B. 1, it is desired to find the incremental change in attenuation $\Delta\eta$ os a signal passing between reference planes 1 and 2 when the complex permittivity of the ferroelectric changes by an incremental amount $\Delta\epsilon$. It is assumed that wall losses can be omitted and that the system is well matched so that reflection losses are negligible.

Between reference planes 1 and 2 the fields within the junction must be solutions to the Maxwell curl equations. These are:

$$\nabla \times \vec{E} = - j \omega \mu_0 \vec{H} \qquad \nabla \times \vec{E}' = - j \omega \mu_0 \vec{H}'$$

$$\nabla \times \vec{H} = j \omega \epsilon \vec{E} \qquad \nabla \times \vec{H}' = j \omega (\epsilon + \Delta\epsilon) \vec{E}' \quad , \tag{C. 1}$$

where the primed quantities refer to the conditions existing after ϵ has been changed to $\epsilon + \Delta\epsilon$. As discussed in Appendix B, assume that the relation between the fields at the reference planes can be expressed as:

$$\vec{E}_2 = \vec{E}_1 e^{- \eta - j\phi} \qquad \vec{E}_2' = \vec{E}_1' e^{- \eta' - j\phi'}$$

$$\vec{H}_2 = \vec{H}_1 e^{- \eta - j\phi} \qquad \vec{H}_2' = \vec{H}_1' e^{- \eta' - j\phi'} \quad , \tag{C. 2}$$

where for small changes in ϵ one has

$$\vec{E}' = \vec{E} + \Delta\vec{E}$$

$$\vec{H}' = \vec{H} + \Delta\vec{H} \tag{C. 3a}$$

and

$$\phi' = \phi + \Delta\phi$$
$$\eta' = \eta + \Delta\eta \qquad \text{(C. 3b)}$$

The incremental attenuation $\Delta\eta$ can be computed by considering the vector identity

$$\nabla \cdot (\vec{E} \times \vec{H}'^* + \vec{E}' \times \vec{H}^*) = \vec{H}'^* \cdot (\nabla \times \vec{E}) - \vec{E} \cdot (\nabla \times \vec{H}'^*) + \vec{H}^* \cdot (\nabla \times \vec{E}') - \vec{E}' \cdot (\nabla \times \vec{H}^*) \quad , \qquad \text{(C. 4)}$$

where * denotes the complex conjugate. By converting the volume integral of Eq. (C. 4) into a surface integral over the volume enclosed between reference planes 1 and 2, one obtains

$$\oint_S (\vec{E} \times \vec{H}'^* + \vec{E}' \times \vec{H}^*) \cdot d\vec{a} = -j\omega\mu_0 \int_V (\vec{H}' \cdot \vec{H}^* + \vec{H}'^* \cdot \vec{H})\, dv + j\omega\varepsilon_0 \int_{V-V_f} (\vec{E}' \cdot \vec{E}^* + \vec{E}'^* \cdot \vec{E})\, dv + j\omega\Delta\varepsilon^* \int_{V_f} \vec{E}'^* \cdot \vec{E}\, dv \quad , \qquad \text{(C. 5)}$$

where use has been made of Eq. (C. 1) and where S , V , and V_f have the same meaning as discussed in connection with Eq. (B. 5) of Appendix B. By making use of the boundary conditions on the waveguide walls and by substituting Eqs. (C. 2) and (C. 3b) into Eq. (C. 5) the following

equation is obtained:

$$2\cos\Delta\phi^{-2\eta-\Delta\eta}\int_{S_2}(\vec{E}_1\times\vec{H}_1^*)\cdot d\vec{a}-2\int_{S_1}(\vec{E}_1\times\vec{H}_1^*)\cdot d\vec{a}$$

$$=-2j\omega\mu_0\int_V R_e(\vec{H}'\cdot\vec{H}^*)\,dv+2j\omega\varepsilon_0\int_{V-V_f}R_e(\vec{E}'\cdot\vec{E}^*)\,dv$$

$$+2j\omega\varepsilon^*\int_{V_f}R_e(\vec{E}'\cdot\vec{E}^*)\,dv+j\omega\Delta\varepsilon^*\int_{V_f}\vec{E}'^*\cdot\vec{E}\,dv\ , \qquad (C.\ 6)$$

where it has been assumed that the signal level at reference plane 1 has a constant value. By collecting first order terms in Δ and taking the real part of Eq. (C. 6), it is found that

$$2(1-\Delta\eta)e^{-2\eta}R_e\left[\int_{S_2}(\vec{E}_1\times\vec{H}_1^*)\cdot d\vec{a}\right]-2R_e\left[\int_{S_1}(\vec{E}_1\times\vec{H}_1^*)\cdot d\vec{a}\right]$$

$$=-\omega\varepsilon''\int_{V_f}(2|\vec{E}|^2+\vec{E}\cdot\Delta\vec{E}^*+\vec{E}^*\cdot\Delta\vec{E})\,dv$$

$$-\omega\Delta\varepsilon''\int_{V_f}|\vec{E}|^2\,dv\ . \qquad (C.\ 7)$$

One can now simplify this expression by using the relations for input power P_{in}, output power P_{out}, and power lost in the dielectric P_{lost} given by

$$\frac{1}{2}R_e\left[\int_{S_1}(\vec{E}_1\times\vec{H}_1^*)\cdot d\vec{a}\right]=P_{in} \qquad (C.\ 8)$$

$$\frac{1}{2}e^{-2\eta}R_e\left[\int_{S_2}(\vec{E}_1\times\vec{H}_1^*)\cdot d\vec{a}\right]=P_{out} \qquad (C.\ 9)$$

$$\frac{1}{2}\omega\varepsilon''\int_{V_f}|\vec{E}|^2\,dv=P_{lost} \qquad (C.\ 10)$$

By substituting Eqs. (C. 8), (C. 9), and (C. 10) into Eq. (C. 7) and noting that $P_{lost} = P_{in} - P_{out}$, Eq. (C. 7) reduces to

$$4 \Delta\eta P_{out} = 2 \frac{\Delta\epsilon''}{\epsilon'} P_{lost} + \omega\epsilon'' \int_{V_f} (\vec{E} \cdot \Delta\vec{E}^* + \vec{E}^* \cdot \Delta\vec{E}) \, dv \quad . \qquad (C. 11)$$

Observe that no restriction has been placed upon either P_{lost} or ϵ''/ϵ' as was done in the derivation of the phase shift formula. In that derivation it was found that for small losses (a necessary requirement if the phase shifter is to have any practical value) and for $\epsilon''/\epsilon' \ll 1$ the resulting equation for $\Delta\phi$ was independent of the configuration of the device. Here one finds that both $\Delta\epsilon''/\epsilon''$ and the volume integral in Eq. (C. 11) are in general of the same order of magnitude. Therefore, the formula for the incremental attenuation is given by

$$\Delta\eta = \frac{1}{2} \frac{\Delta\epsilon''}{\epsilon''} \frac{P_{lost}}{P_{out}} + \frac{1}{4} \frac{\omega\epsilon''}{P_{out}} \int_{V_f} (\vec{E} \cdot \Delta\vec{E}^* + \vec{E}^* \cdot \Delta\vec{E}) \, dv \quad , \qquad (C. 12)$$

and is correct to first order.

APPENDIX D

THE INCREMENTAL BEHAVIOR OF ELECTRICALLY TUNABLE CAVITIES

To determine the general incremental behavior of resonant cavities containing ferroelectric samples, consider the arbitrary cavity configuration shown in Fig. D. 1. The ferroelectric sample is assumed to be of arbitrary shape and size and the cavity walls are assumed to be perfectly reflecting. The resonant frequencies of such a system are the natural

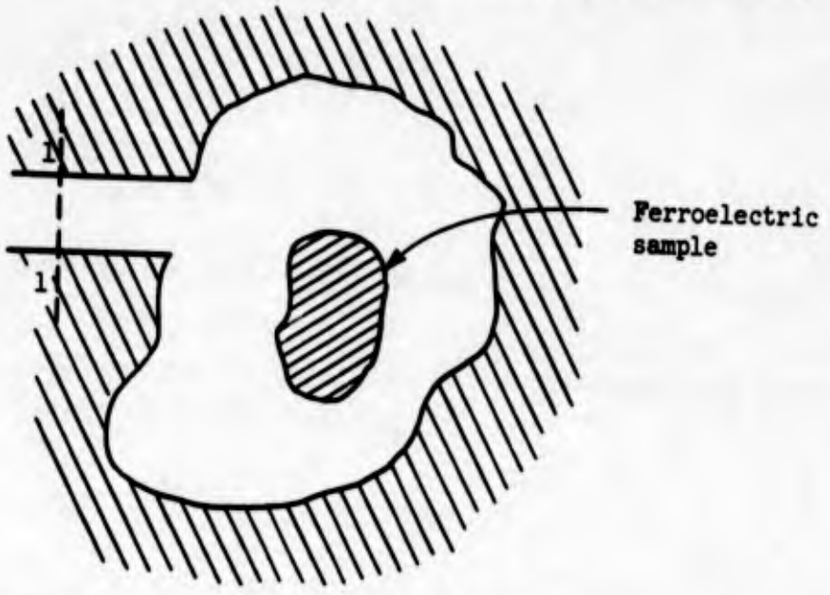

FIG. D. 1--Arbitrary cavity configuration with ferroelectric sample.

modes of vibration of the fields enclosed within the volume bounded by reference plane 1-1 and can be found by placing an electric short at the reference plane. Then by allowing the complex permittivity of the nonlinear ceramic to change from ϵ to $\epsilon + \Delta\epsilon$, it is possible to determine the resultant fractional change in the resonance of the cavity $\Delta\omega/\omega$.

For each value of permittivity the cavity fields are governed by

Maxwell's equations:

$$\nabla \times \vec{E} = - j\omega\mu_0 \vec{H}$$

$$\nabla \times \vec{H} = j\omega\epsilon \vec{E} \qquad \text{(D. 1)}$$

and

$$\nabla \times \vec{E}' = - j (\omega + \Delta\omega) \mu_0 \vec{H}'$$

$$\nabla \times \vec{H}' = j (\omega + \Delta\omega)(\epsilon + \Delta\epsilon) \vec{E}' \qquad \text{(D. 2)}$$

where

$$\vec{E}' = \vec{E} + \Delta\vec{E}$$

$$\vec{H}' = \vec{H} + \Delta\vec{H} \quad . \qquad \text{(D. 3)}$$

The incremental change in resonance $\Delta\omega$ is most easily found by considering the vector identity given by Eq. (B. 4) of Appendix B. From this identity one can easily show, by making use of the divergence theorem and by utilizing Eqs. (D. 1) and (D. 2), that

$$\oint_S (\vec{E} \times \vec{H}'^* - \vec{E}' \times \vec{H}^*) \cdot d\vec{a} = - j\omega\mu_0 \int_V \vec{H} \cdot \vec{H}'^* \, dv$$

$$+ j (\omega + \Delta\omega)\mu_0 \int_V \vec{H}' \cdot \vec{H}^* \, dv + j (\omega + \Delta\omega)(\epsilon + \Delta\epsilon)^* \int_V \vec{E} \cdot \vec{E}'^* \, dv$$

$$- j\omega\epsilon^* \int_V \vec{E}' \cdot \vec{E}^* \, dv \quad , \qquad \text{(D. 4)}$$

where V is the volume of the cavity enclosed by the surface S which extends over reference plane 1-1. The surface integral in Eq. (D. 4) vanishes identically due to the boundary conditions on the cavity walls

and on the surface of the reference plane. Hence, one can write

$$\mu_0 \int_V \left[\left(1 + \frac{\Delta\omega}{\omega}\right) \vec{H}' \cdot \vec{H}^* - \vec{H} \cdot \vec{H}'^* \right] dv$$
$$+ \int_V \left[\left(1 + \frac{\Delta\omega}{\omega}\right)(\epsilon + \Delta\epsilon)^* \vec{E} \cdot \vec{E}'^* - \epsilon^* \vec{E}' \cdot \vec{E}^* \right] dv = 0 \,. \quad \text{(D. 5)}$$

Substitution of Eq. (D. 3) into Eq. (D. 5) results in the following equation, correct to first order changes:

$$\frac{\Delta\omega}{\omega} \int_V \left(\mu_0 |\vec{H}|^2 + \epsilon^* |\vec{E}|^2 \right) dv + 2j\mu_0 \int_V \mathrm{Im}\,(\vec{H}^* \cdot \Delta\vec{H})\, dv$$
$$+ \Delta\epsilon^* \int_V |\vec{E}|^2 dv + 2j\epsilon^* \int_V \mathrm{Im}\,(\vec{E} \cdot \Delta\vec{E}^*)\, dv = 0 \quad , \quad \text{(D. 6)}$$

where Im denotes the imaginary part. If one takes the real part of this expression and observes that ϵ is only complex over the volume of the ferroelectric sample V_f and can only undergo a change $\Delta\epsilon$ in this volume, one finds

$$\frac{\Delta\omega}{\omega} \left\{ \mu_0 \int_{V-V_f} |\vec{H}|^2 dv + \epsilon_0 \int_{V-V_f} |\vec{E}|^2 dv + \epsilon' \int_{V_f} |\vec{E}|^2 dv \right\}$$
$$+ \Delta\epsilon' \int_{V_f} |\vec{E}|^2 dv - 2\epsilon'' \int_{V_f} \mathrm{Im}\,(\vec{E} \cdot \Delta\vec{E}^*)\, dv = 0 \quad . \quad \text{(D. 7)}$$

It has been assumed here that in the volume outside the ferroelectric $V-V_f$ the permittivity is that of free space ϵ_0 .

An examination of the integrals appearing within the braces on the left hand side of Eq. (D. 7) reveals that they can be written in terms of the energy stored in the cavity. Therefore, in the low loss approximation, i.e., when $\epsilon''/\epsilon' \ll 1$, Eq. (D. 7) reduces to the following first order expression:

$$8 \frac{\Delta\omega}{\omega} U_E + 4 \frac{\Delta\epsilon'}{\epsilon'} U_{diel} = 0 \quad , \quad \text{(D. 8)}$$

where U_E is the average electric energy stored in the cavity, including the dielectric

$$U_E = \frac{1}{4}\ \epsilon_0 \int_{V-V_f} |\vec{E}|^2\, dv + \frac{1}{4}\ \epsilon' \int_{V_f} |\vec{E}|^2\, dv \ ,$$

and where U_{diel} is the average energy stored in the dielectric sample,

$$U_{diel} = \frac{1}{4}\, \epsilon' \int_{V_f} |\vec{E}|^2\, dv \ .$$

Note that for <u>small losses</u> one has

$$U_E \approx U_H = \frac{1}{4}\, \mu_0 \int_V |\vec{H}|^2\, dv \ ;$$

use has been made of this relation in deriving Eq. (D. 8).

Equation (D. 8) can be simplified considerably by writing U_E and U_{diel} in terms of the unloaded Q of the cavity containing the dielectric, i.e.,

$$Q = \frac{2\omega\, U_E}{P_{lost}} \ , \qquad \text{(D. 9)}$$

and the dielectric Q , Q_{diel} , given by

$$Q_{diel} = \frac{1}{\tan \delta} = \frac{2\omega\, U_{diel}}{P_{lost}} \ . \qquad \text{(D. 10)}$$

In Eqs. (D. 9) and (D. 10) P_{lost} represents the power consumed in the ferroelectric sample. Combining Eqs. (D. 8), (D. 9), and (D. 10) with $\epsilon' = \epsilon_0\, \kappa'$ produces

$$\frac{\Delta\omega}{\omega} = -\frac{1}{2}\, \frac{1}{Q \tan \delta}\, \frac{\Delta\kappa'}{\kappa'} \ ,$$

which is the desired result.

APPENDIX E

CALCULATION OF THE CONVERSION EFFICIENCY OF THE RESONANT HARMONIC GENERATOR

The objective of this appendix is to obtain an expression for the conversion efficiency of the resonant harmonic generator discussed in the first half of Chapter IV. In this calculation it will be assumed that the fundamental response is much larger than the third harmonic response. The analysis is consequently limited to the case of low, or at most, moderate, conversion efficiencies.

The set of coupled nonlinear algebraic equations given by Eqs. (42) and (43) completely describes the behavior of the harmonic generator. When $|V_1|>|V_3|$, one can linearize these equations with respect to V_3 and rewrite them as

$$I_g = [(g_{01} + Y_1) + 3(g_{21} + j\omega c_2)(V_1 V_1^* - V_1^{*2} V_3/V_1)] V_1 \qquad \text{(E. 1)}$$

$$(g_{23} + 3\, j\omega c_2) V_1^3 = [(g_{03} + Y_3) + 6\,(g_{23} + 3\, j\omega c_2) V_1 V_1^*] V_3 \,. \qquad \text{(E. 2)}$$

Solutions to Eqs. (E. 1) and (E. 2) can be obtained most easily by using the method of successive approximations (iterations) in which a linear algebraic equation is solved at each stage. Observe that since this calculation applies in the low efficiency region, one can assume as a first approximation that the product of the nonlinear coefficients with the square of the voltage is small compared to the linear terms, or that

$$V_1 \approx \frac{I_g}{g_{01} + Y_1} \qquad \text{(E. 3)}$$

and

$$V_3 \approx \frac{(g_{23} + j\omega c_2)}{(g_{03} + Y_3)} V_1^3 \,. \qquad \text{(E. 4)}$$

This first approximation is valid when I_g has very small amplitude.

To obtain the second approximation, Eqs. (E. 1) and (E. 2) are solved for V_1 and V_3, respectively, and Eqs. (E. 3) and (E. 4) are substituted into these expressions. In the second approximation it is assumed that one can neglect terms in the product of the nonlinear coefficients squared with the voltage to the fourth power. To this order of approximation one has

$$V_1 = \frac{I_g}{(g_{01} + Y_1) + 3(g_{21} + j\omega c_2)\left[\frac{|I_g|^2}{|g_{01} + Y_1|^2}\right]} \qquad \text{(E. 5)}$$

and

$$V_3 = \frac{(g_{23} + 3j\omega c_2)\, V_1^3}{(g_{03} + Y_3) + 6(g_{23} + 3j\omega c_2)\left[\frac{|I_g|^2}{|g_{01} + Y_1|^2}\right]} \,. \qquad \text{(E. 6)}$$

Equations (E. 5) and (E. 6) are valid when $|V_1| > |V_3|$ and when I_g is small or when the efficiency is moderately low.

The conversion efficiency can now be found by calculating the third harmonic output power P_{out} in terms of the input pump power P_{in}. Considering the on-resonance ($\omega = \Omega_1$) high Q ($n^2 Y_0 \gg G_1$ and $m^2 Y_0 \gg G_3$) behavior, Eqs. (E. 5) and (E. 6) become

$$V_1 = \frac{I_g}{(g_{01} + n^2 Y_0) + 3(g_{21} + j\Omega_1 c_2)\dfrac{|I_g|^2}{(g_{01} + n^2 Y_0)}} \qquad \text{(E. 7)}$$

and

$$V_3 = \frac{3(g_{21} + j\Omega_1 c_2)\, V_1^3}{(3\, g_{01} + m^2 Y_0) + 18\,(g_{21} + j\Omega_1 c_2)\dfrac{|I_g|^2}{(g_{01} + n^2 Y_0)^2}} \,, \qquad \text{(E. 8)}$$

where use has been made of the relation $g_{n3} = 3g_{n1}$. By combining Eqs. (E. 7) and (E. 8) and requiring that the system be well matched at the input and output terminals [Eqs. (51) and (52)], one obtains

$$V_3 = \left\{ \frac{3(g_{21} + j\,\Omega_1\, c_2)\, I_g^3}{6g_{01} + \frac{9}{2}(g_{21} + j\,\Omega_1\, c_2)\frac{|I_g|^2}{g_{01}^2}} \right\} \left\{ \frac{1}{2g_{01} + \frac{3}{4}(g_{21} + j\,\Omega_1\, c_2)\frac{|I_g|^2}{g_{01}^2}} \right\}^3 . \qquad \text{(E. 9)}$$

From Eq. (E. 9) the output power given by

$$P_{out} = 2\, g_{03}\, |V_3|^2 = 6\, g_{01}\, |V_3|^2 \qquad \text{(E. 10)}$$

can easily be found. In order to relate P_{out} to P_{in} (P_{in} is equal to P_{inc} since the system is matched), Eq. (46) is used, i.e.,

$$|I_g|^2 = 2\, n^2\, Y_0\, P_{inc} = 2\, g_{01}\, P_{inc} \quad . \qquad \text{(E. 11)}$$

By substituting Eqs. (E. 9) and (E. 11) into (E. 10) and neglecting all terms of higher order than the product of P_{inc} with the nonlinear coefficients, one finds after some algebraic manipulation that

$$P_{out} = \frac{3\,(g_{21}^2 + \Omega_1^2\, c_2^2)}{16\, g_{01}^4 \left[1 + \left(\frac{15}{2}\right)\left(\frac{g_{21}}{g_{01}^2}\right) P_{inc}\right]} P_{inc}^3 \quad . \qquad \text{(E. 12)}$$

It should be emphasized that Eq. (E. 12), which is the desired result, is consistent with the approximations used in deriving Eqs. (E. 5) and (E. 6).

The conversion efficiency $\eta = (P_{out}/P_{in}) \times 100\%$ can be computed from Eq. (E. 12) by inspection and is given as Eq. (54) in the text.

APPENDIX F

DETERMINATION OF POWER FLOW IN THE HARMONIC GENERATOR CIRCUIT

A general relation for the power distribution in the harmonic generator network can be obtained from the nonlinear algebraic circuit equations given by Eqs. (42) and (43). These are rewritten here for convenience as Eqs. (F. 1) and (F. 2):

$$I_g = (g_{01} + Y_1)\, V_1 + 3\,(g_{21} + j\omega c_2)(V_1^2\, V_1^* + 2\, V_1\, V_3\, V_3^* - V_1^{*2}\, V_3) \qquad \text{(F. 1)}$$

$$0 = (g_{03} + Y_3)\, V_3 - (g_{23} + 3j\omega c_2)(V_1^3 - 6\, V_1\, V_1^*\, V_3 - 3\, V_3^2\, V_3^*) \quad . \qquad \text{(F. 2)}$$

With reference to Fig. F. 1, the power delivered by the generator P_{gen} at ω and the power transferred to the load P_{out} at 3ω can be expressed as

$$P_{gen} = 2\, R_e\, (V_1^*\, I_g) \qquad \text{(F. 3)}$$

and

$$P_{out} = 2\, m^2\, Y_0\, |V_3|^2 \quad . \qquad \text{(F. 4)}$$

By substituting Eqs. (F. 1) and (F. 2) into Eqs. (F. 3) and (F. 4) and simplifying, one has

$$P_{gen} = P_{lost,\,\omega} + 6\, R_e \left\{(g_{21} + j\omega c_2)(|V_1|^4 + 2\, |V_1|^2\, |V_3|^2 - V_1^{*3}\, V_3)\right\} \qquad \text{(F. 5)}$$

$$P_{out} = - P_{lost,\,3\omega} + 2\, R_e \left\{(g_{23} + 3j\omega c_2)(V_1^3\, V_3^* - 6\, |V_1|^2\, |V_3|^2 - 3\, |V_3|^4)\right\}, \qquad \text{(F. 6)}$$

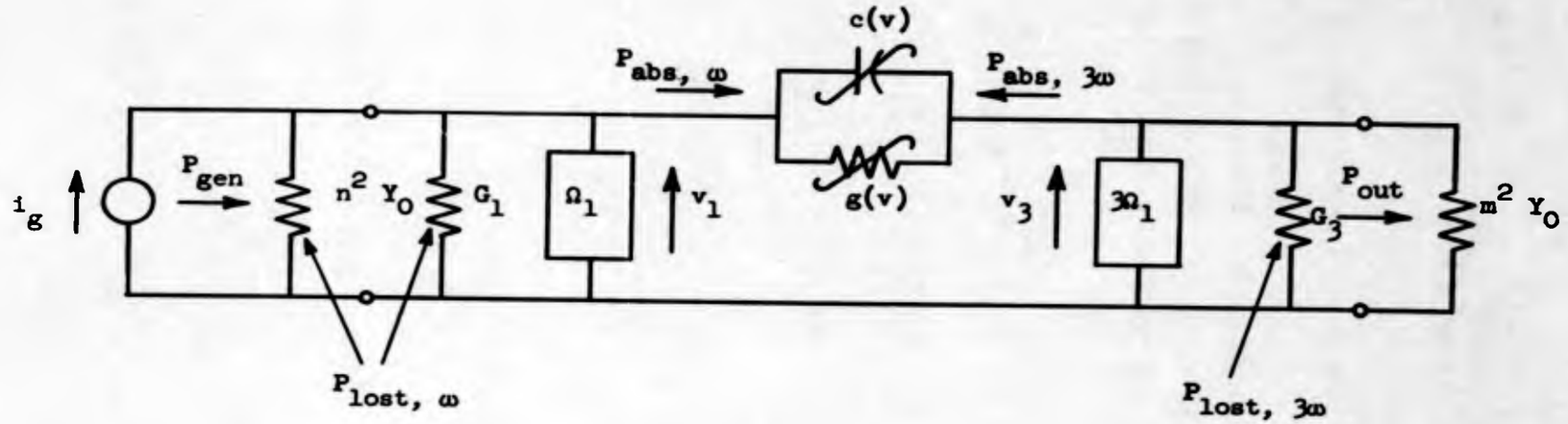

FIG. F. 1--Simplified equivalent circuit of the harmonic generator shown in Fig. 16. Here Ω_1 and $3\Omega_1$ refer to the L - C resonant tanks tuned to Ω_1 and $3\Omega_1$, respectively. The arrows indicated in the figure have been chosen to illustrate graphically the power flow in the network.

where

$$P_{lost,\ \omega} = 2\ (g_{01} + G_1 + n^2\ Y_0)\ |V_1|^2 \qquad \text{(F. 7)}$$

and

$$P_{lost,\ 3\omega} = 2(g_{03} + G_3)\ |V_3|^2 \quad . \qquad \text{(F. 8)}$$

Observe that the linear loss terms in the nonlinear conductance $g(v)$ have been included in the expressions for the power lost P_{lost} in the ω and 3ω resonant circuits. By subtracting Eq. (F. 6) from (F. 5) and making use of conservation of power, one obtains the following relation for the total absorbed power $P_{abs} = P_{abs,\ \omega} + P_{abs,\ 3\omega}$:

$$P_{abs} = 6\ R_e\left\{(g_{21} + j\omega c_2)(|V_1|^4 + 2\ |V_1|^2\ |V_3|^2 - V_1^{*3}\ V_3)\right\}$$
$$- 2\ R_e\left\{(g_{23} + 3j\omega c_2)(V_1^3\ V_3^* - 6\ |V_1|^2\ |V_3|^2 - 3\ |V_3|^4)\right\} . \qquad \text{(F. 9)}$$

This equation can be simplified considerably by noting that $g_{23} = 3\ g_{21}$; whence

$$P_{abs} = 6\ g_{21}\ \left[|V_1|^4 + 3\ |V_3|^4 + 8\ |V_1|^2\ |V_3|^2 - (V_1^{*3}\ V_3 + V_1^3\ V_3^*)\right] . \qquad \text{(F. 10)}$$

It should be emphasized that the power absorbed in the nonlinear coupling element shown in Fig. F. 1 is due only to the conductance $g(v)$, as expected.

APPENDIX G

RESPONSE FUNCTIONS $A_k(z)$ AND $B_k(z)$ FOR THE NONLINEAR TRANSMISSION LINE

The functions $A_k(z)$ and $B_k(z)$ appearing in Eq. (68) have been computed to second order in the perturbation parameter $\zeta = 3lc_2$ by successive integrations of Eqs. (63). Approximate solutions were therefore obtained for the fundamental, third, and fifth harmonic frequencies. The final results of the computations are given by the following expressions:

$$A_1(z) = V_G e^{-\alpha_1 z}\left\{1 - \frac{3}{16}\zeta_1 u\left(1 - e^{-2\alpha_1 z}\right) - \frac{9}{512}\frac{u^2}{\beta_1}\left[8\omega\zeta_1\alpha_1 + \left(\omega^2 - 3\zeta_1^2\right)\beta_1\right]\left(1 - 2e^{-2\alpha_1 z} + e^{-4\alpha_1 z}\right) - \frac{9}{1024}u^2\left(\omega^2 - \zeta_1^2\right)\left[1 - (1 + 4\alpha_1 z)\, e^{-4\alpha_1 z}\right]\right\} \tag{G. 1}$$

$$B_1(z) = \frac{3}{16}\omega u V_G e^{-\alpha_1 z}\left\{\left(1 - e^{-2\alpha_1 z}\right) - \frac{3}{32}u\zeta_1\left[1 - (1 + 4\alpha_1 z)\, e^{-4\alpha_1 z}\right] + \frac{3}{32}\frac{u}{\omega\beta_1}\left[2\alpha_1\left(3\omega^2 - \zeta_1^2\right) - 4\omega\zeta_1\beta_1\right]\left(1 - 2e^{-2\alpha_1 z} + e^{-4\alpha_1 z}\right)\right\} \tag{G. 2}$$

plus

$$A_e(z) = -\frac{3}{8} uV_G e^{-3\alpha_1 z} \left\{ \zeta_1 \alpha_1 z + \frac{9}{32} u(\omega^2 - \zeta_1^2) \left[1 + 2\alpha_1 z - (1 + 4\alpha_1 z) e^{-2\alpha_1 z} \right] \right\} \quad \text{(G. 3)}$$

$$B_3(z) = \frac{3}{8} \omega u V_G e^{-3\alpha_1 z} \left\{ \alpha_1 z - \frac{9}{16} u\zeta_1 \left[1 + 2\alpha_1 z - (1 + 4\alpha_1 z) e^{-2\alpha_1 z} \right] \right\} \quad \text{(G. 4)}$$

$$A_5(z) = \frac{9}{128} u^2 \frac{\alpha_1^2 z}{\beta_1} \left[2\omega\zeta_1 - 5(\omega^2 - \zeta_1^2)\beta_1 z \right] V_G e^{-5\alpha_1 z} \quad \text{(G. 5)}$$

$$B_5(z) = -\frac{9}{128} u^2 \frac{\alpha_1^2 z}{\beta_1} \left[(\omega^2 - \zeta_1^2) + 10\omega\zeta_1\beta_1 z \right] V_G e^{-5\alpha_1 z} , \quad \text{(G. 6)}$$

where

$$u = \omega \frac{z_0^2}{\alpha_1 \beta_1} c_0 c_2 V_G^2 ,$$

and α_1 and β_1 are, respectively, the attenuation and phase constants determined from the real and imaginary parts of the complex propagation constant given by Eq. (64). These expressions are valid when $\beta_1 \gg \alpha_1$ which applies in the case of ferroelectrics.

APPENDIX G

RESPONSE FUNCTIONS $A_k(z)$ AND $B_k(z)$ FOR THE NONLINEAR TRANSMISSION LINE

The functions $A_k(z)$ and $B_k(z)$ appearing in Eq. (68) have been computed to second order in the perturbation parameter $\zeta = \beta c_2$ by successive integrations of Eqs. (63). Approximate solutions were therefore obtained for the fundamental, third, and fifth harmonic frequencies. The final results of the computations are given by the following expressions:

$$A_1(z) = V_G e^{-\alpha_1 z} \left\{ 1 - \frac{3}{16} \zeta_1 u \left(1 - e^{-2\alpha_1 z}\right) - \frac{9}{512} \frac{u^2}{\beta_1} \left[8\omega\zeta_1\alpha_1 + \left(\omega^2 - 3\zeta_1^2\right)\beta_1\right] \left(1 - 2e^{-2\alpha_1 z} + e^{-4\alpha_1 z}\right) - \frac{9}{1024} u^2 \left(\omega^2 - \zeta_1^2\right) \left[1 - (1 + 4\alpha_1 z) e^{-4\alpha_1 z}\right] \right\} \tag{G. 1}$$

$$B_1(z) = \frac{3}{16} \omega u V_G e^{-\alpha_1 z} \left\{ \left(1 - e^{-2\alpha_1 z}\right) - \frac{3}{32} u\zeta_1 \left[1 - (1 + 4\alpha_1 z) e^{-4\alpha_1 z}\right] + \frac{3}{32} \frac{u}{\omega\beta_1} \left[2\alpha_1 \left(3\omega^2 - \zeta_1^2\right) - 4\omega\zeta_1\beta_1\right] \left(1 - 2e^{-2\alpha_1 z} + e^{-4\alpha_1 z}\right) \right\} \tag{G. 2}$$

plus

$$A_e(z) = -\frac{3}{8} uV_G e^{-3\alpha_1 z} \left\{ \zeta_1 \alpha_1 z + \frac{9}{32} u(\omega^2 - \zeta_1^2) \left[1 + 2\alpha_1 z - (1 + 4\alpha_1 z) e^{-2\alpha_1 z} \right] \right\} \quad \text{(G. 3)}$$

$$B_3(z) = \frac{3}{8} \omega u V_G e^{-3\alpha_1 z} \left\{ \alpha_1 z - \frac{9}{16} u\zeta_1 \left[1 + 2\alpha_1 z - (1 + 4\alpha_1 z) e^{-2\alpha_1 z} \right] \right\} \quad \text{(G. 4)}$$

$$A_5(z) = \frac{9}{128} u^2 \frac{\alpha_1^2 z}{\beta_1} \left[2\omega\zeta_1 - 5(\omega^2 - \zeta_1^2)\beta_1 z \right] V_G e^{-5\alpha_1 z} \quad \text{(G. 5)}$$

$$B_5(z) = -\frac{9}{128} u^2 \frac{\alpha_1^2 z}{\beta_1} \left[(\omega^2 - \zeta_1^2) + 10\omega\zeta_1\beta_1 z \right] V_G e^{-5\alpha_1 z} \quad , \quad \text{(G. 6)}$$

where

$$u = \omega \frac{z_0^2}{\alpha_1 \beta_1} c_0 c_2 V_G^2 \quad ,$$

and α_1 and β_1 are, respectively, the attenuation and phase constants determined from the real and imaginary parts of the complex propagation constant given by Eq. (64). These expressions are valid when $\beta_1 \gg \alpha_1$ which applies in the case of ferroelectrics.

APPENDIX H

WAVE PROPAGATION IN NONLINEAR RECTANGULAR WAVEGUIDES

The problem of wave propagation in nonlinear waveguides has been solved formally in Eqs. (78), (79), and (80). To illustrate the behavior of these solutions and to show how the example given in section C of Chapter IV must be modified when the transverse variations in the waveguide fields are taken into account, consider the problem of illuminating the rectangular guide of Fig. H. 1 in a TE_{10} mode. The waveguide walls are assumed to be perfectly conducting so that the boundary conditions

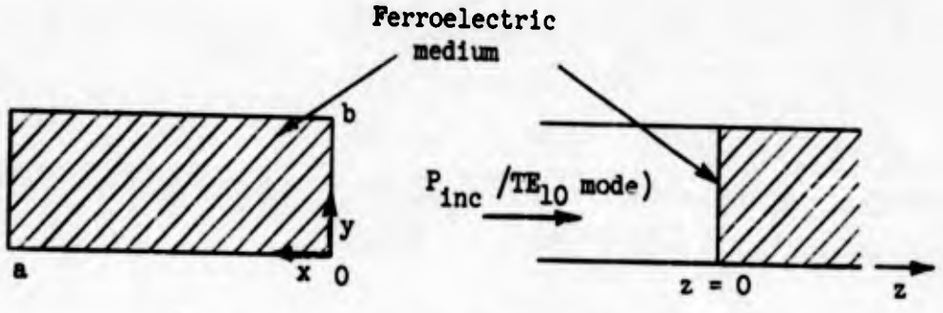

FIG. H. 1--Nonlinear rectangular waveguide.

$\hat{n} \times \vec{E} = 0$ and $\hat{n} \cdot \vec{H} = 0$ are satisfied where $\hat{n}$ is the unit vector normal to the waveguide surface.

Solutions to Eqs. (79) can be found by successive integrations. For $p = 1, 2$ Eqs. (79) reduce to

$$\nabla \times \vec{E}_k^{(1,2)} = -jk\omega\mu_0 \vec{H}_k^{(1,2)}$$

$$\nabla \times \vec{H}_k^{(1,2)} = jk\omega\epsilon_0 (\kappa'_1 - j\kappa''_1) \vec{E}_k^{(1,2)} \quad . \qquad \text{H. 1)}$$

These are linear equations and give as possible solutions all TE and TM modes. From the continuity relations at $z = 0$ given by Eq. (80) it can be seen that only the TE_{10} at angular frequency ω is of concern. Thus by including both an incident and reflected wave in the TE_{10} mode for $z < 0$ and by matching these solutions at $z = 0$ to the TE_{10} mode in the region $z > 0$, one has as the first order solutions in the electric field E_y

$$E_y\Big|_{z<0} = -j\omega_0\left(\frac{\pi}{a}\right)A \sin\frac{\pi}{a}x \left[e^{-\gamma_1 z} + \left(1 - \frac{2\gamma_1}{\gamma_1 + \Gamma_{1,1}}\right) e^{\gamma_1 z}\right] e^{j\omega t} \qquad \text{(H. 2)}$$

$$E_y^{(1)}\Big|_{z>0} = -j\omega\mu_0\left(\frac{\pi}{a}\right)\left(\frac{2\gamma_1}{\gamma_1 + \Gamma_{1,1}}\right) \sin\frac{\pi}{a}x\, e^{-\Gamma_{1,1} z}\, e^{j\omega t} \,. \qquad \text{(H. 2)}$$

Here A is the amplitude of the drive which is chosen to be real and is related to the incident power P_{inc} in the TE_{10} mode by

$$A^2 = \frac{P_{inc}}{\omega\mu_0\pi^2 (b/a)\sqrt{\omega^2\mu_0\epsilon_0 - (\pi/a)^2}} \,. \qquad \text{(H. 4)}$$

The propagation constants γ_1 and $\Gamma_{1,1}$ for the TE_{10} mode in the region $z < 0$ and $z > 0$, respectively, are given by

$$\gamma_1^2 = \left(\frac{\pi}{a}\right)^2 - \omega^2\mu_0\epsilon_0 \qquad \text{(H. 5)}$$

$$\Gamma_{1,1}^2 = \left(\frac{\pi}{a}\right)^2 - \omega^2\mu_0\epsilon_0 (\kappa'_1 - j\kappa''_1) \,. \qquad \text{(H. 6)}$$

Note that the second order fields which are any linear combination of the normal modes of propagation vanish at $z = 0$ for all frequencies including the fundamental frequency [see Eq. (80)]. One can therefore choose the second order solutions to Eqs. (H. 1) to have zero amplitude.

The third order solutions can be found in terms of the first order solutions from Eqs. (79). The governing equations for the third order fields are

$$\nabla \times \bar{E}_k^{(3)} = - jk\omega\mu_0 \bar{H}^{(3)}$$

$$\nabla \times \bar{H}_k^{(3)} = jk\omega\epsilon_0 (\kappa'_1 - j\kappa''_1) \bar{E}_k^{(3)} + \sum_{m,n=-\infty}^{\infty} jk\omega\epsilon_0 (\kappa'_3 - j\kappa''_3)(\bar{E}_{m-n}^{(1)} \cdot \bar{E}_n^{(1)}) \bar{E}_{k-m}^{(1)} \quad . \tag{H. 7}$$

This set of equations can easily be shown to give third order solutions for $k = 1$ and $k = 3$ only. By combining the resulting equations at the fundamental $(k = 1)$ and third $(k = 3)$ harmonics one obtains the following inhomogeneous Helmholtz equations for $\bar{E}_1^{(3)}$ and $\bar{E}_3^{(3)}$:

$$\nabla^2 \bar{E}_1^{(3)} + \omega^2\mu_0\epsilon_0 (\kappa'_1 - j\kappa''_1) \bar{E}_1^{(3)} = - \omega^2\mu_0\epsilon_0 (\kappa'_3 - j\kappa''_3) \left[(\bar{E}_1^{(1)} \cdot \bar{E}_1^{(1)}) \bar{E}_{-1}^{(1)} + 2 (\bar{E}_1^{(1)} \cdot \bar{E}_{-1}^{(1)}) \bar{E}_1^{(1)} \right] \tag{H. 8}$$

and

$$\nabla^2 \bar{E}_3^{(3)} + 9\,\omega^2\mu_0\epsilon_0 (\kappa'_1 - j\kappa''_1) \bar{E}_3^{(3)} = - 9\,\omega^2\mu_0\epsilon_0 (\kappa'_3 - j\kappa''_3)(\bar{E}_1^{(1)} \cdot \bar{E}_1^{(1)}) \bar{E}_1^{(1)} \quad . \tag{H. 9}$$

Particular integrals to Eqs. (H. 8) and (H. 9) can be found by any of the standard techniques. The general solutions to these equations can then be determined by adding the complementary solutions to the particular integrals and invoking the continuity relations at $z = 0$ given by Eq. (80). The solutions derived in this way contain those modes included in the inhomogeneous terms involving $\bar{E}_1^{(1)}$ and $\bar{E}_{-1}^{(1)} = E_1^{(1)*}$ in Eqs. (H. 8) and (H. 9), i.e., the inhomogeneous terms represent a volume distribution of sources which excites these modes in the nonlinear medium.

By finding the solutions to Eqs. (H. 8) and (H. 9) and combining them with Eq. (H. 3), one finds that the expression for the electric field in the region $z > 0$ correct to third order is given by

$$E_y = - j\omega\mu_0 \left(\frac{\pi}{a}\right)\left(\frac{2\,\gamma_1}{\gamma_1 + \Gamma_{1,1}}\right) A \sin\frac{\pi}{a} \times \Bigg\{ e^{j\omega t - \Gamma_{1,1} z}$$

$$- 9\,\omega^2\mu_0^3\epsilon_0 \left(\frac{\pi}{a}\right)^2 \frac{(\kappa'_3 - j\kappa''_3)}{[(2\,\Gamma_{1,1} + \Gamma_{1,1}^*)^2 - \gamma_1^2]} \left|\frac{\gamma_1}{\gamma_1 + \Gamma_{1,1}}\right|^2 A^2 \left[e^{(-\Gamma_{1,1} + \Gamma_{1,1}^*)z} - 1\right] e^{j\omega t - \Gamma_{1,1} z}$$

$$+ 27\,\omega^4\mu_0^3\epsilon_0 \left(\frac{\pi}{a}\right)^2 \frac{(\kappa'_3 - j\kappa''_3)}{(9\,\Gamma_{1,1}^2 - \Gamma_{3,1}^2)} \times \left(\frac{\gamma_1}{\gamma_1 + \Gamma_{1,1}}\right)^2 A^2 \left(e^{-3\,\Gamma_{1,1} z} - e^{-\Gamma_{3,1} z}\right) e^{3j\omega t} \Bigg\} - 6\,j\omega^5\mu_0^4\epsilon_0$$

$$\times \left(\frac{\pi}{a}\right)^3 \left(\frac{\gamma_1}{\gamma_1 + \Gamma_{1,1}}\right) A^3 \sin\frac{3\pi}{a} \times \Bigg\{ \frac{(\kappa'_3 - j\kappa''_3)}{\left[(2\,\Gamma_{1,1} + \Gamma_{1,1}^*)^2 - \Gamma_{1,3}^2\right]}$$

$$\times \left|\frac{\gamma_1}{\gamma_1 + \Gamma_{1,1}}\right|^2 \left[e^{-(2\,\Gamma_{1,1} + \Gamma_{1,1}^*)z}\right] e^{j\omega t} - 3\,\frac{(\kappa'_3 - j\kappa''_3)}{(9\,\Gamma_{1,1}^2 - \Gamma_{3,3}^2)}$$

$$\times \left(\frac{\gamma_1}{\gamma_1 + \Gamma_{1,1}}\right)^2 \left(e^{-3\,\Gamma_{1,1} z} - e^{-\Gamma_{3,3} z}\right) e^{3j\omega t} \Bigg\} \,, \qquad \text{(H. 10)}$$

where use has been made of Eq. (78a). The propagation constants $\Gamma_{3,1}$,

$\Gamma_{1,3}$, and $\Gamma_{3,3}$ appearing in this equation can be expressed as

$$\Gamma_{3,1}^2 = \left(\frac{\pi}{a}\right)^2 - 9\,\omega^2\mu_0\epsilon_0\,(\kappa'_1 - j\kappa''_1) \qquad \text{(H. 11)}$$

$$\Gamma_{1,3}^2 = \left(\frac{3\pi}{a}\right)^2 - \omega^2\mu_0\epsilon_0\,(\kappa'_1 - j\kappa''_1) \qquad \text{(H. 12)}$$

$$\Gamma_{3,3}^2 = \left(\frac{3\pi}{a}\right)^2 - 9\,\omega^2\mu_0\epsilon_0\,(\kappa'_1 - j\kappa''_1) \quad . \qquad \text{(H. 13)}$$

The solution for the electric field in the region $z < 0$ has already been given in Eq. (H. 2). To determine the magnetic field in the guide it is only necessary to substitute Eqs. (H. 2) and (H. 10) into the equation for the curl of $\vec{E}$ and integrate with respect to time.

REFERENCES

1. D. A. Johnson, Microwave Laboratory Report No. 825, Stanford University (1961).
2. L. Davis and L. G. Rubin, J. Appl. Phys. 24, 1194 (1953).
3. T. S. Benedict and J. L. Durand, Phys. Rev. 109, 1091 (1958).
4. C. B. Sharpe and C. G. Brockus, Report No. 2732-4-F, University of Michigan Research Institute (1959).
5. H. J. Schmitt, Z. Angew. Physik 9, 107 (1957).
6. W. Känzig, in Solid State Physics, edited by F. Seitz and D. Turnbull (Academic Press, Inc., New York, 1957), Vol. 4.
7. A. Von Hippel, Revs. Modern Phys. 22, 221 (1950).
8. G. Shiranev, F. Jona, and R. Pepinsky, Proc. IRE 43, 1738 (1955).
9. A. Von Hippel, Dielectric and Waves, (John Wiley and Sons, Inc., New York, 1954).
10. C. Kittel, Solid State Physics, (John Wiley and Sons, Inc., New York, 1962) 2nd ed.
11. A. J. Dekker, Solid State Physics, (Prentice-Hall, Inc. Englewood Cliffs, New Jersey, 1957).
12. S. Roberts, Phys. Rev. 71, 890 (1947).
13. W. J. Merz, Phys. Rev. 76, 1221 (1949).
14. A. F. Devonshire, Advances in Physics 3, 85 (1954).
15. E. T. Jaynes, Ferroelectricity, (Princeton University Press, Princeton, New Jersey, 1953).
16. H. H. Wieder, Phys. Rev. 99, 1161 (1955).
17. A. L. Stanford, Jr., Phys. Rev. 124, 408 (1961).
18. J. G. Powles and W. Jackson, Proc. IEE (London) 96, part III, 383 (1949).
19. C. Kittel, Phys. Rev. 83, 458 (1951).
20. E. T. Jaynes and V. Varenhorst, Microwave Laboratory Report No. 287, Stanford University (1955).
21. W. Jackson and W. Reddish, Nature 156, 717 (1945).
22. E. T. Jaynes, Proc. IRE 43, 1733 (1955).

23. H. Diamond, J. Appl. Phys. 32, 909 (1961).
24. D. A. Kleinman, Phys. Rev. 126, 1977 (1962).
25. G. Rupprecht and R. O. Bell, Phys. Rev. 125, 1915 (1962).
26. B. D. Silverman, Phys. Rev. 125, 1921 (1962).
27. M. Di Domenico, Jr. D. A. Johnson, and R. H. Pantell, J. Appl. Phys. 33, 1697 (1962).
28. R. F. Soohoo, Theory and Applications of Ferrites, (Prentice-Hall, Inc., Englewood Cliffs, New Jersey, 1960).
29. W. Shockley, Bell Syst. Tech. J. 28, 436 (1949).
30. W. J. Gemulla and R. D. Hall, Microwave J. 3, 47 (February, 1960).
31. F. Reggia and E. G. Spencer, Proc. IRE 45, 1510 (1957).
32. R. H. Hardin, E. J. Downey, and J. Munushian, Proc. IRE 48, 944 (1960).
33. R. E. Collin, Field Theory of Guided Waves, (McGraw-Hill Book Co., Inc., New York, N.Y., 1960).
34. P. H. Vartanian, W. P. Ayres, and A. L. Helgesson, IRE, Trans. PGMTT, MTT-6, 215 (1958).
35. M. DiDomenico, Jr. and R. H. Pantell, IRE, Trans. PGMTT, MTT-10, 179 (1962).
36. See reference 33, p. 182 therein.
37. E. L. Ginzton, Microwave Measurements, (McGraw-Hill Book Co., Inc., New York, N.Y., 1957).
38. R. D. Hall, private communication, Sylvania Electric Products, Inc. Electron Defense Lab., Mountain View, Calif. (1961).
39. W. H. Higa, J. Appl. Phys. 27, 775 (1956).
40. Y. Aoki, IRE, Trans. PGMTT, MTT-8, 465 (1960).
41. R. Landauer, J. Appl. Phys. 31, 479 (1960).
42. I. Goldstein, Proc. IRE 48, 1665 (1960).
43. J. M. Manley and H. E. Rowe, Proc. IRE 44, 906 (1956).
44. K. K. N. Chang, RCA Rev. 19 455 (1958).
45. D. B. Leeson and S. Weinreb, Proc. IRE 47, 2076 (1959).
46. C. H. Page, J. Research Natl. Bur. Standards 56, 179 (1956).
47. R. H. Pantell, Proc. IRE 46, 1910 (1958).
48. R. B. Riley, Technical Report No. 1707-1, Stanford Electronics Laboratories, Stanford University (1961).
49. D. L. Hedderly, Proc. IRE 48, 1658 (1960).
50. J. Brown, Proc. IRE 49, 825 (1961).

51. B. A. Auld, H. J. Shaw, and D. K. Winslow, J. Appl. Phys. 32, 317 S (1961).
52. I. Bady, IRE, Trans. PGMTT, MTT-10, 55 (1962).
53. G. S. Kino, J. Pavkovich, and J. Krenz, Microwave Laboratory Report No. 745, Stanford University (1960).
54. P. A. Franken, A. E. Hill, C. W. Peters, and G. Weinreich, Phys. Rev. Letters 7, 118 (1961).
55. J. J. Stoker, Nonlinear Vibrations (Interscience Publishers, Inc. New York, 1950), pp. 94-96.
56. See reference 1, p. 19 or Figs. 3 and 4.
57. B. A. Auld, M. DiDomenico, Jr., and R. H. Pantell, Microwave Laboratory Report No. 907, Stanford University (1962); (To be published in J. Appl. Phys.)
58. L. D. Landau and E. M. Lifshitz, Fluid Mechanics, (Addison - Wesley Publishing Company, Inc., Reading, Massachusetts, 1959).
59. M. J. Lighthill, in Surveys in Mechanics, edited by G. K. Batchelor and R. M. Davies (Cambridge University Press, Cambridge, 1956).
60. R. Landauer and L. H. Thomas, Bull. Am. Phys. Soc. Ser. II 4, 424 (1959).
61. A. V. Gaponov and G. I. Freidman, Soviet Phys. JETP 9, 675 (1959).
62. R. V. Khokhlov, Radio Engineering and Electronics 6, No. 6, 77 (1961).
63. R. Landauer, IBM J. Research Develop. 4, 391 (1960).
64. B. A. Auld, J. Appl. Phys. 31, 106S (1960).
65. See reference 34, pp. 203-207 therein.
66. G. S. Kino and B. A. Auld, "A Large-Signal Theory of Traveling-Wave Parametric Amplifiers and Harmonic Generators," presented at the Eighteenth Conference on Electron Tube Research, Seattle, Washington (June 1960).
67. G. Kron, Proc. IRE 32, 289 (1944).
68. J. R. Whinnery and S. Ramo, Proc. IRE 32, 284 (1944).
69. J. L. Melchor, W. P. Ayres, and P. H. Vartanian, Proc. IRE 45, 643 (1957).

DISTRIBUTION LIST

CONTRACT NONR 225(48)

2 Chief of Naval Research
Department of the Navy
Washington 25, D. C.
Attention: Code 427

1 Commanding Officer
Office of Naval Research
Branch Office
1030 E. Green Street
Pasadena, California

1 Commanding Officer
Office of Naval Research
Branch Office
346 Broadway
New York 13, New York

Director
Naval Research Laboratory
Washington 25, D. C.
1 Attention: Code 3400
1 3600
1 3900
1 3930
1 3940

2 Chief, Bureau of Naval Weapons
Department of the Navy
Washington 25, D. C.
Attention: RREN

1 Director
Naval Electronics Laboratory
San Diego 52, California

1 Director
Naval Ordnance Laboratory
White Oak, Maryland

10 ASTIA
Arlington Hall Station
Arlington 12, Virginia

1 Commanding Officer
Office of Naval Research
Branch Office
1000 Geary Street
San Francisco 9, California

1 Commanding Officer
Office of Naval Research
Branch Office
John Crerar Library Building
86 E. Randolph Street
Chicago 1, Illinois

10 Commanding Officer
Office of Naval Research
Navy 100
Fleet Post Office Box 39
New York, New York

2 Chief, Bureau of Ships
Navy Department
Washington 25, D. C.
Attention: Code 670

2 Chief, Bureau of Aeronautics
Navy Department
Washington 25, D. C.
Attention: Code AV

Chief, Naval Operations
Navy Department
Washington 25, D. C.
1 Attention: Code Op 30
1 Op 91

1 U. S. Naval Post Graduate School
Monterey, California

1 Commander
Naval Air Missile Test Center
Point Mugu, California

1 Chief, European Office
Air Research and Development Command
47 Rue Cantersteen
Brussels, Belgium

Commanding General
Air Force Research Division
Air Research and Development Command
Bedford, Massachusetts
8 Attention: CRRE
1 ERRSA-1

1 Director
Air University
Maxwell Air Force Base
Alabama
Attention: Cr 4582

1 Assistant Secretary of Defense
(Research and Development)
Department of Defense
Washington 25, D. C.
Attention: Technical Library

1 Chief, West Coast Office
USASRDL Building No. 6
75 South Grande Avenue
Pasadena 2, California

1 Chief Signal Officer
Department of the Navy
Washington 25, D. C.
Attention: SIGRD

1 Commanding Officer
U. S. Army Signal Missile Support Agency
White Sands Missile Range
White Sands, New Mexico

1 Commanding General
U. S. Army Ordnance Missle Ground
Huntsville, Alabama
Attention: ORDAB-T

1 Commanding Officer
U. S. Naval Proving Ground
Dahlgren, Virginia

1 Commander
U. S. Naval Air Development Center
Johnsville, Pennsylvania

1 Commanding Officer
Office of Ordnance Research
Box CM, Duke Station
Durham, North Carolina

1 Airborne Instrument Laboratory
Comac Road
Deer Park, L. I., New York
Attention: John Dyer

1 U. S. Coast Guard
1300 E. Street, N. W.
Washington 25, D. C.
Attention: EEE

1 Secretary
Commission on Electrics
Office of the Assistant Secretary of Defense
(Research and Development)
Department of Defense
Washington 25, D. C.

1 Director of Army Research
Office, Chief of Research and Development
Washington 25, D. C.

1 Chief Signal Officer
Department of the Army
Washington 25, D. C.
Attention: SIGC005b4

1 Commanding General
U. S. Army Electronic Proving Ground
Fort Huachuca, Arizona
ATTN: Technical Library,
Greely Hall

1 Commanding General
Naval Ordnance Laboratory
Corona, California

32 Signal Property Agent
Building 2504, Watson Area
Fort Monmouth, New Jersey
Attention: Office of Research Operations

1 Bell Telephone Laboratories
Murray Hill Laboratory
Murray Hill, New Jersey
Attention: Dr. J. R. Pierce

1 Office of the Chief of Engineers
Department of the Army
Washington 25, D. C.

1 California Institute of Technology
Department of Electrical Eng.
Pasadena, California
Attention: Professor L. M. Field

1 Commanding Officer
Engineering Research and Development Laboratory
Ft. Belvoir, Virginia

1 Ballistics Research Laboratory
Aberdeen Proving Ground
Aberdeen, Maryland
Attention: D. W. W. Delsasso

2 Chief of Staff
United States Air Force
Washington 25, D. C.
Attention: AFDRD-SC-3

2 Commanding General
Rome Air Development Center
Griffiss Air Force Base
Rome, New York

5 Commander
Air Force Office of Scientific Research
Attention: SRYA
Washington 25, D. C.

1 National Science Foundation
1951 Constitution Avenue, N. W.
Washington 25, D. C.

1 Commander
Air Force Armament Center
Attention: Technical Library
Eglin Air Force Base, Florida

1 Commander
Air Force Missile Development Center
Attention: Technical Library
Holloman Air Force Base
New Mexico

1 Office of the Chief of Ordnance
Department of the Army
Washington 25, D. C.
Attention: ORDTU

1 Commanding Officer
Frankford Arsenal
Bridesburg
Philadelphia, Pennsylvania

Commander
Wright Air Development Division
Wright-Patterson Air Force Base
Ohio
2 Attention: WCLC
4 WCLRC
1 WCLRC
1 WCLRA
1 WPLJ
1 WCLJH
1 WCRE
2 WCRED
1 WCRET

1 AEMTC (AEMTC Technical Library-MU 135)
Patrick Air Force Base
Cocoa, Florida

1 Chief, Physics Branch, Division Division of Research
U. S. Atomic Energy Commision
1901 Constitution Avenue, N.W.
Washington 25, D. C.

1 Commander
Arnold Engineering Development Center
Attention: Technical Library
Tullahome, Tennessee

1 Commander
Air Force Special Weapons Center
Attention: Technical Library
Kirtland Air Force Base
New Mexico

1 Commandant
Air Force Institute of Tech.
Attention: MCLI, Tech. Library
Wright-Patterson Air Force Base
Ohio

1 Commander
Air Force Ballistic Missile Division
Headquarters ARDC
Attention: WDSOT
Post Office Box 262
Inglewood, California

40 Stanford University
Stanford, California

1 Sylvania Electric Products, Inc.
500 Evelyn Avenue
Mountain View, California
Attention: Special Tube Operations

1 Ohio State University
Department of Electrical Eng.
Columbus 10, Ohio
Attention: Professor E. M. Boone

1 University of Michigan
Willow Run Research Center
Engineering Research Institute
Ann Arbor, Michigan
Attention: Dr. H. Goode

1 Director
Electronics Defense Group
Engineering Research Institute
University of Michigan
Ann Arbor, Michigan

1 Columbia University
Columbia Radiation Laboratory
New York 27, New York
Attention: Mr. Bernstein

1 Cruft Laboratory
Harvard University
Cambridge, Massachusetts

1 Dr. Winston H. Bostick
Department of Physics
Stevens Institute of Technology
Hoboken, New Jersey

1 Raytheon Manufacturing Company
1481 California Street
Newton, Massachusetts

1 Sperry Gyroscope Company
Great Neck, L. I., New York
Attention: Technical Library

1 Sylvania Electric Products, Inc.
70 Forsyth Street
Boston, Massachusetts
Attention: Charles E. Arnold

1 Varian Associates
611 Hansen Way
Palo Alto, California
Attention: Technical Library

1 University of Texas
Defense Research Laboratory
Austin, Texas
Attention: Harold D. Kirck, Sr.

1 Massachusetts Institute of Technology
Research Laboratory of Electronics
Cambridge 39, Massachusetts
Attention: Mr. Hewitt Librarian

1 Brooklyn Polytechnic Institute
Microwave Research Institute
55 Johnson Street
Brooklyn 1, New Jersey
Attention: Mr. Jerome Fox

1 Dr. Paul D. Coleman
Electrical Engineering Depart.
Control Systems Laboratory
University of Illinois
Urbana, Illinois

1 Dr. John R. whinnery
Division of Electrical Eng.
University of California
Berkeley 4, California

1 Professor Hans Motz
Oxford University
Oxford, England

1 Lincoln Laboratory
Massachusetts Institute of Technology
P. O. Box 73
Lexington, Massachusetts

1 Gilfillian Brothers
1815 Venice Blvd.
Los Angeles, California
Attention: Countermeasures Laboratories

1 Hallicrafters
4401 West 5th Street
Chicago, Illinois
Attention: William Frankart

1 The Maxson Corporation
460 West 34th Street
New York 1, New York

1 Motorola, Incorporated
8330 Indiana Avenue
Riverside, California
Attention: Robert W. Barton

1 Raytheon Manufacturing Corp.
Waltham 54, Massachusetts
Attention: Research Division Library

1 Mr. Paul C. Yuen
Research Engineer
Electronics Research Laboratory
Illinois Institute of Tech.
Technology Center
Chicago 16, Illinois

1 Sperry Gyroscope Company
Electronic Tube Division
Great Neck, L. I., New York
Attention: T. Sege

4 Office of Ordnance
U. S. Army
Box CM, Duke Station
Durham, North Carolina

1 Electron Tube Division of the Research Laboratory
General Electric Company
The Knolls
Schenectady, New York

1 Glenn L. Martin Company
Baltimore, Maryland
Attention: Mary E. Exxo

1 Hughes Aircraft Company
Florence Ave. and Teale St.
Culver City, California
Attention: Mr. Nicholas E. Devereux Technical Document Ctr.

1 Melpar, Incorporated
Corvey Division
2601 Jefferson-Davis Highway
Alexandria, Virginia

1 The Rand Corporation
1700 Main Street
Santa Monica, California
Attention: Margaret Anderson Librarian

1 Dr. Walter Higa
Engineering Specialist
Research Group Supervisor
California Institute of Tech.
4800 Oak Grove Drive
Pasadena 3, California

1 General Electric Microwave Lab.
601 California Avenue
Palo Alto, California
Attention: Librarian

1 Mr. Kjell Blåtekjær
Norwegian Defense Research
Establishment
Radar Division
Bergen, Norway

1 Pacific Union College
Physics Department
Angwin, California
Attention: Dr. Ivan Neilson

1 Dr. A. D. Berk
4134 Del Rey Avenue
Venice, California

1 Dr. A. F. Pierce
Imperial College of Science
and Technology
South Kensington
London, S. W., England

1 The Mitre Corporation
P. O. Box 208
Lexington 73, Massachusetts

1 Mr. Jack Summers
Varian Associates
611 Hansen Way
Palo Alto, California

1 General Electric Company
Power Tube Division
Electronic components Division
Building 269, Room 205
One River Road
Schenectady 5, New York

1 Litton Industries
Electron Tube Division
960 Industrial Road
San Carlos, California

1 Eitel-McCullough, Inc.
Research Library
301 Industrial Way
San Carlos, California

1 Stanford Research Insititute
Menlo Park, California
Attention: Documents Center

1 Bendix Corporation
Red Bank Division
Eatontown, New Jersey
Attention: Mr. S. Barbasso

1 High-Power Klystron Department
G. 38
Attention: Dr. John Romaine
Sperry Gyroscope Company
Great Neck, L. I., New York

1 Dr. Bertil Agdur
Microwave Department
Royal Institute of Technology
Stockholm, Sweden

1 California Institute of Technology
Electron Tube Laboratory
Pasadena, California

1 Pacific Semiconductors, Inc.
10451 West Jefferson Blvd.
Culver City, California
Attention: Mr. H. Q. North

1 Robert Vehn
Watkins-Johnson Company
3333 Hillview Avenue
Palo Alto, California

1 Sperry Electronic Tube Division
Sperry Rand Corporation
Gainsville, Florida

1 Research Division Library
Raytheon Company
28 Seyon Street
Waltham 54, Massachusetts

1 Mr. J. F. Kane
Kane Engineering Laboratories
845 Commercial Street
Palo Alto, California

1 Phillips Laboratories
Division of North American
Phillips Company, Inc.
Irvington-on-Hudson
New York
Attention: Robert C. Bohlinger

1 Director
U. S. Naval Research Labs.
Washington 25, D. C.
Attention: Code 5300

1 Sperry Phoenix Company
Division of Sperry Rand Corp.
Phoenix, Arizona
Attention: Tech. Librarian

1 TUCOR, Incorporated
18 Marshall Street
South Norwalk, Connecticut
Attention: Mrs. Marion Osband

1 Professor H. W. Konig
Institute fur
Hochfrequenztechnik
Technische Hochschule
Vienna 4,
Gusshausstrasse 25
Austria

1 Dr. V. L. Stout, Manager
Physical Electronic Research
Laboratory
P. O. Box 1088
Schenectady, New York

1 Institute for Defense Analysis
Research andEngineering
Suppot Division
1825 Connecticut Ave., N. W.
Washington 25, D. C.
Attention: Technical Information
Office

1 Director
National Security Agency
Fort George G. Meade, Maryland
Attention: CREF-332 (Rm. 20087)
Miss Creswell
Librarian

1 Research Center for the Airtron
Division of Litton Industries
200 East Hanover Avenue
Morris Plains, New Jersey
Attention: J. W. Neilson, Manager
Solid State Materials
Laboratory

1 Commanding Officer
U. S. Army Research Office
Durham
Box CM, Duke Station
Dunham, North Carolina
Attention: CRD-AA-IP, Mr. Ulsh

1 Cornell University
School of Electrical Engineering
Ithaca, New York
Attention: Professor G. C.
Dalman

1 Carlyle Barton Lab.
The Johns Hopkins University
Charles and 34th Streets
Baltimore 18, Maryland
Attention: Librarian

1 Professor Sanai Mito
Osaka City University
Department of Engineering
12 Nishi-Ogimachi, Kitaku
Osaka, Japan

CERN
Service d'Information Scientifique
Attn: Mme L. Goldschmit-Clermont
Geneve 23, Switzerland

Amphenol-Borg Electronics Corporation
2801 South 25th Avenue
Broadview, Illinois
ATTN: Mr. R. C. Becker
Senior Staff Engineer

Dr. Glen Wade
Spencer Laboratories
Burlington, Massachusetts

Mr. Charles Turner
585 Kenton Rd., Kenton, Harrow
Middlesex, England

Scientific Attache
Swedish Embassy
2249 R Street, N. W.
Washington 8, D. C.

Dr. Yen
Department of Electrical Eng.
University of Toronto
Toronto 5, Ontario
Canada

M. A. Allen
Microwave Associates Inc.
Burlington, Massachusetts

Commanding Office (3 copies)
U. S. Army Research Office (Durham)
ATTN: CRD-AA-IP, Box CM
Duke Station
Durham,, North Carolina

Raytheon Company
Research Division
Waltham 54, Massachusetts
ATTN: Mrs. Madaleine Benett
Librarian

USNPG
Monterey, California
ATTN: Prof. Gray
Electronics Department

Dr. E. A. Ash
Standard Telecommunications Lab., Ltd.
London Road
Harlow, Essex, England

Dr. W. Veith
Siemens and Halske Aktiengesellschaft
St. Martin Strasse 76
Munchen 8, Germany

Dr. Humio Inaba
Electrical Engineering Department
Tohoku University
Sensai, Japan

Dr. T. Rossing
St. Olaf College
Northfield, Minnesota

Carnegie Institute of Technology
Department of Electrical Eng.
Schenley Park
Pittsburgh 13, Pennsylvania

UNCLASSIFIED

UNCLASSIFIED